



Erasmus Mundus Joint
Master Degree in
Marine Environment
UPV/EHU-SOTON-UBx-ULiège
www.merplus.eu



MASTER THESIS PROJECT

Detection and Explanation of Shifts in the Climatic Controls of Norwegian Glaciers

Author: Syed Danish Ali

Supervisor: Dr. habil. Sebastian G. Mutz

**Department: School of Geographical & Earth Sciences
University of Glasgow**

PLENTZIA (UPV/EHU), SEPTEMBER 2025



UNIVERSITY OF
Southampton



LIÈGE
université



UAc
UNIVERSIDADE
DOS AÇORES



Dr. Manu Soto as teaching staff of the MER Master of the University of the Basque Country

CERTIFIES:

That the research work entitled **“Detection and explanation of shifts in the climatic controls on Norwegian glaciers.”** has been carried out by **Syed Danish Ali** in **University of Glasgow** under the supervision of **Dr. habil. Sebastian G. Mutz** from **School of Geographical & Earth Sciences, University of Glasgow (Scotland, U.K.)** in order to achieve 30 ECTS as a part of the MER Master program.

In Plentzia (Spain), September 2025

Presenter: **Prof. Manu Soto**

Supervisor(s): **Dr. habil. Sebastian G. Mutz**

Sign.

Sign.

Sign

PLENTZIA (UPV/EHU), SEPTEMBER 2025

Detection and Explanation of Shifts in the Climatic Controls of Norwegian Glaciers

MSc Marine Environment & Resources

Syed Danish Ali

August 2025



Supervisor: Dr. habil. Sebastian G. Mutz

School of Geographical & Earth Sciences

University of Glasgow

Declaration of Authorship

I hereby declare that this thesis, entitled "**Detection and Explanation of Shifts in the Climatic Controls of Norwegian Glaciers**", is the result of my own independent work, and has not been submitted, in whole or in part, for any other degree or qualification at this or any other institution. All sources of information, data, figures, and references from the published or unpublished work of others have been fully acknowledged in the text and listed in the bibliography section.

August 2025

Glasgow, Scotland

A handwritten signature consisting of stylized, fluid lines.

Sign

Acknowledgements

I would like to express my sincere gratitude to my supervisor, Dr. habil. Sebastian G. Mutz, for his invaluable guidance, support, and encouragement throughout the course of this research. His expertise and constructive feedback have greatly contributed to the development and completion of this thesis. The experience of learning from him will remain invaluable throughout my career. My appreciation extends to the School of Geographic and Earth Sciences at University of Glasgow for providing the resources, facilities, and academic environment necessary for carrying out this research. I would also like to thank my colleagues and friends from the master for a memorable time. Special thanks to Sam and Dr. Daniel Boateng for their help to debug errors faced during programming. Finally, I am eternally grateful to my family for their unwavering love, patience, and encouragement throughout all my academic endeavors. Their belief in me has been a constant source of motivation and without it, I would not be where I am today.

Abstract

Norwegian glaciers have undergone accelerated mass loss since 2000, indicating a shift in the climatic controls on their mass balance. This study analyzes the relationships between large-scale variability and the mass balance of 11 Norwegian glaciers (situated 57–72° N) via correlation analyses, computed separately for pre-2000 and post-2000 using DJF (accumulation) and MJJAS (ablation) windows. These relationships for each glacier are then transferred to an empirical statistical downscaling framework with six regressors and three feature-selection methods. Four key patterns emerge: (1) pre-2000, NAO, precipitation, and temperature strongly influenced mass balance, with B_w closely linked to accumulation-season precipitation (P_{acc}); (2) post-2000, sensitivity shifts toward summer temperature (T_{abl}) and surface solar radiation (SSRD), with weaker B_w –NAO coupling; (3) B_w – P_{acc} correlations decline while B_w – T_{acc} correlations rise; and (4) a persistent maritime–continental gradient, with coastal glaciers more precipitation sensitive and inland glaciers increasingly temperature dominated. The findings point to transition of B_a from winter (accumulation) to summer (ablation) dominated for 9/11 glaciers. In modelling, linear regressors (RidgeCV, Bayesian Ridge, ARD) paired with Recursive or Tree-based selectors consistently outperform non-linear models. Predictability ranks $B_w > B_a > B_s$, with the best models achieving glacier-specific R^2 up to 0.81 and RMSE as low as 0.30 m w.e. The model framework presented here does not consider glacier dynamics or geometry. The findings confirm a post-2000 shift to a more temperature-dominated regime and provide a transferable machine-learning framework for projecting Norwegian glacier mass balance under future scenarios.

Abstract (en français)

Depuis 2000, les glaciers Norvégiens ont subi une perte de masse accélérée, indiquant un changement dans les contrôles climatiques de leur bilan de masse. Cette étude analyse les relations entre la variabilité à grande échelle et le bilan de masse de 11 glaciers norvégiens (situés entre 57° et 72° N) à travers des analyses de corrélation, calculées séparément pour les périodes avant et après 2000, en utilisant les fenêtres DJF (accumulation) et MJJAS (ablation). Ces relations, propres à chaque glacier, sont ensuite intégrées dans un cadre de réduction d'échelle statistique empirique utilisant six régressions et trois méthodes de sélection de variables. Quatre tendances clés se dégagent : (1) avant 2000, l'oscillation nord-atlantique (NAO), les précipitations et la température influençaient fortement le bilan de masse, avec Bw étroitement lié aux précipitations hivernales d'accumulation (Pacc) ; (2) après 2000, la sensibilité se déplace vers la température estivale (Tabl) et le rayonnement solaire incident en surface (SSRD), avec un affaiblissement du couplage Bw–NAO ; (3) les corrélations Bw–Pacc diminuent tandis que les corrélations Bw–Tacc augmentent ; et (4) un gradient maritime–continental persistant, avec des glaciers côtiers plus sensibles aux précipitations et des glaciers continentaux de plus en plus dominés par la température. Les résultats indiquent une transition de Ba, passant d'un régime hivernal (accumulation) à un régime estival (ablation) pour 9 glaciers sur 11. En modélisation, les régressions linéaires (RidgeCV, Bayesian Ridge, ARD) associées à des sélecteurs récursifs ou basés sur les arbres surpassent systématiquement les modèles non linéaires. La prévisibilité suit l'ordre Bw > Ba > Bs, les meilleurs modèles atteignant un R² spécifique au glacier allant jusqu'à 0,81 et un RMSE aussi bas que 0,30 m équ. eau. Le cadre de modélisation présenté ici ne prend pas en compte la dynamique ou la géométrie des glaciers. Les résultats confirment un passage, après 2000, à un régime davantage dominé par la température et proposent un cadre de machine learning transférable pour projeter le bilan de masse des glaciers norvégiens dans de futurs scénarios.

Contents

| | |
|---|-----------|
| <u>LIST OF FIGURES</u> | 1 |
| <u>LIST OF TABLES</u> | 4 |
| <u>LIST OF ACRONYMS</u> | 5 |
| <u>INTRODUCTION</u> | 7 |
| 1.1. BACKGROUND | 7 |
| 1.2. HOLOCENE GLACIER VARIABILITY | 7 |
| 1.3. GLACIER DISTRIBUTION & CLASSIFICATION | 9 |
| 1.4. CLIMATIC SETTING OF NORWAY | 11 |
| 1.5. GLACIER MASS BALANCE REGIME | 13 |
| 1.6. IMPACT OF CLIMATE CHANGE | 13 |
| 1.7. IMPACT OF GLACIER LOSS | 14 |
| 1.8. MODELLING APPROACHES | 15 |
| 1.9. AIMS OF THIS STUDY | 16 |
| <u>2. METHODOLOGY</u> | 17 |
| 2.1. DATA SOURCES & SELECTION | 17 |
| 2.2. EMPIRICAL ORTHOGONAL FUNCTION ANALYSIS | 18 |
| 2.3. CORRELATION ANALYSIS | 20 |
| 2.4. MODEL DEVELOPMENT | 21 |
| <u>3. RESULTS</u> | 24 |
| 3.1. ANNUAL MASS BALANCE TRENDS | 24 |
| 3.2. WINTER MASS BALANCE TRENDS | 26 |
| 3.3. SUMMER MASS BALANCE TRENDS | 28 |
| 3.4. MASS BALANCE CONTROL TRENDS | 30 |
| 3.5. MODELLING ANNUAL MASS BALANCE | 32 |
| 3.6. MODELLING WINTER MASS BALANCE | 35 |

| | |
|--|-----------|
| 3.7. MODELLING SUMMER MASS BALANCE | 37 |
| 4. DISCUSSION | 39 |
| 4.1. TRENDS IN ANNUAL MASS BALANCE | 39 |
| 4.2. TRENDS IN WINTER MASS BALANCE | 42 |
| 4.3. TRENDS IN SUMMER MASS BALANCE | 44 |
| 4.4. EVALUATION OF MODEL PERFORMANCE | 45 |
| 4.4.1. ANNUAL MASS BALANCE | 45 |
| 4.4.2. WINTER MASS BALANCE | 46 |
| 4.4.3. SUMMER MASS BALANCE | 46 |
| 4.5. INTERPRETATION & COMPARISON WITH OTHER STUDIES | 47 |
| 5. CONCLUSION | 49 |
| 5.1. PART A | 49 |
| 5.2. PART B | 50 |
| BIBLIOGRAPHY | 51 |
| APPENDIX | 64 |
| I. EOF ANALYSIS | 64 |
| II. COMPARISON BETWEEN HURRELL's NAO AND EOF DERIVED NAO | 66 |
| III. REGIME SHIFT IN B_w ~NAO COUPLING | 67 |
| IV. COMPLETE GLACIER-WISE MODELLING RESULTS | 68 |
| TABLE A1: ANNUAL MASS BALANCE (B_A) | 68 |
| TABLE A2: WINTER MASS BALANCE (B_w): | 72 |
| TABLE A3: SUMMER MASS BALANCE (B_s) | 77 |

List of Figures

| | |
|--|----|
| FIG 1: TIMELINE SUMMARIZING THE GLACIER VARIABILITY IN SCANDINAVIA DURING THE HOLOCENE, HIGHLIGHTING PERIODS OF RETREAT, DISAPPEARANCE, REFORMATION, ADVANCEMENT, AND RECENT ACCELERATED MELTING..... | 8 |
| FIG 2: (A) LOCATION OF GLACIERS INCLUDED IN THIS STUDY (INSET SHOWS GLACIER LOCATIONS IN THE SOUTHERN CLUSTER): ALF- ÅLFOTBREEN, AUS- AUSTDALSBUEREN, ENG-ENGABREEN, GRÅS- GRÅSUBRENN, GRÅ- GRÅFJELLSBREA, HAN- HANSEBREEN, HELL-HELLSTUGUBRENN, LAN- LANGFJORDJØKELEN, NIG- NIGARDSBREEN, REM-REMESDALSKÅKA, STO- STORBREEN, AND; (B) TOPOGRAPHIC SETTING OF NORWAY WITH AN OVERVIEW OF GLACIER LOCATIONS. | 10 |
| FIG 3: (A) AVERAGE ANNUAL PRECIPITATION (MM YR-1) FOR THE PERIOD 1950-2023, SHOWING A DISTINCT ZONE OF HIGH PRECIPITATION ALONG THE COASTAL REGION. (B) MONTHLY MEAN TEMPERATURE ABOVE SURFACE ($^{\circ}$ C), WHERE THE SPATIAL PATTERN REFLECTS TOPOGRAPHY, WITH HIGHER TEMPERATURES IN LOWER-ELEVATION COASTAL AREAS AND COOLER CONDITIONS IN HIGH-ELEVATION INLAND REGIONS. [DATA SOURCE: ECMWF ERA5 REANALYSIS DATA]..... | 11 |
| FIG 4: 2D ILLUSTRATION OF PCA. PC1 CAPTURES THE MAXIMUM VARIANCE (MAJOR AXIS), WHILE PC2 IS ORTHOGONAL AND REPRESENTS THE SECOND-LARGEST VARIANCE (MINOR AXIS). | 19 |
| FIG 5: SCHEMATIC SUMMARY OF THE STEPS UNDERTAKEN FOR THE CORRELATION ANALYSIS WORKFLOW..... | 20 |
| FIG 6: SCHEMATIC OF THE MODELLING ROUTINE. PREDICTORS ARE CONSTRUCTED FROM ERA5 DATASETS TO GENERATE EMPIRICAL-STATISTICAL MODELS & THEIR METRICS. THE RESULTING MODEL'S PERFORMANCE FOR EACH MASS BALANCE COMPONENT IS EVALUATED USING THE DEFINED METRICS TO IDENTIFY ANY SIGNIFICANT PATTERNS. THE BEST PERFORMING MODEL(S), INDIVIDUALLY OR IN AN ENSEMBLE, CAN BE COUPLED WITH A GCM TO MAKE FUTURE PREDICTIONS. DATA SOURCES: MASS BALANCE [NVE] & ERA5 REANALYSIS [ECMWF] | 22 |
| FIG 7: CUMULATIVE B_A (M W.E.) FOR 11 NORWEGIAN GLACIERS FROM 1950 TO 2020. THE DASHED VERTICAL LINE AT THE YEAR 2000 INDICATES A MARKED ACCELERATION IN CUMULATIVE MASS LOSS FOR MOST GLACIERS AFTER 2000. THIS SHOWS A TRANSITION | |

| | |
|---|----|
| TOWARD INCREASINGLY NEGATIVE MASS BALANCE REGIMES FOR ALL 11 GLACIERS IN THE 21ST CENTURY | 24 |
| FIG 8: CORRELATION (R) HEAT-MAPS FOR B_A (M W.E.) WITH SELECTED CLIMATE VARIABLES, FOR BEFORE AND AFTER 2000. RED R VALUES IN DENOTE STATISTICALLY INSIGNIFICANT RESULTS ($P > 0.05$). GRAY CELLS LABELLED ‘NAN’ REPRESENT CASES WITH LACK OF SUFFICIENT DATA TO COMPUTE A CORRELATION, WHILE ‘N/A’ DENOTES VARIABLES FOR WHICH CORRELATION WAS NOT APPLICABLE BY DESIGN..... | 25 |
| FIG 9: 5-YEAR ROLLING MEAN OF B_w (M W.E.) FOR 11 NORWEGIAN GLACIERS FROM 1950 TO 2020. THE DASHED VERTICAL LINE AT THE YEAR 2000 MARKS A TRANSITION PERIOD. WHILE B_w REMAINS RELATIVELY STABLE FOR MANY GLACIERS, SOME DISPLAY A GREATER INTERANNUAL VARIABILITY POST-2000..... | 26 |
| FIG 10: CORRELATION (R) HEAT-MAPS FOR B_w (M W.E.) WITH SELECTED CLIMATE VARIABLES, FOR BEFORE AND AFTER 2000. RED R VALUES IN DENOTE STATISTICALLY INSIGNIFICANT RESULTS ($P > 0.05$). GRAY CELLS LABELLED ‘NAN’ REPRESENT CASES WITH LACK OF SUFFICIENT DATA TO COMPUTE A CORRELATION, WHILE ‘N/A’ DENOTES VARIABLES FOR WHICH CORRELATION WAS NOT APPLICABLE BY DESIGN..... | 27 |
| FIG 11: 5-YEAR ROLLING MEAN OF B_s (M W.E.) FOR 11 NORWEGIAN GLACIERS FROM 1950 TO 2020. THE DASHED VERTICAL LINE MARKS THE YEAR 2000, INDICATIVE OF A MORE PRONOUNCED NEGATIVE TREND IN B_s FOR SEVERAL GLACIERS..... | 28 |
| FIG 12: CORRELATION (R) HEAT-MAPS FOR B_s (M W.E.) WITH SELECTED CLIMATE VARIABLES, FOR BEFORE AND AFTER 2000. RED R VALUES IN DENOTE STATISTICALLY INSIGNIFICANT RESULTS ($P > 0.05$). GRAY CELLS LABELLED ‘NAN’ REPRESENT CASES WITH LACK OF SUFFICIENT DATA TO COMPUTE A CORRELATION, WHILE ‘N/A’ DENOTES VARIABLES FOR WHICH CORRELATION WAS NOT APPLICABLE BY DESIGN..... | 29 |
| FIG 13: HEAT-MAP DISPLAYING THE PEARSON CORRELATION OF B_A WITH B_w & B_s PRE- & POST-2000. RESULTS SHOW A CLEAR SHIFT IN INFLUENCE OF B_s IN DETERMINING B_A POST 2000..... | 30 |
| FIG 14: (A) SCATTERPLOTS DISPLAYING THE PEARSON CORRELATION OF B_A WITH B_w (PRE-2000) & WITH B_s (POST-2000). (B) SCATTERPLOT DISPLAYING THE CORRELATION OF B_A WITH B_w & B_s (POST-2000). THE PLOT OUTLINES THE SEASONAL SHIFT IN THE MASS BALANCE CONTROL. A GENERAL SHIFT FROM A B_w DOMINATED MASS BALANCE REGIME TO A B_s DOMINATED REGIME IS OBSERVED FOR 9 OUT OF 11 GLACIERS POST 2000. B_A OF SOME GLACIERS CONTINUES TO BE CONTROLLED BY B_w POST-2000..... | 31 |

| | |
|--|----|
| FIG 15: (A) TEST PERFORMANCE METRICS (R^2) BOXPLOTS FOR B_A (M W.E.) FOR 6 REGRESSORS (RIDGEBCV, BAGGING, ARD, RANFOMFOREST, XGBOOST, BAYESIANRIDGE) AND 3 REGRESSORS (RECURSIVE, SEQUENTIAL, TREEBASED). (B) HEAT-MAP SHOWING TEST RMSE VALUES FOR A COMBINATION OF REGRESSOR AND SELECTOR FOR EACH GLACIER. ARD-TREE, BAG-TREE, AND RF-REC HAVE THE BEST PERFORMANCE ACROSS ALL 11 GLACIERS. CORRELATION WAS NOT APPLICABLE BY DESIGN. | 32 |
| FIG 16: (A) TEST PERFORMANCE METRICS (R^2) BOXPLOTS FOR B_W (M W.E.) FOR 6 REGRESSORS (RIDGEBCV, BAGGING, ARD, RANFOMFOREST, XGBOOST, BAYESIANRIDGE) AND 3 REGRESSORS (RECURSIVE, SEQUENTIAL, TREEBASED). (B) HEAT-MAP SHOWING TEST RMSE VALUES FOR A COMBINATION OF REGRESSOR AND SELECTOR FOR EACH GLACIER. ARD-TREE, BAG-TREE, AND RF-REC HAVE THE BEST PERFORMANCE ACROSS ALL 11 GLACIERS. CORRELATION WAS NOT APPLICABLE BY DESIGN. | 35 |
| FIG 17: (A) TEST PERFORMANCE METRICS (R^2) BOXPLOTS FOR B_s (M W.E.) FOR 6 REGRESSORS (RIDGEBCV, BAGGING, ARD, RANFOMFOREST, XGBOOST, BAYESIANRIDGE) AND 3 REGRESSORS (RECURSIVE, SEQUENTIAL, TREEBASED). (B) HEAT-MAP SHOWING TEST RMSE VALUES FOR A COMBINATION OF REGRESSOR AND SELECTOR FOR EACH GLACIER. B_s PREDICTION DISPLAYS LOW R^2 AND HIGH RMSE FOR ALL GLACIERS AND MODELS, PROVING TO BE DIFFICULT TO ESTIMATE. | 37 |
| FIG 18: INTER-ANNUAL VARIABILITY OF WINTER PRECIPITATION (TOP) AND THE NAO INDEX (BOTTOM) FOR THE PERIOD 1950-2023. PRECIPITATION EXPRESSED AS SEASONAL MEANS (DEC-FEB) IN MM, WHILE NAO IS PRESENTED AS STANDARDIZED ANOMALIES. BOTH SERIES EXHIBIT SIMILAR INTERANNUAL FLUCTUATIONS, WITH HIGHER PRECIPITATION GENERALLY COINCIDING WITH POSITIVE NAO PHASES. FIGURE INSPIRED FROM NESJE ET AL. (2000). [DATA: ECMWF- ERA5 REANALYSIS PRODUCT] | 40 |
| FIG 19: SCATTERPLOT DISPLAYING THE CORRELATION BETWEEN NAO INDEX AND WINTER PRECIPITATION. PEARSON CORRELATION YIELDED $R= 0.62$, INDICATING A STRONG CORRELATION AND COUPLING BETWEEN THE TWO VARIABLES. [DATA: ECMWF- ERA5 REANALYSIS PRODUCT] | 41 |
| FIG 20: CORRELATION BETWEEN B_W AND B_A AND BETWEEN B_s AND B_A FOR 11 NORWEGIAN GLACIERS. THE ANALYSIS SHOWS THAT B_A FOR MARITIME GLACIERS (ÅLFOTBREEN, ENGABREEN, GRAFJELLSBREA, REMBESDALSKÅKA) IS MAINLY CONTROLLED BY B_W WHEREAS B_A OF CONTINENTAL GLACIERS (GRASUBREEN, HELLSTUGUBREEN, STOREBREEN) IS CONTROLLED BY B_s . FIGURE ADAPTED FROM NESJE ET AL. (2023)..... | 43 |

List of Tables

| | |
|---|----|
| TABLE 1: SELECTED B_A MODEL PERFORMANCE METRICS | 34 |
| TABLE 2: SELECTED B_W MODEL PERFORMANCE METRICS..... | 36 |
| TABLE 3: SELECTED B_S MODEL PERFORMANCE METRICS | 38 |

List of Acronyms

AAR – Accumulation Area Ratio

acc/abl – Climate variable measured during accumulation or ablation seasons

AO – Arctic Oscillation

b – mass balance (*ba*: annual/net balance *bw*: winter, *bs*: summer)

CMIP6 – Coupled Model Intercomparison Project Phase 6

EA – East Atlantic Oscillation

ECMWF – European Centre for Medium-Range Weather Forecasts

ELA – Equilibrium Line Altitude

EOF – Empirical Orthogonal Function

ERA5 – ECMWF Reanalysis Dataset v5

ESD – Empirical Statistical Downscaling

GCM – Global Climate Model

GHG – Greenhouse Gas

ML – Machine Learning

m a.s.l. – meters above sea level

NAO – North Atlantic Oscillation

NCAR – National Center for Atmospheric Research

NVE – Norwegian Water Resources and Energy Directorate (Norges vassdrags- og energidirektorat)

PCA – Principal Component Analysis

PCA-ANA – Principal Component Analysis: All North Atlantic (Northern Hemisphere) domain

PCA-NA – Principal Component Analysis: North Atlantic domain

PC – Principal Component

PCC – Pearson Correlation Coefficient

POPs – Persistent Organic Pollutants

pyESD – Python Empirical Statistical Downscaling package

RCM – Regional Climate Model

SIS – Scandinavian Ice Sheet

SLP – Sea Level Pressure

SSPs – Shared Socioeconomic Pathways

Φ – Latitude

Introduction

1.1. Background

Glaciers are among the most sensitive and dynamic components of the Earth's climate system, serving an important role as key indicators of climate change. The advances and retreats of mountain glaciers are one of the most visible signs of the effects of climate change (Lemke et al., 2007). Glaciers have been regularly monitored globally and for more than the past six decades in Norway (Andreassen et al., 2005a; Liestøl, 1967). The second longest continuous mass balance record (1949 - Present) is from Storbreen (Jotunheimen) in central southern Norway (Nesje & Bakke, 2007). Although Norway is a relatively small country with a land area of approximately 385,199 km², it holds particular significance for glaciological research due to its proportionately high glacier coverage compared to most other European countries (Østrem & Haakensen, 1973; Winsvold et al., 2014).

Norway has the largest share of ice-covered land in mainland Europe (Beniston et al., 2018). With Norwegian glaciers occupying around $2,692 \pm 81$ km² (using $\pm 3\%$ as uncertainty) of the mainland (Andreassen et al., 2020; Andreassen & Winsvold, 2012), they account for ~ 0.8 to 0.9% of the total area. Glacier inventory made by (Østrem & Haakensen, 1993) listed 1,627 glaciers in Norway. However, 2,534 glaciers have been identified in the most recent inventories (Andreassen & Winsvold, 2012; Winsvold et al., 2014). They occur primarily as icecaps, cirque glaciers, outlet glaciers, and small valley glaciers (Andreassen & Winsvold, 2012). Norway's glaciers hold substantial economic potential, contributing to sectors such as tourism, climate science, and hydroelectric energy production (Andreassen, Elvehøy, et al., 2020). They play a considerable role in electricity generation. Hydroelectric power generation in Norway was responsible for nearly 92% of the total power production in the country in April 2025 (SSB 2025), a share that not only remained dominant but also increased compared to the preceding year, reaffirming its central role in Norway's energy budget. Glaciers in Norway were among the first ones to experience the effects of climate change (Vaughan et al., 2013).

1.2. Holocene Glacier variability

The glaciers in Scandinavia have exhibited pronounced cycles of retreat and advancement throughout the Holocene (Fig. 1), closely tied to climatic variability (Nesje & Bakke, 2007). Following the Last Glacial Maximum (c. 26 - 18 ka) in Norway (Hughes et al., 2013; Mangerud

et al., 2011), rapid deglaciation of the SIS began around 9700 BCE. Several outlet glaciers from the SIS retreated significantly in early Holocene c. 9800 - 9500 BCE (Dahl et al., 2002). During 8,000 - 4,000 BCE, most glaciers in Norway disappeared at least once due to warmer summer temperatures and/or reduced winter precipitation (Nesje & Bakke, 2007). Norwegian glaciers reformed between approximately 6,000 and 2,000 BCE (Dahl et al., 2002; Nesje, Matthews, Dahl, Berrisford, et al., 2001), with many reaching their maximum ‘Neoglacial’ extents during the Little Ice Age (roughly 18th - 19th centuries CE), marked by cooler conditions and increased winter snowfall (Matthews & Karlén, 1992). However, a general pattern of retreat has dominated following the ‘Neoglacial’ state, with brief phases of advance in 1950s and early 1990s (Andreassen et al., 2005b; Nesje & Dahl, 2000).

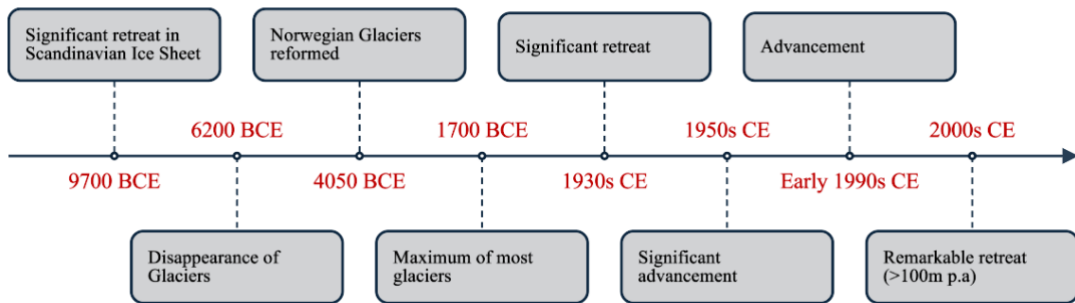


Fig 1: Timeline summarizing the glacier variability in Scandinavia during the Holocene, highlighting periods of retreat, disappearance, reformation, advancement, and recent accelerated melting.

Since the turn of the 21st century (2000), Norwegian glaciers have entered a phase of rapid and widespread retreat, exceeding 100 m per year, which has largely been attributed to increased summer temperatures (Nesje & Bakke, 2007). A ‘regime shift’ has been reported by several researchers as all Norwegian glaciers exhibit remarkable mass-balance deficits (Andreassen et al., 2005b; Andreassen et al., 2020; Nesje, 2023; Nesje & Bakke, 2007; Winsvold et al., 2014). This shift marks the most negative mass-balance period on record due to accelerated retreat rates, driven by increased summer temperatures (Andreassen & Winsvold, 2012).

These observations motivate the central hypothesis of my thesis: “The turn of the century marks the transition to a new glacier regime, characterized by a change in the climatic controls on annual mass balances.” A secondary project goal is to capture the empirical relationships between climatic controls on glacier mass balance by developing empirical statistical models for B_a , B_w , and B_s and evaluating the performance of different models.

1.3. Glacier Distribution & Classification

Systematic observation and measurement of Norwegian glacier's mass balance began in the 1960s, revealing both temporal and spatial variability. The Norwegian mass balance record is now maintained and published by the NVE: Norwegian Water Resources and Energy Directorate (Norwegian: Norges vassdrags- og energidirektorat). Glacier inventories in Norway, such as those by Østrem (1969, 1973, 1988) and Andreassen & Winsvold (2014), use the concept of 'glacier units', which is defined as individual glacier masses with distinct accumulation-ablation zones that drain into one single hydrological basin, exhibiting an independent flow regime. From these inventories, Norway has 3,143 'glacier units' (Andreassen & Elvehøy, 2021; Kjøllmoen, 2011) with approximately 2,534 'contiguous glaciers' (Winsvold et al., 2014). A 'contiguous glacier' refers to a physically connected ice mass that may be comprised of multiple glacier units, each functioning dynamically as a separate entity. An ice cap, often referred to as a plateau glacier, is a dome-shaped ice body that covers the underlying topography with a radial flow (Andreassen & Winsvold, 2012). For context: Jostedalsbreen is the largest ice cap in Norway, covering 487 km² and is the largest continuous ice mass in continental Europe. It is divided into 61 individual glacier units (Ostrem & Haakensen, 1993).

The glaciers in Norway are concentrated in two main areas (Ostrem & Haakensen, 1993): (1) Southern Norway's mountain ranges, housing dominating ice caps like Jostedalsbreen and Folgefonna; and (2) Northern Norway, particularly Nordland County, which is the narrowest part of Norway between 66° and 68°N (Fig. 2). While the initial focus of NVE was on the southern glaciers (six of which have records since 1963), measurements on northern glaciers began in 1989 on an east-facing maritime ice cap Langfjordjøkelen (Andreassen, Nordli, et al., 2012). They constitute a west - east profile extending from the maritime Ålfotbreen to the continental Gråsubreen (Winsvold et al., 2014). The critical mountain height above which glaciers can form is known as the glaciation level (Andreassen & Winsvold, 2012). Glaciers below this do not retain enough snow to sustain glaciation. The ELAs (Equilibrium Line Altitude) in southern Norway ranges from 1,200 m a.s.l. on the western coast to 2,200 m a.s.l. in east in Jotunheimen (Ostrem & Haakensen, 1993).

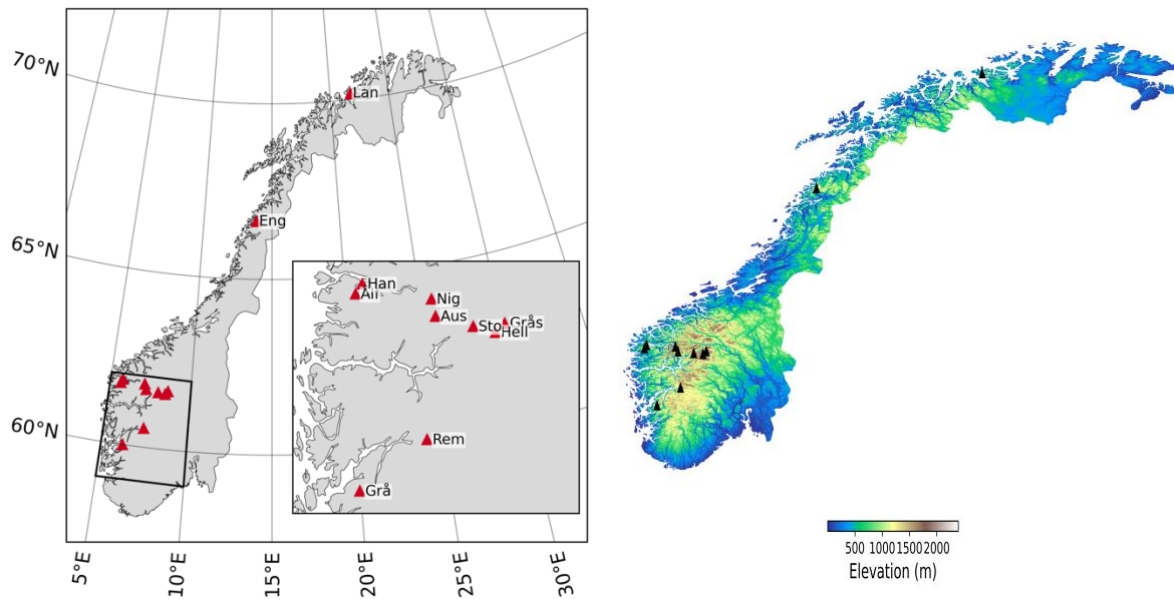


Fig 2: (a) Location of glaciers included in this study (Inset shows glacier locations in the Southern cluster): Alf- Ålfotbreen, Aus- Austdalsbreen, Eng- Engabreen, Grå- Gråsubreen, Grå-Gråfjellsbreen, Han- Hansebreen, Hell- Hellstugubreen, Lan- Langfjordjøkelen, Nig- Nigardsbreen, Rem-Rembesdalskåka, Sto- Storbreen, and; (b) Topographic setting of Norway with an overview of glacier locations.

Corresponding ELAs range from 1,160 m a.s.l. at Ålfotbreen in the west to 2,130 m a.s.l. at Gråsubreen in the east, and from 870 m a.s.l. at Langfjordjøkelen to 1,340 m a.s.l. at Okstindbreen in the north (Andreassen et al., 2005a). These spatial patterns reflect the transition from maritime to continental conditions (Østrem & Haakensen, 1973), with ELAs increasing inland due to drier conditions and decreasing northward due to latitude driven climate conditions (Winsvold et al., 2014).

The heterogeneity in glaciation levels is tied to both glacier type (e.g. cirque, valley, ice-cap) and climate setting (maritime vs continental), and is influenced by temperature, precipitation, and debris cover (Kraaijenbrink et al., 2017; Yao et al., 2012). These factors also affect glacier retreat and mass balance sensitivity to climate change (Han et al., 2023). Maritime glaciers, exposed to heavier precipitation and warmer conditions, are typically more sensitive to climate change than their continental counterparts (O’Neil et al., 2014; Xu et al., 2012). Because of their limited size and faster reaction times, mountain glaciers respond more quickly to climatic fluctuations than polar glaciers, making them reliable indicators of climate variability (Bach et al., 2018). Their retreat impacts hydrology, ecosystems, hydropower generation, geohazard risks, tourism, etc. (Nesje, 2023).

1.4. Climatic setting of Norway

Mainland Norway has a complex climate setting due to its large geographical extent, stretching from 58° to 71°N and 5° to 31°E, and a wide range of physical factors influencing it (Fig. 2a). According to the Köppen classification, Norway spans five climate zones, straddling both temperate and polar climate zones. This is due to its location on the western edge of the Scandinavian Peninsula and proximity to the North Atlantic Current (Beylich, 2021). We can observe the strong influence of the westerlies along Norway's long coastline (~1,700 km), leading to a coupling with North Atlantic climate systems (Ketzler et al., 2021).

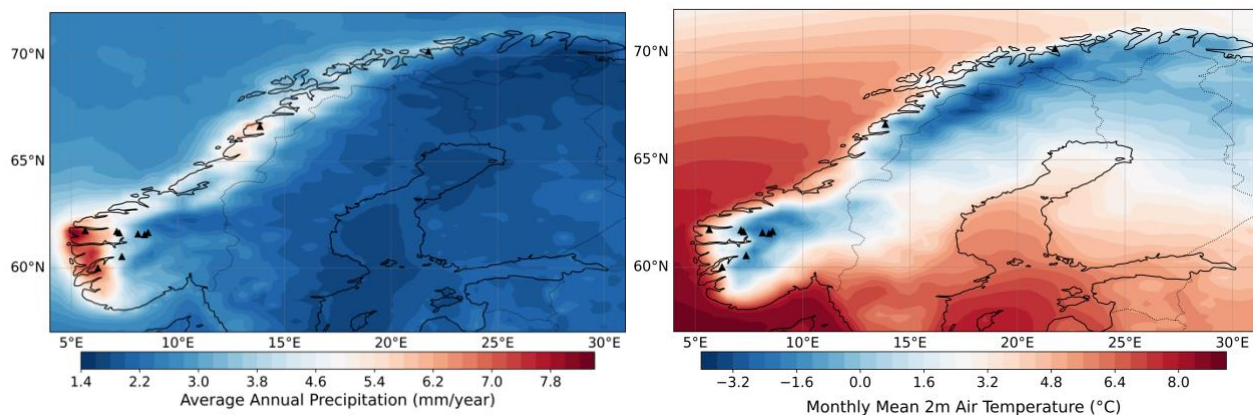


Fig 3: (a) Average annual precipitation (mm yr⁻¹) for the period 1950–2023, showing a distinct zone of high precipitation along the coastal region. (b) Monthly mean temperature above surface (°C), where the spatial pattern reflects topography, with higher temperatures in lower-elevation coastal areas and cooler conditions in high-elevation inland regions. (Data source: ECMWF ERA5 Reanalysis data)

This leads to more advection of moist maritime air masses with significant regional and local climate variability. The coastal lowlands of southwest Norway have a temperate climate, where moist air from the Atlantic is lifted by westerly winds over the mountainous areas (reaching up to 2,469 m a.s.l; Fig. 2b). This leads to high annual precipitation in the coastal regions, with values exceeding 2,500 mm/a (Fig. 3a). This annual precipitation pattern persists throughout the year, as also confirmed by Ketzler et al. (2021). A clear maritime (coast) to continental (inland) gradient exists as well as a north to south gradient with southern regions generally receiving more precipitation (Fig. 3a) due to higher temperatures and stronger westerly winds. In contrast, Eastern Norway is drier, while the elevated mountain plateaus, especially in Northern Norway, display subarctic features, including permafrost. Norway's temperature regime is affected by the North Atlantic Current (also known as the Norwegian Current), which

transports warm oceanic water northward. This thermal influence leads to relatively mild winters and moderate summers along the coast (Seppälä, 2005). During winter, when sea surface temperatures exceed those of the overlying air, increased evaporation produces humid air masses that are advected inland by the prevailing westerlies. In spring and summer, this effect reverses, as warmer air flows over cooler ocean surfaces and loses heat, further stabilizing coastal temperatures. As a result, coastal areas exhibit a narrow annual temperature range, while inland regions display stronger seasonal contrasts due to reduced maritime influence (Ketzler et al., 2021). Temperature gradients become increasingly continental from west to east and from coastal lowlands to the elevated interior (Fig. 3b).

The North Atlantic eddy-driven jet stream governs the atmospheric circulation in the Euro-Atlantic sector (Mellado-Cano et al., 2019), amongst which the North Atlantic Oscillation (NAO) is the dominant mode of wintertime variability in the region (Pinto & Raible, 2012). With the exception of the summer season (July-August; (Folland et al., 2009)), it is defined by a characteristic meridional pressure dipole between the Azores High and Icelandic Low (Hurrell, 1995) (Fig. A1). Positive NAO phases enhance westerly airflow, leading to warm and wet conditions in central and northern Europe as well as precipitation deficits in southern Europe, while the opposite pattern is observed during negative phases (e.g., Trigo et al., 2002). However, the NAO's influence is non-stationary and can vary over time due to shifts in the position and strength of these pressure systems (Vicente-Serrano & López-Moreno, 2008).

Some of the limitations to characterize the European climate variability can be partially overcome by complementing the NAO with other patterns of variability. The second pattern of climate variability in the region is the East Atlantic (EA) pattern (Barnston & Livezey, 1987). It is a dipole in the pressure field whose centers of variability are shifted southeastwards and more zonally oriented as compared to those of the NAO (Fig. A3). However, recent works characterize it as a well-defined sea level pressure (SLP) monopole south of Iceland and west of Ireland (Comas-Bru & Hernández, 2018). The variability of the North Atlantic eddy-driven jet stream can be largely described using a combination of NAO and EA (Mellado-Cano et al., 2019). Fluctuations in the strength of these meridional pressure gradients control the westerly winds. The response of these climate streams to climate change will strongly decide the state of future regimes (Peings et al., 2018).

1.5. Glacier Mass Balance Regime

The term ‘glacier regime’ has been defined as a summary of several factors, namely: seasonal and annual mass balances (b), which are directly related to volume change, mass turnover (α), equilibrium-line altitude (ELA), and accumulation-area ratio (AAR) (M. Dyurgerov, 2003). This thesis focuses on the mass balance components in this study. The variation in mass input and output corresponds to changes in the volume of a glacier (Dyurgerov & Meier, 2000). Accumulation refers to the process of mass gain and it generally corresponds to the winter season. It is primarily determined by atmospheric precipitation (snowfall). Ablation on the other hand is the loss of mass and corresponds to the summer season. It is governed by melting and evaporation processes (Dyurgerov & Meier, 2000). Mass balance measurements comprise of accumulated snow (winter balance, b_w) and measurements of snow and ice removed by ablation (summer balance, b_s) (Andreassen et al., 2005b; Andreassen & Winsvold, 2012). This thesis focuses mainly on the interannual variation of the mass balance. The b_a (net balance) is the sum of these two components:

$$b_a = b_w + b_s \quad \dots(1)$$

where b_s is negative. If the b_w is greater than the b_s , the b_a is positive and the glacier increases in volume. Alternatively, if the melting of snow and ice during the summer is larger than the b_w , the b_a is negative and the ice volume decreases.

The mass balance calculation and measurement methods have remained constant over the years (Andreassen & Elvehøy, 2021; Kjøllmoen, 2011; Østrem & Stanley, 1966). The maximum balance value during one balance year is the winter balance. The time when this maximum value is reached (i.e., the end of the accumulation period) divides the year into a winter season and a summer season (Østrem & Brugman, 1991). While Dyurgerov (2003) used the term regime to reflect the covariance amongst atmospheric variables and the state and behaviour of a glacier, this thesis refers to ‘regime’ as a state of conditions of the glacier, influenced by the atmospheric variables, mass balance, and their interactions (Winkler et al., 2010).

1.6. Impact of Climate Change

The contemporary theory of anthropogenic climate change has been well documented along with the steady increase of greenhouse gas emissions (GHG) since industrialization (Calvin et

al., 2023). This has had widespread impacts on human and natural systems, e.g. atmospheric and ocean warming, decreasing snow and ice cover, and sea level rise. Modelled scenarios and pathways are used to predict future emissions, climate change impacts and risks. The five Shared Socio-economic Pathways (SSP1 to SSP5) are designed to span a range of challenges to climate change mitigation and adaptation (Calvin et al., 2023). The assessed best estimates, along with the very likely ranges of warming for 2081-2100 relative to 1850-1900 is an increase by +1.4 °C (1.0 to 1.8 °C) in the very low GHG emissions scenario (SSP1-1.9). In the intermediate scenario (SSP2-4.5), emissions remain near present-day levels until mid-century, with warming of about +2.7 °C (2.1 to 3.5 °C). They are expected to roughly double from current levels by, 4.4 °C (3.3 to 5.7 °C) in the very high GHG emissions scenario (SSP5-8.5). This projected increase in temperature poses a significant threat to glaciers worldwide, accelerating mass loss and altering their seasonal accumulation-melt dynamics. Such changes have cascading impacts on sea level, freshwater availability, and downstream ecosystems, as discussed in the following section.

1.7. Impact of Glacier Loss

Global warming stresses the importance of sustainable alternative energy sources, such as hydropower which is threatened by the potential disappearance of glaciers (S. Mutz et al., 2016). Glacier area in mainland Norway has decreased by 326 km² corresponding to a 11 % decrease in glacier inventories conducted between 1950s-2000s (Winsvold et al., 2014). This decrease is more apparent in western Norway than in eastern parts, while northern glaciers have retreated more than southern ones (Andreassen & Oerlemans, 2009; Andreassen & Winsvold, 2012; Winsvold et al., 2014). Some effects of glacier loss are:

- Global glacier retreat has contributed 27 ± 22 mm to global mean sea-level rise between 1961 to 2016. Glaciers in Scandinavia contributed to sea level rise by $+0.47 \pm 0.23$ m w.e. (Zemp et al., 2019). Present mass-loss rates indicate that glaciers will continue to contribute to sea-level rise beyond 2100 (Zemp et al., 2019).
- The effect of the retreat of glaciers is readily observed on river runoff. Most of the water discharge in glacier catchments (up to ~80%) is due to summer melting (Nesje & Bakke, 2007). The melting maintains high discharge in dry and warm summers as well. Nesje & Bakke (2007) reported severe consequences for river run-off, water temperature and sediment transport due to predicted reduction in glacier dimensions.

- Constant summer melting may lead to the annual run-off equaling the annual precipitation resulting in the destabilization of ice or glacio-fluvially dammed water bodies triggering sudden outburst floods (*jökulhlaups*) as observed at Søndre Folgefonna in 2002 and at Flatbreen in Fjærland in 2004 (Nesje & Bakke, 2007).
- Glacier meltwater can act as a source of anthropogenic contaminants like POPs, black carbon, and trace elements (Daly & Wania, 2005; Gabrielli et al., 2008; Hodson, 2014). These substances can be released during glacier retreat and ablation periods (Bizzotto et al., 2009; Bogdal et al., 2009). Elevated concentrations of pesticides have been observed in glacier-fed streams compared to non-glacial ones (Villa et al., 2006), posing risks to aquatic ecosystems due to their bioavailability in low-organic-matter environments (Slemmons et al., 2013).
- Norway's present-day ice caps are highly vulnerable to surface mass balance changes due to their distinct hypsometry (Åkesson et al., 2016). In recent years, glaciers across Norway have undergone significant transformations, with pronounced retreat of glacier termini. For instance, Bødalsbreen has retreated significantly in recent years, leading to the termination of glacier measurements in 2015. The terminus had retreated beyond the steep cliffs and is now considered dangerous to approach the glacier due the danger of rockfalls (Andreassen, Elvehøy, et al., 2020).

1.8. Modelling approaches

Various types of models exist that are used to study glaciers, with a wide range of complexity and application. Over the past few decades, numerous models have been developed, with a wide scope and approaches. Energy-balance models adopt a physically based framework, calculating melt by quantifying the energy fluxes to and from the glacier surface. In contrast, temperature-index models also known as degree-day models, use an empirical relationship between air temperature and melt, based on the well-established correlation often observed between these variables (Hock, 2005).

1.9. Aims of this study

The primary aim of this thesis is to investigate and explain regime shifts in the climatic controls on Norwegian glaciers. The secondary aim is to develop empirical statistical models for all the mass balance components, identify any underlying patterns and then evaluate model performance.

The main workflow of this thesis is:

Part A: Identifying the Regime Shift:

- Assess correlations between glacier mass balance components and key climate variables.
- Compare glacier-climate relationships before and after 2000 to detect potential regime shifts.

Part B: Statistical Downscaling & Model Development:

- Develop and train empirical-statistical models using multiple machine learning (ML) techniques.
- Assimilate performance of models trained on six regressors and 3 selector techniques.
- Evaluate model performances using standard metrics (R^2 and RMSE).

2. Methodology

This section outlines the complete methodological framework of my study, covering data collection and predictor processing (2.1), atmospheric teleconnections reconstruction via Empirical Orthogonal Functions (2.2), correlation analysis (2.3), and empirical statistical model development (2.4). The workflow integrates observational datasets with machine learning based empirical modelling to identify and evaluate past climatic controls on glacier mass balance.

2.1. Data Sources & Selection

The mass balance data (predictand) was sourced from NVE: Norwegian Water Resources and Energy Directorate (Norwegian: Norges vassdrags- og energidirektorat). They have collected and maintained data pertaining to glacier regimes since 1949. Eleven glaciers were selected for this study in such a manner that they possessed at least 20 years of data to make any result obtained statistically viable. The eleven glaciers chosen are: Ålfotbreen, Austdalsbreen, Engabreen, Gråfjellsbrea, Grasubreen, Hansebreen, Hellstugubreen, Langfjordjøkelen, Nigardsbreen, Rembesdalskåka, and Storbreen. The mass balance record for each of these glaciers varies in coverage but generally spans from 1950s to 2022. The mass balance data has 3 components as mentioned in section 1.5. The accumulation months (b_w) correspond to December to February inclusive (DJF) while the ablation months (b_s) are May to September inclusive (MJJAS). While many studies define the accumulation period as October-April or December-February, most researchers tend to adopt the DJF period, as it yields a stronger statistical relationship. Andreassen et al. (2020) reported stronger correlations between the NAO and Arctic Oscillation (AO) and mass balances for nearly all glaciers when using the shorter DJF period. The mean value of mass balance components for a single glacier are expressed in the units m w.e. which are metres of water equivalent.

The climate variables (predictor) used in this study are obtained from the ERA5 monthly reanalysis dataset, produced by the European Centre for Medium-Range Weather Forecasts (ECMWF). ERA5 provides a globally gridded reanalysis of the atmosphere by including a wide range of historical observations into a numerical weather prediction model. The dataset is structured on a regular latitude-longitude grid, with a horizontal resolution of $0.25^\circ \times 0.25^\circ$ for atmospheric variables, corresponding to 31 km grid spacing (Hersbach et al., 2020). It is available for years 1950 to 2023. The predictors were chosen based on their physical relevance

to the glacier mass balance regime: 2 m air temperature (t2m), precipitation (tp), 10 m wind components (u10, v10), surface solar radiation downwelling (ssrd), and mean sea level pressure (msl). The msl field is used to construct and extract teleconnection indices like the NAO, EA, and the AO indices.

2.2. Empirical Orthogonal Function Analysis

To construct the teleconnection indices mentioned in section 2.1, the statistical technique of Principal Component Analysis (PCA) was employed. PCA otherwise also referred to as Empirical Orthogonal Functions (EOF) in atmospheric and oceanographic sciences, is one of the most popular multivariate statistical tools used for identifying dominant modes of variability (Wilks, 2011). It was first used by (Obukhov, 1947) and popularized by (Lorenz, 1956) and then (Davis, 1976) to reconstruct teleconnection indices from pressure field patterns. Its purpose is to reduce the dimensionality of a dataset, by decomposing a spatio-temporal field (like msl) into two components: (1) orthogonal spatial patterns also called loadings, eigenvectors or EOFs; and (2) temporally uncorrelated time components called principle components or scores (Lingis & Michaelides, 2009). The first PC is the linear combination of the original variables that explains the largest possible amount of variance, corresponding to the largest eigenvalue. The second PC captures the next largest fraction of variance, while remaining orthogonal (uncorrelated) with the first, and so on. This process continues for higher-order components, sequentially explaining decreasing amounts of variance along orthogonal directions (Jolliffe, 2011; Wilks, 2011). While conducting EOF analysis on gridded datasets (like ERA5), spatial weighting may be necessary to compensate for unequal distribution of grid points in the data matrix (Baldwin, 2008). This accounts for the convergence of meridians at higher latitudes and ensures that the resulting EOF modes are from grid-related biases.

Graphically, PCA can be visualized as fitting an ellipse (in 2D) or an ellipsoid (in 3D) to the data points (Jolliffe, 2002). The PC1 corresponds to the axis of the ellipse or ellipsoid that captures the maximum variance, it is the direction along which the data are most spread out. Mathematically, PC1 is the major axis, that passes through the multidimensional mean of the dataset and minimizes the sum of squared perpendicular distances from the data points to the line (Jolliffe, 2002). The PC2 is orthogonal to PC1 and usually corresponds to the minor axis (Fig. 4).

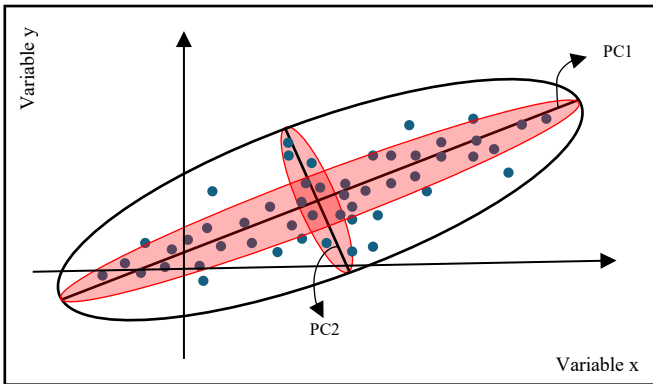


Fig 4: 2D illustration of PCA. PC1 captures the maximum variance (major axis), while PC2 is orthogonal and represents the second-largest variance (minor axis).

The NAO can be reconstructed either from station-based pressure differences (as mentioned in section 1.4) or via EOF analysis of gridded SLP data. Although these methods produce minor differences, the resulting signals generally match well. Two PCA analyses were performed: one for the North Atlantic sector, referred to as PCA-NA, and another for the entire Northern Hemisphere Atlantic region, referred to as PCA-ANA. To compensate for converging meridians on a latitude-longitude grid, each grid point was weighted by the formula $\sqrt{\cos(\Phi)}$, where Φ is the latitude (NCAR, 2013). After performing PCA-NA, the resulting PC1-NA and PC2 -NA time series were standardized to remove scale differences and ensure comparability. For PCA-NA, the standardized PCs were then aggregated into seasonal means to derive indices corresponding to the NAO and EA. This was achieved by reshaping the monthly series into seasonal matrices, where each row represents a complete season comprising three consecutive months, followed by averaging across the rows to compute seasonal indices. For DJF, December values were assigned to the following year to preserve correct winter season continuity. On the other hand, the PC1 from PCA-ANA was used to compute the Arctic Oscillation (AO) index (Fig. A4), following the same standardization and seasonal aggregation procedure.

To confirm the consistency of the two methods of computing NAO, the NAO index derived from PCA-NA was compared with the Hurrell station-based NAO index, obtained from the NCAR Climate Data Guide (Hurrell, 1995). The comparison of the two time series revealed a high degree of similarity (Fig. A5). A strong Pearson correlation ($r = 0.76$) confirms that the EOF-derived NAO index captures the same large-scale atmospheric variability as the established station-based index (Fig. A6).

2.3. Correlation Analysis

The remaining climate variable's data (section 2.1) was extracted from the gridded ERA5 data and processed before it was ready to be utilized. The temperature data was converted to celsius from kelvin and the precipitation data was converted from meters to millimeters to ensure consistency. The most important step was to subset data for all climate variables to focus on the Norwegian mainland region which covers latitudes 57°N to 72°N and longitudes 4°E to 31°E. Temporal averages were computed as long-term means for each grid cell giving us climatology maps (Fig. 3), while spatial averages were calculated as regional means over Norway for each time step leading to monthly time series. The dataset was further divided into pre-2000 and post-2000 periods and aggregated over DJF representing the accumulation season and MJJAS representing the ablation season. December values were assigned to the following year to ensure correct winter season alignment. Following the processing of data, the climate variables were correlated with the mass balance components for the 11 selected glaciers. Given the geographic differences in climatic forcing (Section 1.3), the Northern glaciers (Fig. 2) were correlated with the AO, while the Southern glaciers were correlated with the NAO and EA.

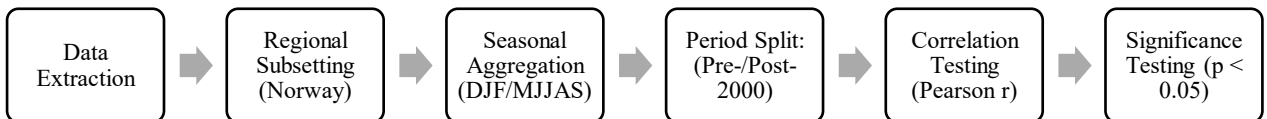


Fig 5: Schematic summary of the steps undertaken for the correlation analysis workflow.

The analysis used was the Pearson correlation coefficient (PCC) to quantify the strength of the statistical relationship between the mass balance components and the climate variables split over the two time periods (eq. 2). PCC evaluates the linear correlation between the model predictions y_i and observed data x_i . The PCC for n samples is defined as:

$$PCC(x, y) = \frac{\sum_{i=1}^n (x_i - \bar{x})(y_i - \bar{y})}{\sqrt{\sum_{i=1}^n (x_i - \bar{x})^2} \times \sqrt{\sum_{i=1}^n (y_i - \bar{y})^2}} \quad ... (2)$$

Where x and y are the means of the x_i and y_i values respectively. Correlations were computed only when at least 10 valid data points where available. Statistical significance was also assessed by only considering results with p-values less than 0.05. The results were visualized by generating heat-maps.

2.4. Model Development

Empirical statistical downscaling (ESD) is an umbrella term for methods that statistically relate local elements of the climate system (like temperature recorded at weather stations) to relevant synoptic to mesoscale atmospheric variability (Hewitson et al., 2014). It is computationally less expensive than dynamic downscaling and considers local factors like topography and micro-climatic controls (Mutz et al., 2021; Robertson et al., 2012).

The model development procedure in this thesis project follows the ‘perfect prognosis’ (PP) approach for the ESD routine. The PP-ESD approach has many advantages, the key one being that it is RCM- and GCM- agnostic. As opposed to its counterpart (Model Output Statistics), the PP-ESD models can be coupled to any RCM or GCM (S. G. Mutz et al., 2021). This is due to the usage of observational data (like ERA5) for predictors that allows seamless integration with RCM/GCMs to make predictions. The modelling routine in this thesis was carried out with the Python Empirical-Statistical Downscaling (pyESD) package. ‘pyESD’ adopts an object-oriented programming (OOP) style and treats the predictand data archives as objects with many functionalities and attributes relevant to ESD modeling (Boateng & Mutz, 2023). pyESD comprises a collection of utilities and methods for data preparation, predictor selection, data transformation, predictor construction, model selection and training, evaluation, statistical testing, and visualization (Boateng & Mutz, 2023).

The modelling pipeline employed in this thesis consists of 4 main steps (Fig. 6). They are (1) predictor selection, (2) model selection and training, (3) validation, followed by (4) model performance evaluation. The modeling routine involves the training and testing with a combination of 6 regressors (Ridge Regression with Cross Validation, Bagging, Automatic Relevance Determination, Random Forest, XGBoost, and Bayesian Ridge Regression) and 3 feature selectors (Recursive, Tree-Based, and Sequential). After this, the performance of all 18 combinations is evaluated using standard metrics like coefficient of determination (R^2) and the root mean squared error (RMSE), to assess prediction skill across all glaciers.

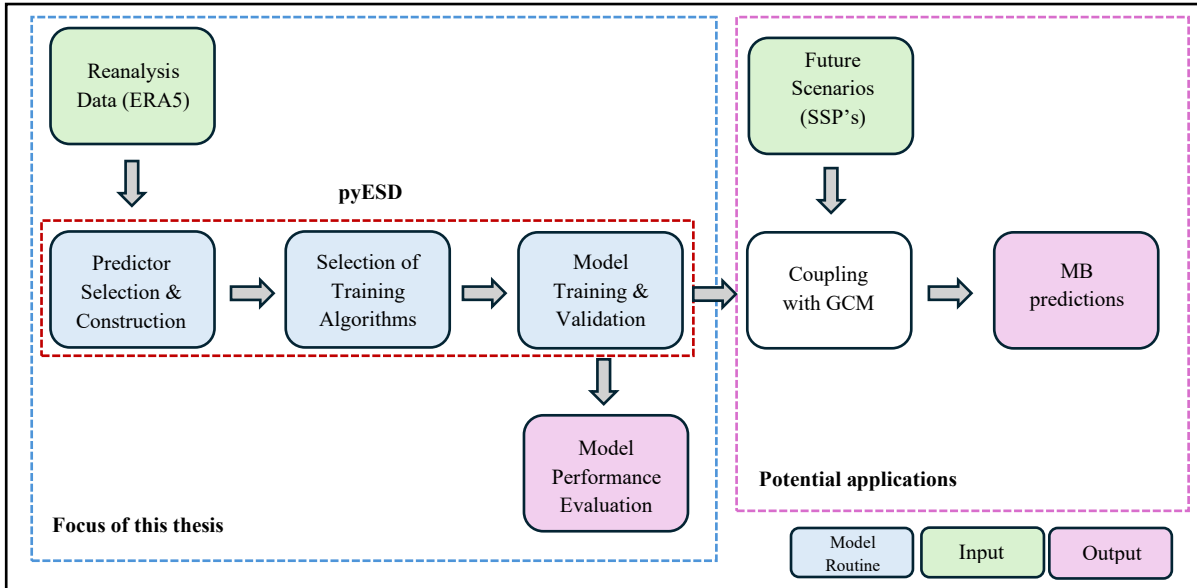


Fig 6: Schematic of the modelling routine. Predictors are constructed from ERA5 datasets to generate Empirical-statistical models & their metrics. The resulting model's performance for each mass balance component is evaluated using the defined metrics to identify any significant patterns. The best performing model(s), individually or in an ensemble, can be coupled with a GCM to make future predictions. Data Sources: Mass balance [NVE] & ERA5 Reanalysis [ECMWF]

The R^2 represents the fraction of the predictand's observed variance that can be explained by the predictors (eq. 3). It can be seen as a measure of how well the model predicts the unseen data (Wilks, 2011). Simply put, it is the ratio of sum of squared residuals (SSR) to the sum of squares (SST). The R^2 for the predicted values \hat{y}_i in relation to the observed data y_i for $i = 1, \dots, n$ samples, is defined as:

$$R^2(y, \hat{y}) = 1 - \frac{\sum_{i=1}^n (y_i - \hat{y}_i)^2}{\sum_{i=1}^n (y_i - \bar{y})^2} \quad \dots(3)$$

where \bar{y} is the mean of the observed data. R^2 can range from $-\infty$ to 1, where 1 is the best possible score and negative values are indicative of a worse model. The second metric used to evaluate is the root mean squared error (RMSE) that estimates the mean magnitude of error between the predictions and observations (eq. 4). RMSE is computed in the units of the values to be predicted. So, in this project, it has the same unit as mass balance which is m w.e. The RMSE for predictions \hat{y}_i and observations y_i of n samples, is calculated as:

$$\text{RMSE } (y, \hat{y}) = \sqrt{\frac{1}{n} \sum_{i=1}^n (\hat{y}_i - y_i)^2} \quad \dots(4)$$

This modeling pipeline allows for a comprehensive evaluation of statistical downscaling skill, by utilizing different regressors, feature selection techniques, and validation metrics, ensuring robust glacier mass balance predictions.

3. Results

This section focuses on the trends observed in the results obtained, aiming to validate the hypothesis of this thesis that revolves around the much speculated regime shift in 2000. The results of the analysis (described in section 2.3) are presented in a top-down manner, attempting to illustrate the existence of the regime shift through the trends observed in B_a (section 3.1), followed by supporting evidence from trends of the individual mass balance components (section 3.2 & 3.3).

3.1. Annual Mass Balance Trends

The cumulative annual mass balance for the glaciers for the period of 1960-2000 varied significantly (Fig. 7). Maritime glaciers gained a considerable amount of mass as evidenced by Figure 7. Ålfotbreen (+ 9 m w.e.), Nigardsbreen (+ 17 m w.e.), Rembesdalskåka (+ 5 m w.e.) displayed significant positive balance (Fig. 7). A decline in the cumulative B_a for all 11 glaciers is observed post-2000.

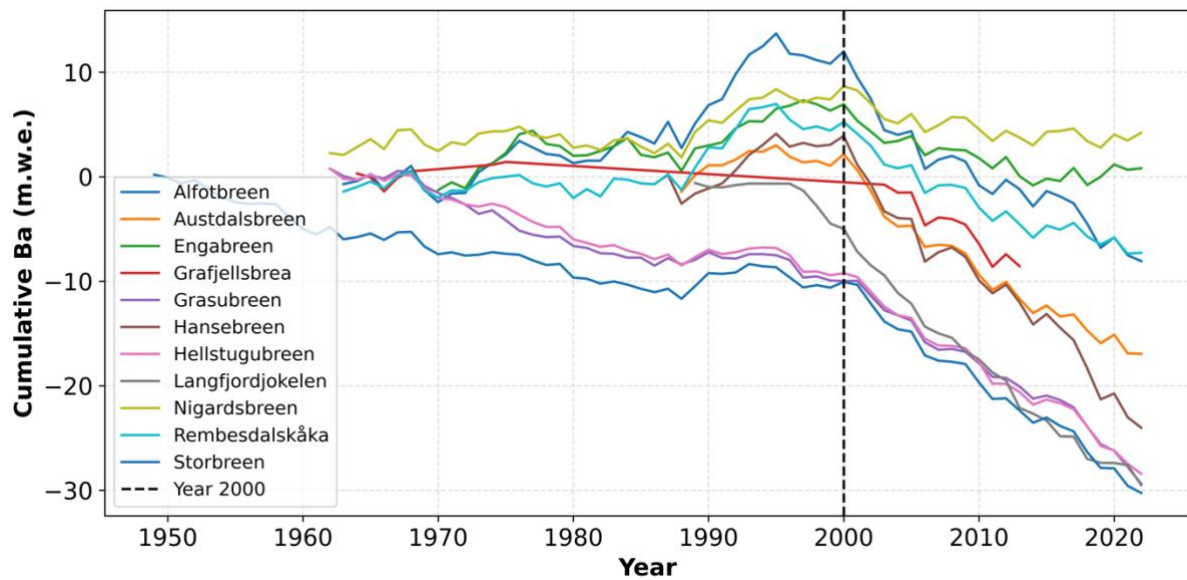


Fig 7: Cumulative B_a (m w.e.) for 11 Norwegian glaciers from 1950 to 2020. The dashed vertical line at the year 2000 indicates a marked acceleration in cumulative mass loss for most glaciers after 2000. This shows a transition toward increasingly negative mass balance regimes for all 11 glaciers in the 21st century.

Pre-2000, B_a is mainly governed by P_{acc} and NAO (Fig. 8). High correlation values for the continental glaciers with NAO (E.g.: Alf: 0.56, Aus: 0.67, Rem: 0.54) are seen. Additionally,

a high correlation with P_{acc} for 6 out of 11 glaciers (E.g.: Ålf: 0.66, Aus: 0.78, Nig: 0.66, Rem: 0.66) is observed. 4 out of 11 glaciers have a moderate-high correlation (E.g.: Ålf: 0.52, Aus: 0.74) with T_{acc} .

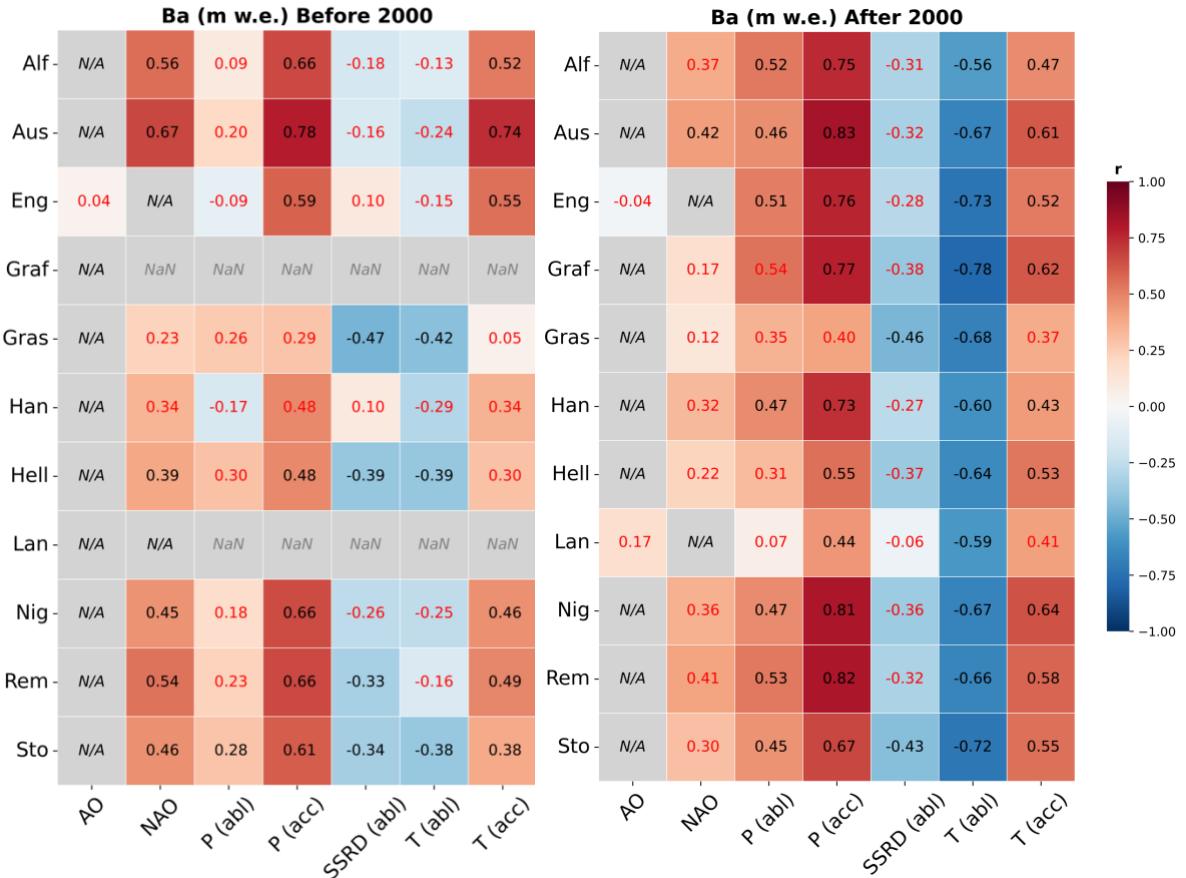


Fig 8: Correlation (r) heat-maps for B_a (m w.e.) with selected climate variables, for before and after 2000. Red r values denote statistically insignificant results ($p > 0.05$). Gray cells labelled 'NaN' represent cases with lack of sufficient data to compute a correlation, while 'N/A' denotes variables for which correlation was not applicable by design.

Post-2000, notable changes are evident in the trends. Correlation with NAO is statistically insignificant for 8 out of 9 glaciers. This insignificance isn't due to a lack of data, but simply due to a lack of a relationship. Other changes include a sharp increase in correlation with P_{acc} for 8 out of 11 glaciers, and an increase in correlation with P_{abl} for 7 out of 11 glaciers. All 11 glaciers show an increase in correlation (negative) for T_{abl} and correlation (positive) for 9 out of 11 glaciers with T_{acc} .

3.2. Winter Mass Balance Trends

A general trend of decreasing B_w is evident between 1990 and 2000 (Fig. 9). 8 out of 11 glaciers have a steeper loss: Ålfotbreen (5 to 3 m w.e.), Austdalsbreen (2.7 to 1.9 m w.e.), Engabreen (3.2 to 2.5 m w.e.), Hansebreen (4.2 to 3 m w.e.), Nigardsbreen (2.7 to 2 m w.e.), and Rembesdalskåka (3 to 1.9 m w.e.).

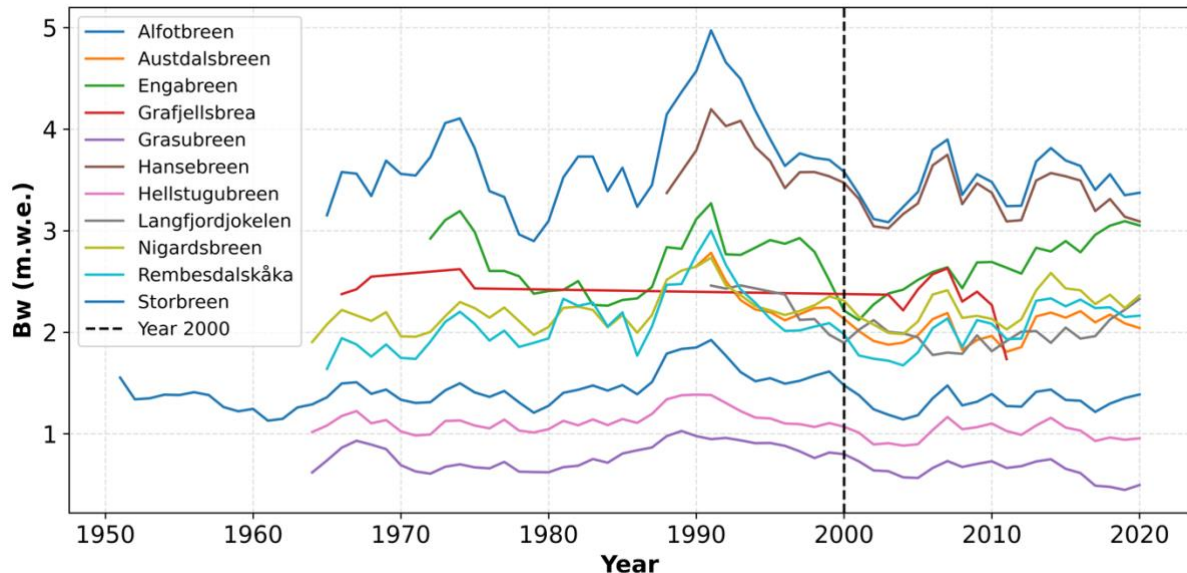


Fig 9: 5-year rolling mean of B_w (m w.e.) for 11 Norwegian glaciers from 1950 to 2020. The dashed vertical line at the year 2000 marks a transition period. While B_w remains relatively stable for many glaciers, some display a greater interannual variability post-2000.

Prior to 2000, the results show a moderate to strong correlation between winter mass balance and the NAO index, with values ranging from 0.4 to 0.7 across most glaciers. The consistently high correlation values with P_{acc} , ranging from 0.4 to 0.9, clearly indicate that P_{acc} is the primary driver of winter mass balance (Fig. 10). The northern glaciers Langfjordjøkelen and Engabreen do not have a statistically significant correlation with the AO index. Temperature and wind components, although important, do not show any consistent trends, while surface solar radiation (SSRD) shows no statistically significant relationship with winter mass balance.

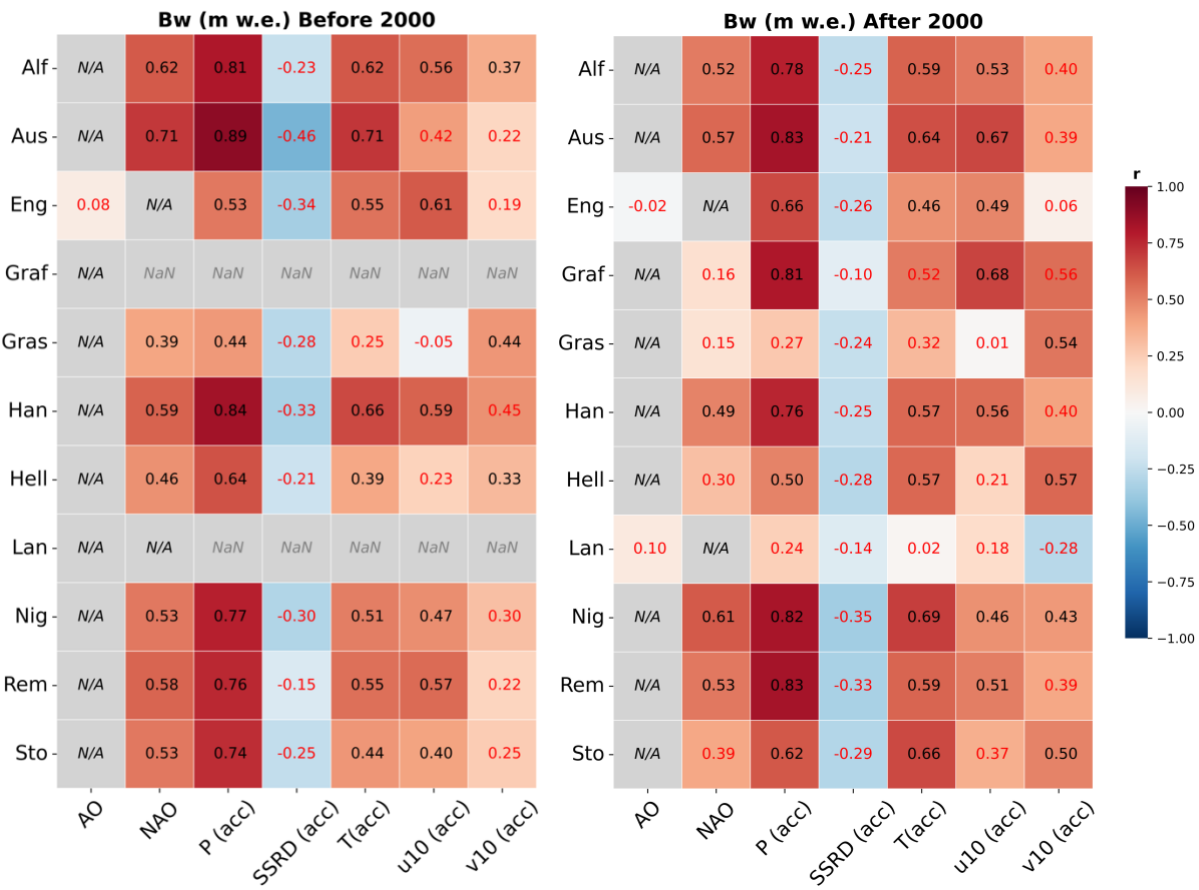


Fig 10: Correlation (r) heat-maps for B_w (m w.e.) with selected climate variables, for before and after 2000. Red r values denote statistically insignificant results ($p > 0.05$). Gray cells labelled ‘NaN’ represent cases with lack of sufficient data to compute a correlation, while ‘N/A’ denotes variables for which correlation was not applicable by design.

After 2000, the correlation with NAO remains positive, but the strength varies more widely across glaciers compared to the earlier period. The correlation weakens for 4 out of 9 glaciers and becomes insignificant for the other 5 (Fig. 10). P_{acc} persists as a dominant driver, with strong correlations observed across nearly all glaciers, typically ranging from 0.5 to 0.9. Notably, a few glaciers like Nigardsbreen (0.82), Austdalsbreen (0.83), and Rembesdalskåka (0.83) show high correlations with P_{acc} , reinforcing its continued importance in shaping winter mass balance post 2000 as well. T_{acc} shows a slight increase in its influence on 4 glaciers post-2000. Wind components continue to lack consistent patterns, and SSRD remains largely uncorrelated with winter mass balance in the post-2000 period.

3.3. Summer Mass Balance Trends

A sharper decline in summer mass balance B_s is evident for many glaciers after the year 2000 (Fig. 11). Glaciers such as Ålfotbreen and Hansebreen experience a decline beginning in the late 1990s. Notable reductions in B_s are observed for Ålfotbreen and Hansebreen (approx. -3 to -5 m w.e.), Langfjordjøkelen (-2.5 to -3.5 m w.e.), Austdalsbreen (-2 to -3.25 m w.e.), Grafjellsbreen and Hellstugubreen (-1 to -1.6 and -2 m w.e., respectively), and Storebreen, where B_s drops from around -1.6 to -2.5 m w.e. These trends highlight a shift in B_s trends after 2000.

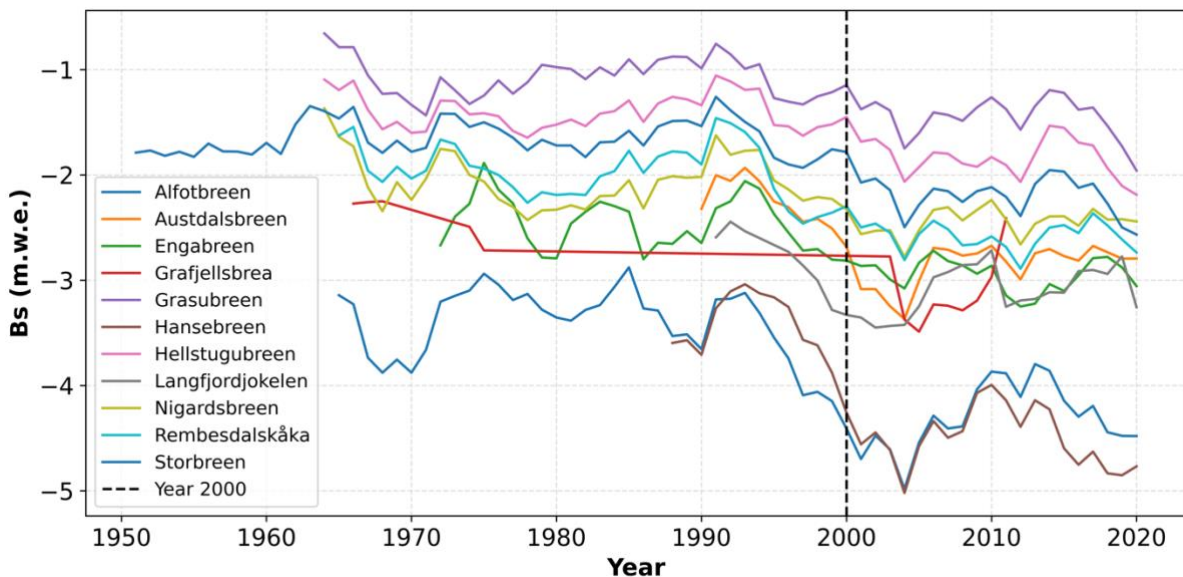


Fig 11: 5-year rolling mean of B_s (m w.e.) for 11 Norwegian glaciers from 1950 to 2020. The dashed vertical line marks the year 2000, indicative of a more pronounced negative trend in B_s for several glaciers.

The results from the correlation analysis of B_s reveal very interesting trends (Fig. 12). There was an absence of statistically significant relationships with P_{abl} for 7 out of 9 glaciers before 2000. The negative correlation strength is low to moderate with SSRD for 5 out of 9 glaciers with available data. This correlation ranges from -0.3 to -0.5. Similar trends are seen in the correlation with T_{abl} where there is a moderate negative correlation ranging from -0.4 to -0.7, which proves it to be a key driver of B_s .

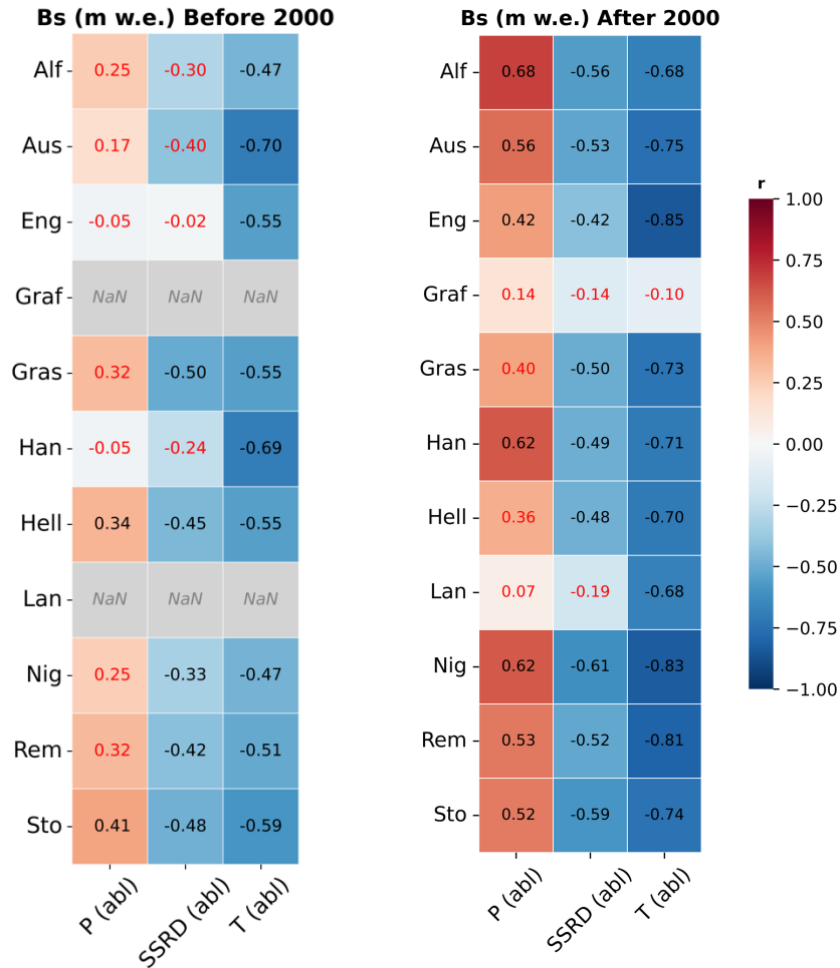


Fig 12: Correlation (r) heat-maps for B_s (m w.e.) with selected climate variables, for before and after 2000. Red r values in denote statistically insignificant results ($p > 0.05$). Gray cells labelled 'NaN' represent cases with lack of sufficient data to compute a correlation, while 'N/A' denotes variables for which correlation was not applicable by design.

Post 2000, the relationship of B_s with P_{abl} becomes statistically significant for 7 out of 11 glaciers, and the positive correlation increases for 7 out of 11 glaciers. Glaciers like Ålfotbreen (0.68), Hansebreen (0.62), Nigardsbreen (0.62) display a strong correlation. An increase in the strength of negative correlation with SSRD for 9 out of 11 glaciers is observed. T_{abl} values range from -0.68 to -0.85, indicating it to be an important driver of B_s post 2000 as well. The negative correlation strength increased for 10 out of 11 glaciers.

3.4. Mass Balance Control Trends

An analysis of the control of the individual mass balance components on determining the annual mass balance (B_a) pre- and post-2000 was carried out. Figure 13 is a heatmap of Pearson correlation between B_a and its seasonal components B_w and B_s , pre- and post-2000. For B_w (pre-2000), correlation values range from 0.53 (Gråsubreen) to 0.85 (Ålfotbreen). For B_w (post-2000), correlations remain high across all glaciers, ranging from 0.64 (Gråsubreen) to 0.87 (Austdalsbreen and Rembesdalskåka). Langfjordjøkelen has a notable decrease in correlation from 0.75 (pre-2000) to 0.40 (post-2000).

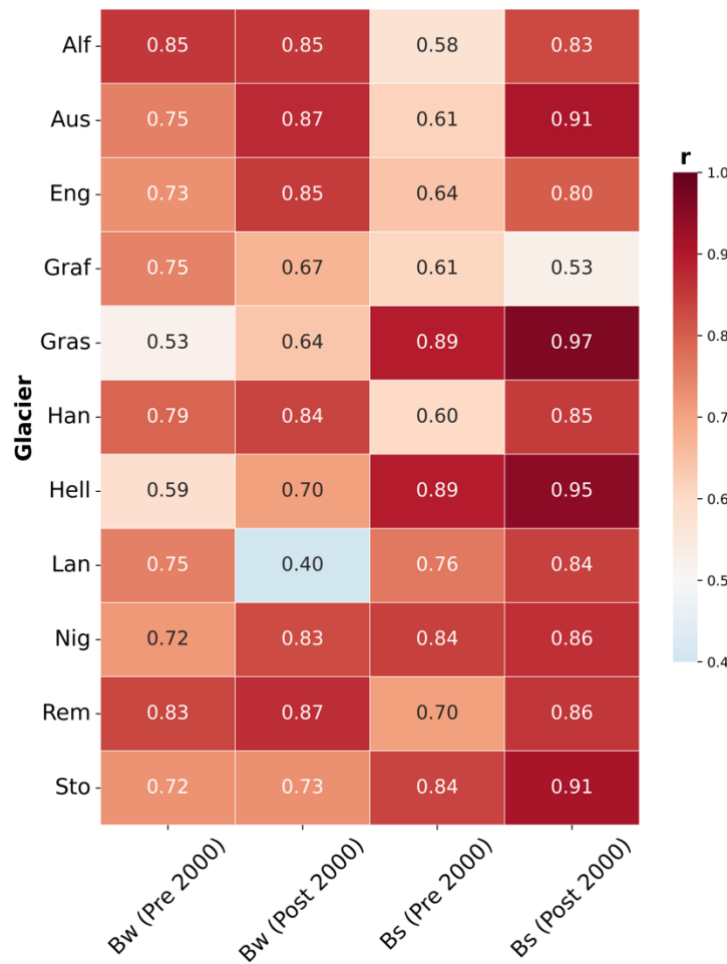


Fig 13: Heat-map displaying the Pearson correlation of B_a with B_w & B_s pre- & post-2000. Results show a clear shift in influence of B_s in determining B_a post 2000.

B_s (pre-2000) correlation values vary between 0.58 (Ålfotbreen) and 0.89 (Gråsubreen and Hellstugubreen). For B_s (post-2000), the highest correlations are observed, with values ranging from 0.80 (Engabreen) to 0.97 (Gråsubreen). Seven glaciers show post-2000 B_s correlations

exceeding 0.85, with four exceeding 0.90. However, a decrease in correlation is observed for Grafjellsbrea from 0.61 to 0.53. Overall, B_s (post-2000) displays the strongest correlations with annual mass balance across most glaciers.

9 out of 11 glaciers transitioned from a winter accumulation dominated (B_w) to a summer ablation dominated (B_s) control post-2000, indicating a shift (Fig. 14). Glaciers like Gråsubreen, Hellstugubreen, Storbrean, and Austdalsbreen display very high Pearson correlation values ($r>0.9$) post-2000 between $B_a \sim B_s$, while the other glaciers maintained a fairly strong $B_a \sim B_s$ correlation post-2000 ($r>0.8$). Ålfotbreen and Grafjellsbrea are the only glaciers that didn't display a shift to a summer dominated control (Fig. 14a).

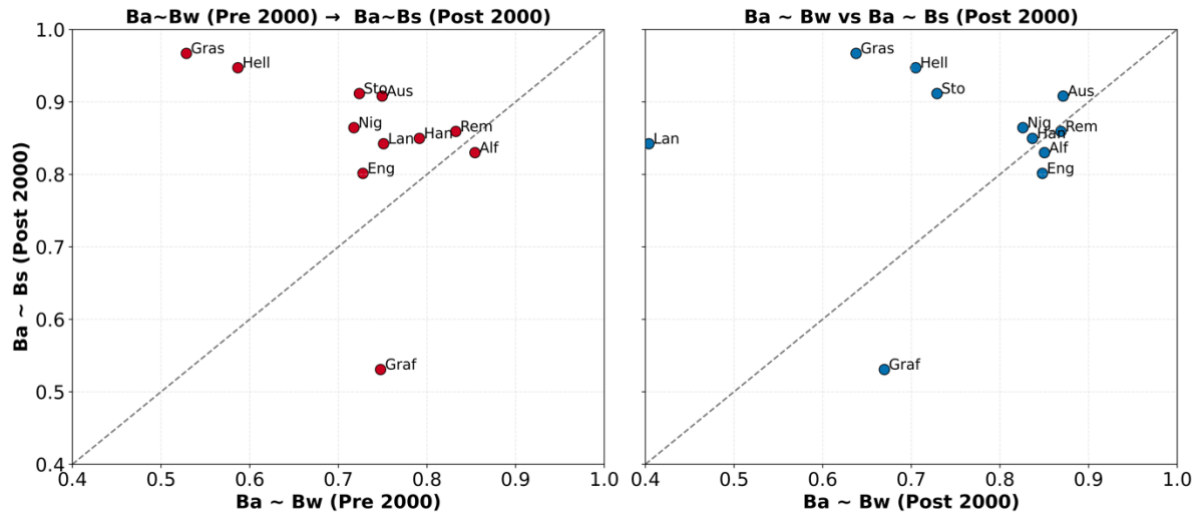


Fig 14: (a) Scatterplots displaying the Pearson correlation of B_a with B_w (pre-2000) & with B_s (post-2000). (b) Scatterplot displaying the correlation of B_a with B_s & B_s (post-2000). The plot outlines the seasonal shift in the mass balance control. A general shift from a B_w dominated mass balance regime to a B_s dominated regime is observed for 9 out of 11 glaciers post 2000. B_a of some glaciers continues to be controlled by B_w post-2000.

The second panel compares $B_a \sim B_w$ and $B_a \sim B_s$ for the post-2000 period (Fig. 14b). 7 glaciers lie above the 1:1 line, indicating a stronger correlation of B_a with B_s than with B_w (>0.8). This pattern is consistent, with Gråsubreen, Hellstugubreen, Storbrean, and Austdalsbreen showing the strongest correlation. The other 4 glaciers (Ålfotbreen, Engabreen, Grafjellsbrea, and Rembesdalskåka) remain below the 1:1 line indicating that they have a higher $B_a \sim B_w$ correlation post-2000.

3.5. Modelling Annual Mass Balance

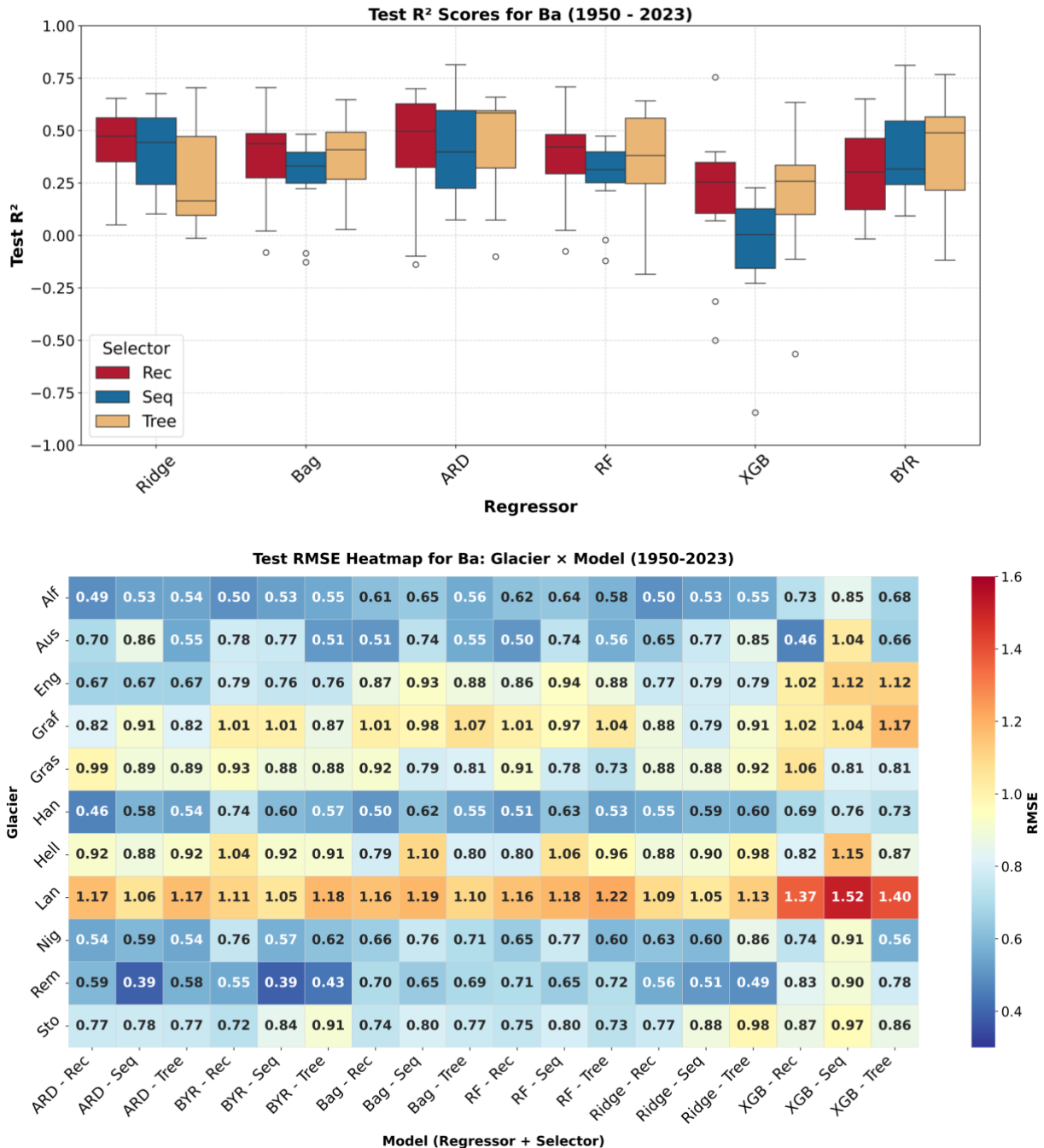


Fig 15: (a) Test performance metrics (R^2) boxplots for B_a (m w.e.) for 6 regressors (RidgeCV, Bagging, ARD, RandomForest, XGBoost, BayesianRidge) and 3 regressors (Recursive, Sequential, TreeBased). **(b)** Heat-map showing Test RMSE values for a combination of Regressor and selector for each glacier. ARD-Tree, Bag-Tree, and RF-Rec have the best performance across all 11 glaciers. correlation was not applicable by design.

The model development procedure (see section 2.4) involved the training and testing 6 regressors and 3 selectors, yielding performance metrics for 18 combinations, for each mass balance component. The results of the modelling routine for B_a for the period 1950-2023 are summarized in Figure 15. In the boxplot of test R^2 scores for each regressor-selector combination (Fig. 15a), values range from below 0.0 to above 0.8, indicating variation in model performance across the glaciers and combinations. Bayesian Ridge + Tree Based (BYR + Tree) and Automatic Relevance Determination + Recursive (ARD + Rec) yield the highest median R^2 scores across all selectors, 0.48 and 0.50 respectively. The Tree-based (Tree) selector consistently produces high median values compared to Recursive (Rec) and Sequential (Seq) selectors, particularly when paired with BYR, XGB, and Random Forest (RF). RF, Bagging (Bag), and ARD appear to have a good performance for B_a with compact boxplots and high median R^2 values.

The test RMSE values for B_a predictions across all glaciers for model combinations for the period 1950- 2023, range from 0.39 to 1.52, indicating high variation in model performance across glaciers and regressors (Fig. 15b). Glaciers like Alfotbreen, Austdalsbreen, Hansebreen, Nigardsbreen, and Rembesdalskåka show a good prediction skill (range of 0.39 ~ 0.8). Higher RMSE values are observed for Grafjellsbrea and Langfjordjøkelen (range of 0.8 ~ 1.52). The lowest RMSE is observed for Rembesdalskåka using the ARD + Tree and BYR + Seq (0.39), while the highest RMSE is found for Langfjordjøkelen with XGB + Seq (1.52). Glaciers like Ålfotbreen and Hansebreen performed well for all models, producing RMSE values below 0.75, reflecting a stronger predictive skill. In contrast, performance is more variable for glaciers like Grafjellsbrea and Hellstugubreen, where several models yield RMSEs ~1.0. Models using ARD, BYR, Bag, and RF regressors generally achieve lower RMSEs across most glaciers, when paired with the Tree-based and Recursive selector.

Table 1: Selected B_a model performance metrics.

| Glacier | Model Combination | Model Type | R² Score | RMSE |
|----------------|-----------------------------|-------------------|----------------------------|-------------|
| Ålfotbreen | Ridge CV + Recursive | Linear | 0.65 | 0.50 |
| | XGBoost + Recursive | Non-Linear | 0.25 | 0.73 |
| Austdalsbreen | Bagging + Recursive | Non-Linear | 0.70 | 0.51 |
| | Random Forest + Recursive | Non-Linear | 0.70 | 0.50 |
| Hansebreen | ARD + Recursive | Linear | 0.69 | 0.46 |
| | XGBoost + Tree Based | Non-Linear | 0.25 | 0.73 |
| Rembesdalskåka | ARD + Sequential | Linear | 0.81 | 0.39 |
| | Bayesian Ridge + Sequential | Linear | 0.81 | 0.39 |
| | Bayesian Ridge + Tree Based | Linear | 0.76 | 0.43 |
| | Random Forest + Recursive | Non-Linear | 0.37 | 0.71 |

3.6. Modelling Winter Mass Balance

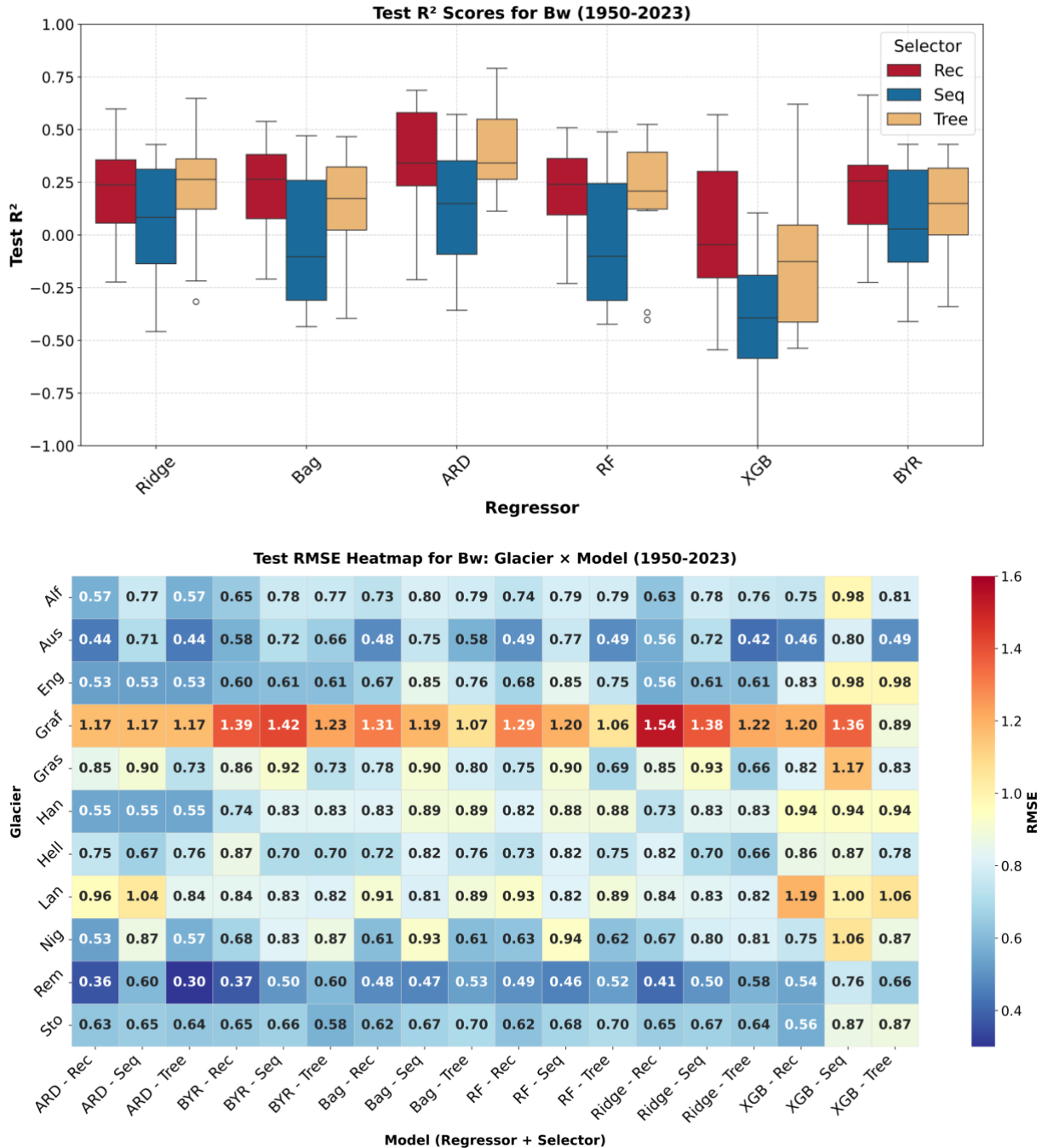


Fig 16: (a) Test performance metrics (R^2) boxplots for B_w (m w.e.) for 6 regressors (RidgeCV, Bagging, ARD, RandomForest, XGBoost, BayesianRidge) and 3 regressors (Recursive, Sequential, TreeBased). (b) Heat-map showing Test RMSE values for a combination of Regressor and selector for each glacier. ARD-Tree, Bag-Tree, and RF-Rec have the best performance across all 11 glaciers. correlation was not applicable by design.

R^2 values range from below -1 to 0.75, indicating a massive variation in model performance across the glaciers and combinations (Fig. 16a). BYR + Rec (0.25), RF + Rec (0.25), and ARD + Rec (0.30) yield the highest median R^2 scores. Recursive and Tree-based selector produce high median values compared to Sequential. RF, Bag, ARD, and BYR appear to have a good performance for B_w with compact boxplots and high median R^2 values.

The test RMSE values for B_w predictions across all glaciers for model combinations for the period 1950- 2023, range from 0.30 to 1.54, indicating high variation in model performance across glaciers and regressors (Fig. 16b). Glaciers like Alfotbreen, Austdalsbreen, Nigardsbreen, Rembesdalskåka, and Storbreen show a good prediction skill (range of 0.30 ~ 0.9). Higher RMSE values are observed for Grafjellsbrea (range of 0.8 ~ 1.54). The lowest RMSE is observed for Rembesdalskåka using the ARD + Tree (0.30), while the highest RMSE is found for Grafjellsbrea with RidgeCV (Ridge) + Rec (1.54). Glaciers like Austdalsbreen and Rembesdalskåka performed well for all models, producing RMSE values below 0.8, reflecting a stronger predictive skill. On the other hand, performance is more variable for glaciers like Grafjellsbrea and Langfjordjøkelen, where several models yield RMSEs ~1.0. Models using ARD, BYR, and Bag, regressors generally achieve lower RMSEs across most glaciers, when paired with the Tree-based and Recursive selector.

Table 2: Selected B_w model performance metrics.

| Glacier | Model Combination | Model Type | R^2 Score | RMSE |
|----------------|----------------------------|------------|-------------|------|
| Ålfotbreen | ARD + Recursive | Linear | 0.25 | 0.57 |
| | XGBoost + Recursive | Non-Linear | -0.28 | 0.75 |
| Austdalsbreen | Ridge CV + Tree Based | Linear | 0.65 | 0.42 |
| | Random Forest + Tree Based | Non-Linear | 0.51 | 0.49 |
| | Random Forest + Sequential | Non-Linear | -0.18 | 0.77 |
| Hansebreen | ARD + Recursive | Linear | 0.48 | 0.54 |
| | XGBoost + Tree Based | Non-Linear | -0.54 | 0.93 |
| Rembesdalskåka | ARD + Tree Based | Linear | 0.79 | 0.30 |
| | Bayesian Ridge + Recursive | Linear | 0.59 | 0.40 |
| | XGBoost + Recursive | Non-Linear | -0.39 | 0.76 |

3.7. Modelling Summer Mass Balance

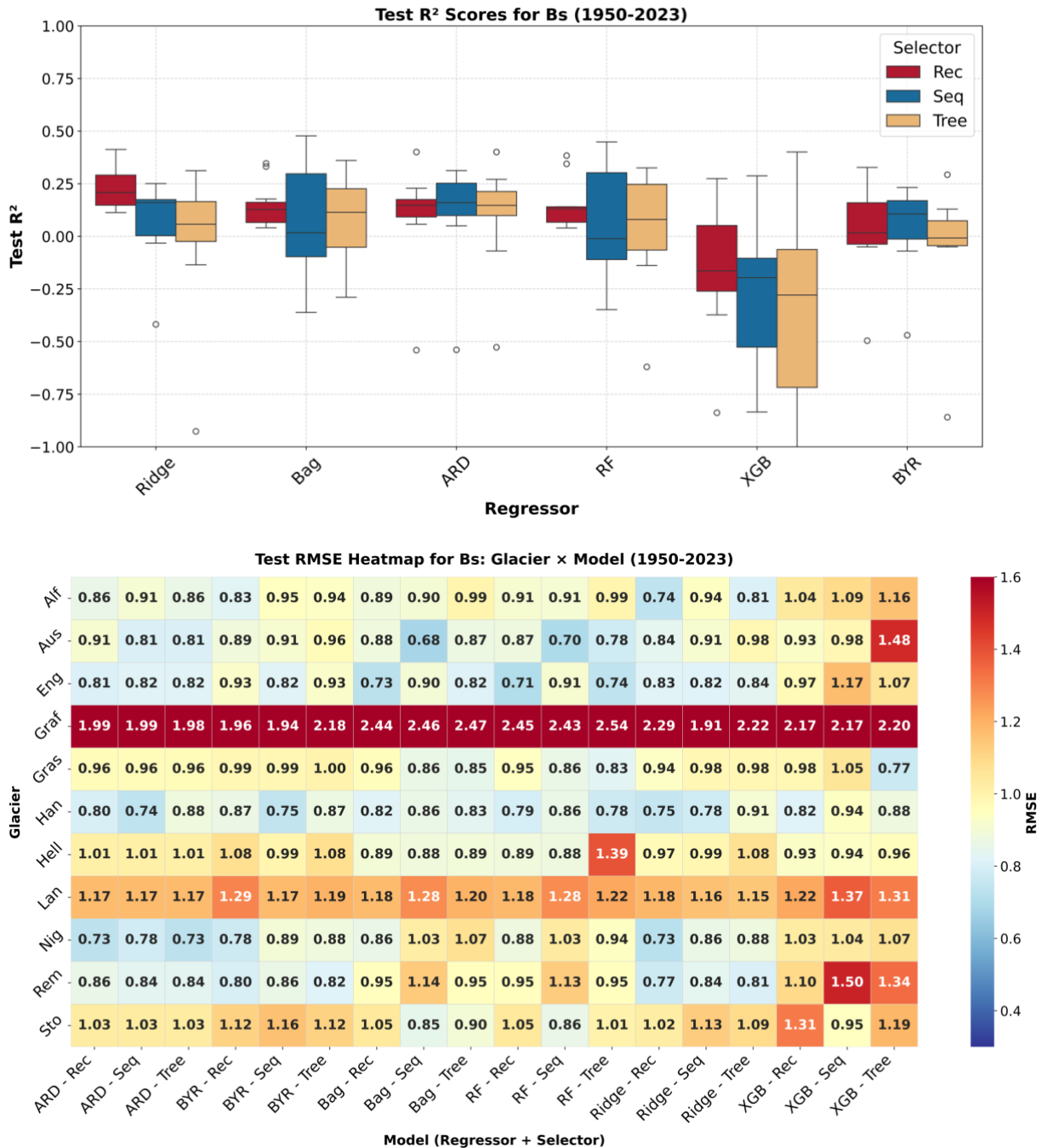


Fig 17: (a) Test performance metrics (R^2) for B_s (m w.e.) for 6 regressors (RidgeCV, Bagging, ARD, RandomForest, XGBoost, BayesianRidge) and 3 regressors (Recursive, Sequential, TreeBased). **(b)** Heat-map showing Test RMSE values for a combination of Regressor and selector for each glacier. B_s prediction displays low R^2 and high RMSE for all glaciers and models, proving to be difficult to estimate.

R^2 values from modelling B_s range from below -1 to 0.50, indicating a poorer performance with increased variation across the glaciers and combinations (Fig. 17a). Overall, ARD, BYR, Bag, and Ridge have acceptable performance for all three selectors, giving a more consistent R^2 output and median values. XGB underperforms with a wide inter-quartile range and increased variation. Ridge + Rec (0.20) yields the highest median R^2 scores. All three selectors have a similar performance for B_s prediction.

The Test RMSE values for B_s predictions across all glaciers for model combinations for the period 1950- 2023, range from 0.68 to 2.54, indicating very high variation in model performance across glaciers and regressors (Fig. 17b). Some glaciers like Engabreen and Hansebreen show a moderate prediction skill (range of 0.7 ~ 1). Very high RMSE values are observed for Grafjellsbrea (range of 0.9 ~ 2.54). The lowest RMSE is observed for Austdalsbreen using the Bag + Seq (0.68), while the highest RMSE is found for Grafjellsbrea with RF + Tree (2.54). Overall, we observe a high variation and high RMSE values for all glaciers and models. The performance is poor for Grafjellsbrea and Langfjordjøkelen, where all models yield RMSEs 1 ~ 2.5.

Table 3: Selected B_s model performance metrics

| Glacier | Model Combination | Model Type | R^2 Score | RMSE |
|----------------|----------------------------|------------|-------------|------|
| Ålfotbreen | Ridge CV + Recursive | Linear | 0.36 | 0.74 |
| | XGBoost + Recursive | Non-Linear | -0.25 | 1.04 |
| Austdalsbreen | ARD + Tree Based | Linear | 0.27 | 0.80 |
| | XGBoost + Recursive | Non-Linear | 0.02 | 0.93 |
| Hansebreen | ARD + Sequential | Linear | 0.25 | 0.74 |
| | XGBoost + Tree Based | Non-Linear | -0.07 | 0.87 |
| Rembesdalskåka | Ridge CV + Recursive | Linear | 0.37 | 0.77 |
| | Bayesian Ridge + Recursive | Linear | 0.32 | 0.80 |
| | XGBoost + Recursive | Non-Linear | -0.26 | 1.09 |

4. Discussion

The goal of this project is to investigate the potential regime shift in the climatic controls on Norway's glaciers in the year 2000. This section follows up on the discussion of the results gathered in the preceding section. This discussion and analysis of trends observed in the 11 glacier regimes will help accept or refuse the hypothesis.

4.1. Trends in Annual Mass Balance

A rapid decline can be observed in the B_a curves for all glaciers post-2000 (Fig. 7). The influence of atmospheric dynamics in driving glacier mass balance has been widely discussed (see sections 1.3 & 1.3). Norway's location at the edge of the Scandinavian peninsula combined with its complex topography, and the intricate coupling with the North Atlantic climate systems enhances the influence of some climate variables, such as precipitation, temperature, and NAO, on glacier regimes. The maritime-continental gradient in the glacier occurrence is also reflected in the correlation results (Fig. 8). For instance, pre-2000, B_a of Nigardsbreen (maritime) has a higher correlation with P_{acc} (0.66) and NAO (0.45), compared to the more continental Hellstugubreen which yielded a weaker correlation to P_{acc} (0.48) and NAO (0.39). Similar parallels can be drawn between other maritime glaciers (Ålfotbreen, Rembesdalskåka) and continental glaciers (Storbreen). Analyses by Nesje & Bakke (2007) showed that accumulation on the maritime glaciers was strongly related to western airflow, and the continental glaciers relied on circulating air in connection with low-pressure systems. The trend lines reflect the inter-annual variation of the glacial regimes (Fig. 7). We can see several glaciers that have had a period of continuous positive B_a pre-2000. Amongst them, Nigardsbreen had continuous positive mass balance since 1973, Ålfotbreen since 1973, and Rembesdalskåka since 1989 (Andreassen et al., 2005a). The mass balance was exceptionally positive in the period 1989-95 due to snow-rich winters, and Ålfotbreen, Nigardsbreen and Rembesdalskåka had a net mass increase of 11, 10 and 8 m w.e., respectively (Andreassen et al., 2005a).

The long-term recorded mass balance for the period 1960-2000 along the West- East profile in the southern glacier cluster in Norway reveals a clear gradient in mean summer and winter mass balance values, where the glaciers located close to the west coast have experienced a much higher mass turnover than those located further inland (Andreassen et al., 2005a). Here, B_w tends to be the more important component of the annual mass balance of the maritime

glaciers, while the more continental glaciers are dominated by variations B_s. A period of glacier advances in the 1980-1990s has been reported by many researchers (Andreassen et al., 2005a; S. Mutz et al., 2016; Nesje & Bakke, 2007). The increase in B_w during this period was likely influenced by a statistically significant increase in P_{acc} as reported in Southwestern and Northern Norway from around 1960 to 1997 (Hanssen-Bauer & Førland, 2000). In contrast, the rapid mass loss of Norwegian glaciers observed post-2000, coincided with a period of below normal P_{acc} around 2000 (Fig. 18) and higher T_{abl} than normal. The 2002 summer was the warmest and the 2003 summer was the fourth warmest on record in Norway since measurements started in 1876. This anomalous summer temperature was accompanied by record high ablation (Andreassen et al., 2005a). On the inter-annual scale, the NAO accounts for the largest amount of variability in climate patterns. After 1980, and especially during early 1990s, the NAO tended to be in an extreme positive phase (Fig. 18), and explains statistically, a substantial part of the observed T_{acc} and P_{acc} in Norway (Hurrell, 1995; Nesje et al., 2000; Nesje et al., 2001).

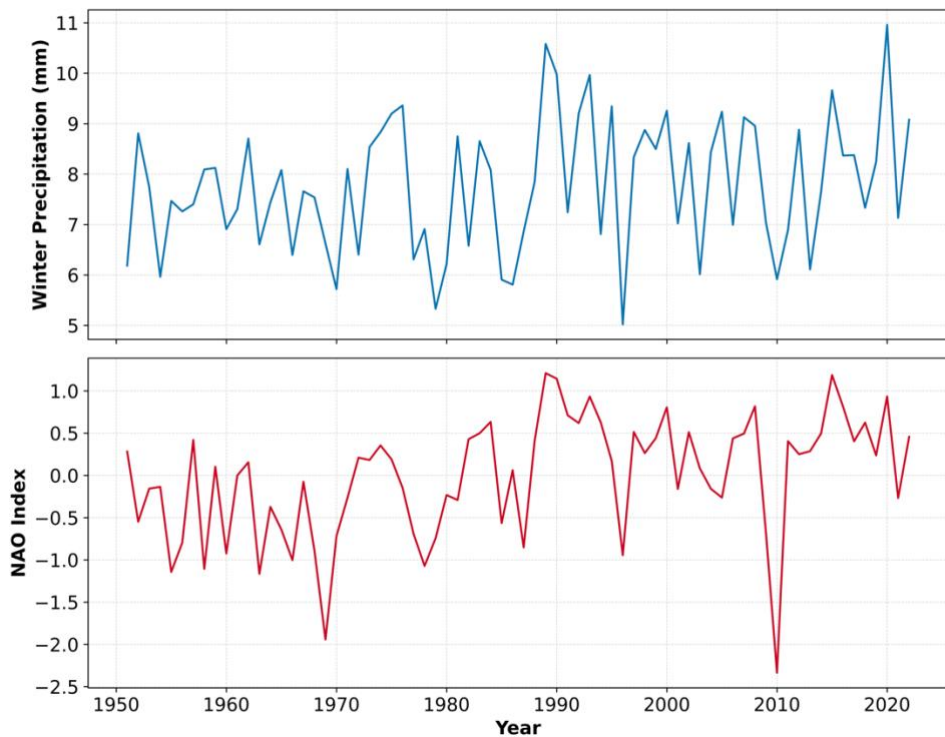


Fig 18: Inter-annual variability of winter precipitation (top) and the NAO index (bottom) for the period 1950-2023. Precipitation expressed as seasonal means (Dec-Feb) in mm, while NAO is presented as standardized anomalies. Both series exhibit similar interannual fluctuations, with higher precipitation generally coinciding with positive NAO phases. Figure inspired from Nesje et al. (2000). [Data: ECMWF- ERA5 Reanalysis product]

The extreme positive phases of the NAO in the early 1990s were synchronous with the precipitation patterns (Fig. 18). The relationship between the NAO index and P_{acc} is further supported by a Pearson correlation of 0.62 (Fig. 19). A similar trend can also be extrapolated to temperature patterns, as both are influenced by the NAO over Norway, characterized by warm and wet winters in positive phases and vice-versa (Hurrell, 1995; Iversen & Burningham, 2015).

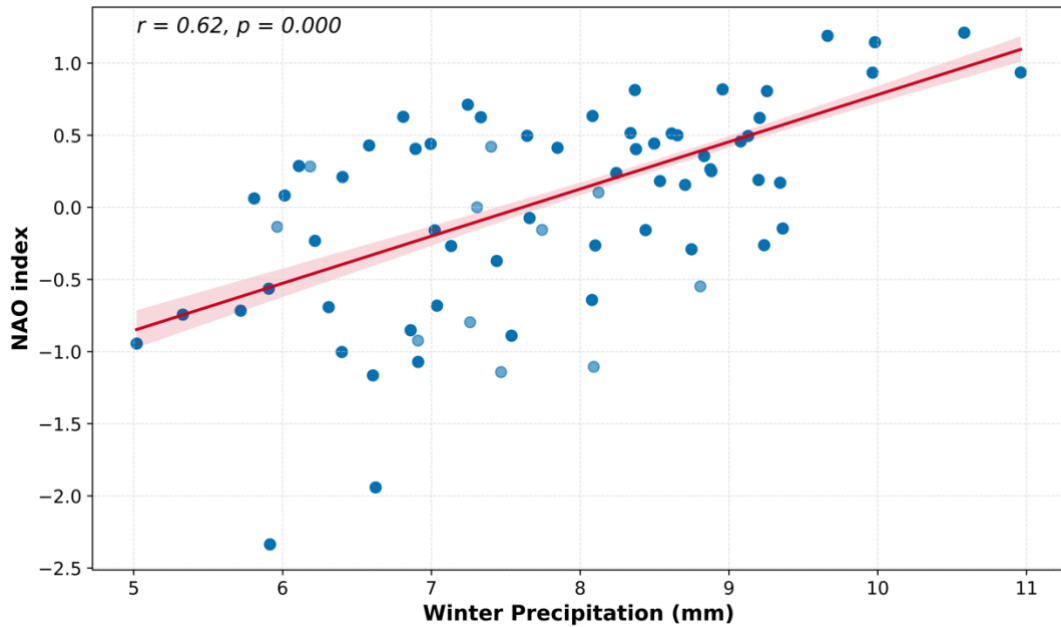


Fig 19: Scatterplot displaying the correlation between NAO index and Winter precipitation. Pearson correlation yielded $r= 0.62$, indicating a strong correlation and coupling between the two variables.
[Data: ECMWF- ERA5 Reanalysis product]

The negative phase of NAO post-2000 (Fig. 18), coupled with anomalous increase in T_{acc} post-2000 (Fig. 8) is associated with colder and drier winters leading to the regime change, which has been the most negative mass balance years on record (Andreassen, Elvehøy, et al., 2020). The drier winters during the negative phase of NAO post-2000 suggest that most precipitation was received as rainfall rather than snowfall. This is reflected in the increase in correlation of B_a with P_{abl} for 7 glaciers and with P_{acc} for 8 glaciers post-2000 (Fig. 8), patterns that coincide with the observed decline in mass balance. A statistically significant increase in correlation with T_{abl} for all 11 glaciers post-2000 can be seen (Fig. 8), supporting the hypothesis of a shift in the glacier regime, to a more energy dominated control post-2000.

A shift in the dominance of seasonal drivers of B_a is also evident when comparing the pre- and post-2000 periods (Fig. 13). Pre- 2000, annual mass balance displayed consistently high alignment with B_w for all glaciers, whereas post- 2000, the influence of B_s increased, particularly for glaciers such as Austdalsbreen, Gråsubreen, Hellstugubreen, and Storbreen, which displayed very strong correlations ($r > 0.9$). The scatterplot corresponds to the hypothesized shift, with 10 glaciers positioned above the 1:1 line, showing a stronger post-2000 correlation between B_a and B_s . This points to the possibility of a growing ablation-driven regime, likely linked to rising summer temperatures. In contrast, Langfjordjøkelen displays a unique pattern compared to the other glaciers. It yields a weaker correlation (0.40) between B_a and B_w post-2000 (Fig. 13). This anomalous result reflects the unique climatic and topographic setting of Langfjordjøkelen in northern Norway. Unlike the maritime southern glaciers that correlate strongly with the NAO, Langfjordjøkelen's mass balance is more closely linked with the AO, which better explains inter-annual variation in B_w and B_a . As a result, it likely did not benefit from the snow-rich winters during the strong positive NAO phase in the 1990s (Andreassen et al., 2012). The sharp increase in $B_a \sim B_s$ correlation post-2000 across most glaciers supports the interpretation of reduced P_{acc} influence during the negative NAO phase and indicates the transition toward a more temperature-driven regime.

4.2. Trends in Winter Mass Balance

A general pattern of decreasing B_w has been observed between 1990 and 2000 (Fig. 9). Among the 8 out of 11 glaciers that experienced mass loss, continental glaciers like Storbreen, Hellstugubreen, Rembesdalskåka, Gråsubreen were amongst the few that experienced a steeper loss. Nesje et al. (2000) report that continental glaciers experienced a significant loss in mass during this period. The years with low NAO index correspond to years of low winter accumulation and low B_w , and vice versa (Nesje et al., 2000), which is reflected in the mass loss observed post-2000 (Fig. 9). Additionally, the weakening of $B_w \sim$ NAO correlation for 7 glaciers observed post-2000 (Fig. 10) corresponds with the shift of NAO into a negative phase (Fig. 18). The consistent strong correlation with P_{acc} post-2000 indicates that P_{acc} is one of the key drivers of B_w , as accumulation in Scandinavian glaciers is mainly influenced by winter precipitation (snowfall) (Bonan et al., 2019; Nesje et al., 2000; Trachsel & Nesje, 2015). Additionally, the correlation with P_{acc} also displays patterns of the maritime-continental gradient, as snowfall decreases with increasing distances from oceanic sources and in precipitation ‘shadows’ in a leeward position of high mountains (Nesje et al., 2000). This is

evident from the higher pre-2000 correlation values with P_{acc} (Fig. 10) for maritime glaciers (like Ålfotbreen: 0.81, Austdalsbreen: 0.89, and Hansebreen: 0.84) compared to continental glaciers (like Hellstugubreen: 0.64 and Gråsubreen: 0.44).

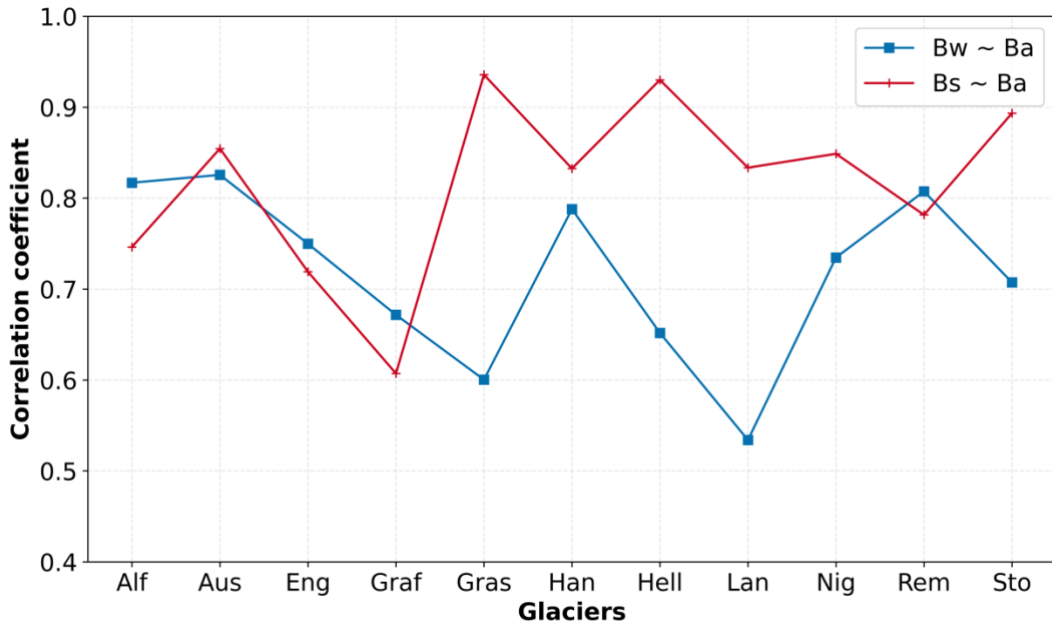


Fig 20: Correlation between Bw and Ba and between Bs and Ba for 11 Norwegian Glaciers. The analysis shows that Ba for maritime glaciers (Ålfotbreen, Engabreen, Grafellsbreen, Rembesdalskåka) is mainly controlled by Bw whereas Ba of continental glaciers (Grasubreen, Hellstugubreen, Storebreen) is controlled by Bs . Figure adapted from Nesje et al. (2023).

Accumulation may also be influenced by wind components, such as wind transport and redistribution of dry snow, by snow avalanches, transport of supercooled vapor etc. Stronger westerly winds (due to a positive phase of NAO) lead to increased snow accumulation in Scandinavia. This process is most common on maritime glaciers (Andreassen, Elvehøy, et al., 2020; Nesje et al., 2000). This pattern is evident from a higher correlation with wind components ($u10$ and $v10$) for maritime glaciers like Ålfotbreen ($u10$: 0.56), Engabreen ($u10$: 0.61), Hansebreen ($u10$: 0.59) as opposed to continental glaciers like Storbreen ($u10$: 0.40) and Nigardsbreen ($u10$: 0.47). The difference in influence of accumulation variables on B_a in maritime versus continental glaciers, as observed in this study, aligns with findings reported by Bonan et al. (2019), Medwedeff & Roe (2017), and Nesje et al. (2000). These researchers report that inter-annual variability in mass balance regimes are greater in maritime settings as opposed to continental ones. This is supported by the interpretation of trends from figure 20,

where we can observe greater control of B_w on B_a for maritime glaciers and of B_s on B_a for their continental counterparts. Finally, a slight increase in correlation with T_{acc} for 4 out of 11 glaciers post-2000 can be seen (Fig 10). The glaciers that display this result are continental glaciers, and this result supports the hypothesized shift towards an energy dominated mass balance control.

4.3. Trends in Summer Mass Balance

A clear decline in B_s is evident in the summer mass balance time series (Fig. 11). The decline in B_s begins in the second half of the 1990s, continuing after 2000. This shift is also reflected in the post-2000 change in correlation patterns (Fig. 12). The key results obtained were a stronger negative correlation between B_s and solar surface radiation (SSRD) for 9 glaciers, and between summer temperature (T_{abl}) for 10 out of 11 glaciers. This correlation supports the interpretation that the glacier ablation increasingly depends on the energy available for melt (Trachsel & Nesje, 2015). An increase in correlation with summer precipitation (P_{abl}) was also seen, mainly in maritime glaciers like Ålfotbreen and Hansebreen. Most studies (Andreassen & Oerlemans, 2009; Engelhardt et al., 2013; Hock et al., 2007; Laumann & Nesje, 2009, 2014; Rasmussen et al., 2007; Rasmussen & Conway, 2005; Schuler et al., 2005) have focused on estimating sensitivities of summer balances to changes in temperature and precipitation. They also reaffirm the primary influence of the NAO on Scandinavian climate patterns and its role in determining the strength of precipitation received by Norway (as established in section 4.1). During negative phases of the NAO, which are typically associated with reduced precipitation, Trachsel & Nesje (2015) highlight an increased relative importance of summer temperature (T_{abl}). As discussed in Section 4.2, the post-2000 negative NAO phases coincide with a decline in the correlation between winter balance and P_{acc} , alongside a corresponding increase in the correlation with T_{abl} , thus suggesting a possible shift in the dominant controls on mass balance regimes. Andreassen & Oerlemans (2009) suggest a minor importance of P_{abl} in determining the summer balance. Apart from P_{abl} , they also emphasized the importance of direct radiation and other ablation related variables in influencing B_s . The statistically significant increase in correlation with the ablation related variables (SSRD and T_{abl}) obtained in my results, supports the interpretation of a shift in the mass balance regime and its dominant controls post-2000, towards a more energy dominated nature.

4.4. Evaluation of Model Performance

The development and evaluation of multiple machine learning models in this study attempts to provide some insights into the ability of these models to estimate glacier mass balance components (B_a , B_w , B_s). To ensure a representative comparison, 6 regressors were selected from both linear and nonlinear model classes. Linear techniques like Ridge regression, Bayesian Ridge, and ARD are useful for data with collinearity, commonly seen in climate datasets (Hoerl & Kennard, 1970). Non-linear techniques like Random Forest and Bagging were included, as they often help in capturing non-linear relationships encountered in climate studies (Breiman, 2001), in this case, between climate variables and glacier mass balance. Furthermore, ensemble-based tree models like XGBoost with their sequential feature selection help in modelling with robustness by making less important predictors redundant (Chen & Guestrin, 2016). Such a mix of models may enable us to effectively understand patterns both glacier-specific and location-specific and evaluate performance and efficacy of different models in such situations.

4.4.1. Annual Mass Balance

Modelling B_a produced R^2 values ranging from 0 to 0.8, with performance varying across different regressor-selector combinations and glaciers. Among all combinations, BYR + Tree and ARD + Rec yielded the highest median R^2 scores of 0.48 and 0.50, respectively. From analysing the modelling routine results, we observe that linear models have generally performed better compared to their non-linear counterparts.

In addition, two key patterns help explain the RMSE values obtained (Fig. 15b). First, glaciers such as Grafjellsbrea and Langfjordjøkelen consistently showed poor performance across all model combinations, with RMSE values exceeding 1.0. This is likely due to the limited and inconsistent training data for these glaciers. Since the models were trained using data from the period 1950–2010, missing or fragmented mass balance records before 2000 for these glaciers may have hindered effective model calibration. Second, a spatial pattern aligned with the maritime-continental gradient is evident. Maritime glaciers such as Ålfotbreen, Hansebreen, Engabreen, and Rembesdalskåka exhibit lower RMSE values and generally stronger model performance compared to more continental glaciers like Grasubreen, Hellstugubreen, and Storbreen.

4.4.2. Winter Mass Balance

Modelling B_w produced R^2 values ranging from around -1 to 0.75, with an increasingly varied performance across the different regressor-selector combinations and glaciers. ARD + Rec (0.30) and BYR + Rec (0.25) were the highest median R^2 scores. Compared to B_a , modelling B_w yields slightly better results; Ålfotbreen, Austdalsbreen, Engabreen, Hansebreen, Hellstugubreen, Rembesdalskåka, and Storbreen see a reduction in RMSE scores. Once again, the maritime glaciers perform better compared to the continental ones (Fig. 16b). Langfjordjøkelen also showed improved performance relative to its results from the B_a modelling routine. In contrast, Grafjellsbrea performance became poorer (compared to B_a) with RMSE values exceeding 1, likely due to the same limitation of insufficient and inconsistent training data. Upon analysing the B_w modelling routine results, once again, the linear models have generally performed better than the non-linear ones.

4.4.3. Summer Mass Balance

The lowest R^2 values produced were from modelling B_s , with median values ranging from around -0.3 to 0.25, with an extremely varied performance across the different regressor-selector combinations and glaciers. We can observe that Ridge, BYR, and ARD were the better performers out of the 6 regressors used (Fig. 17a). Once again, linear models outperformed the non-linear ones. We also see a better performance of the maritime glaciers (Ålfotbreen, Engabreen, Hansebreen, Rembesdalskåka) compared to the poorer performing continental glaciers (Grasubreen, Hellstugubreen, Storbreen) (Fig. 17b). Grafjellsbrea had extremely high RMSE values, explained due to the inconsistent training data. Another key takeaway is the marginally better performance of the linear models compared to the non-linear ones employed. Apart from these patterns, predicting summer mass balance has been difficult with extremely high error values and very low correlation coefficients.

4.5. Interpretation & Comparison with Other Studies

Overall, the modelling results suggest clear patterns in predictability and model performance across the different glacier mass balance components and glaciers. B_w emerged as the most predictable component across all model routines, followed by B_a , with B_s being the most challenging to estimate. The better performance of B_a and B_w models is likely due to the nature of climate variables incorporated. B_a and B_w are strongly influenced by large-scale, seasonal drivers (e.g. temperature, winter precipitation, NAO) with regional impacts (like wind redistribution of snow), that explain most of the variability and are easy to incorporate in statistical models. The coupled influence of winter precipitation (P_{acc}) and NAO (as discussed in section 4.1 and 4.2) and their strong correlations with B_a and B_w (as discussed in section 3.1 and 3.2) possibly makes it easier to predict. B_s on the other hand is harder to model due to its sensitivity to more localized ablation processes. This observation aligns with studies which found that simply using summer temperature (T_{abl}) to model B_s poses problems as crucial variables like the direct effect of radiation and the hypsometry of glaciers, are not entirely accounted for (Trachsel & Nesje, 2015). These influences tend to be important, in transitional seasons where accumulation and ablation can occur simultaneously, especially on a continental glacier (Andreassen & Oerlemans, 2009; Schuler et al., 2005).

Results from this thesis, consistent with findings from other studies in Norway (Andreassen et al., 2005a; Andreassen & Oerlemans, 2009; Giesen & Oerlemans, 2010; Laumann & Nesje, 2009, 2014), support the presence of a spatial gradient. On near-coastal maritime glaciers, B_a is mainly controlled by winter precipitation (P_{acc}) whereas on inland-continental glaciers, B_a is mainly controlled by summer temperature (T_{abl}). The linear models (Ridge, Bayesian Ridge, ARD) outperformed non-linear models (Bagging, Random Forest, XGBoost). This is likely due to the simpler structure of the predictors used, large-scale atmospheric variables with relatively linear relationships to mass balance. In settings where the climatic controls are dominated by straightforward seasonal relationships, linear models have been shown to produce interpretable and robust results (Anilkumar et al., 2023).

Across all glaciers, the B_a models developed in this thesis perform reasonably well, with average performance metrics of $R^2 \approx 0.55$ and $RMSE \approx 0.64$ m w.e. For B_w , the average $R^2 \approx 0.45$ and $RMSE \approx 0.59$ m w.e., while B_s models achieve $R^2 \approx 0.28$ and $RMSE \approx 0.90$ m w.e. These values are comparable to those reported by Mutz et al. (2016), who found correlation

coefficients for B_a ranging from about 0.82 for Ålfotbreen to 0.30 for Gråsubreen. For B_s , their reported R^2 values ranged from -0.70 to -0.40 for Ålfotbreen and around -0.30 for Engabreen, closely matching the results of this study and reflecting the difficulty of statistical models to model summer balance. Ålfotbreen consistently displayed high performance metrics in both studies, reinforcing the observed spatial gradient in which maritime glaciers exhibit higher correlations and are generally easier to model than continental glaciers.

When compared to other modelling approaches and study locations, similar patterns and performance are observed. Mutz & Aschauer (2022) reported average B_a model performance of $RMSE \approx 0.6$ m w.e. and $R^2 \approx 0.5$ for the glaciers in the Andes, closely matching the results obtained here. Masiokas et al. (2016) reconstructed B_a for Echaurren Norte Glacier in the Andes, using a minimal glacier model ($RMSE = 0.77$ m w.e.) (Marzeion et al., 2012) and two regression models ($RMSE = 0.91$ m w.e. and $R^2 = 0.68$). Buttstädt et al. (2009) applied a degree-day model to Martial Este Glacier, also in the Andes, reporting $R^2 = 0.91$ and $RMSE = 0.47$ m w.e. While some of these studies report slightly higher performance scores, this is likely due to their use of more complete datasets and longer measurement records, which improve the ability to capture climate-mass balance relationships during model training. Furthermore, unlike these studies, the models in this thesis rely solely on large-scale atmospheric predictors, whereas others adopt fundamentally different modelling frameworks or incorporate additional local proxy data (e.g., streamflow, snow depth, hypsometry) that provide further relevant information and improve model performance. The models developed in this study achieve $RMSE$ and R^2 values comparable to those reported for similarly constructed mass-balance models in Austria (Schöner & Böhm, 2007) and South America (Mutz & Aschauer, 2022). Despite differences in climatic settings, the performance of some glacier's models in this project falls within the published range for empirical-statistical glacier models of this type.

5. Conclusion

5.1. Part A

The main objective of this study was to investigate the existence of a regime shift in the climatic controls governing Norwegian glaciers. Given the well-established relationship between glacier mass balance and large-scale atmospheric dynamics, an empirical-statistical modelling approach was employed to investigate the link between mass balance components and key climate variables. The correlation patterns observed in this study were consistent with their expected influence. B_a and B_w showed strong relationships with temperature, winter precipitation, and NAO, while B_s correlated well with summer temperature and surface solar radiation. This reiterated their role as dominant drivers of glacier mass balance regimes in Norway. We see a brief period of advancement in the 1990s which temporally coincided with extreme positive phases of the NAO, leading to snow rich winters, and is supported by a strong statistical relationship between B_w and NAO. The findings provide robust evidence of a post-2000 regime shift, characterized by a transition from a winter (accumulation) driven to a summer (ablation) dominated regime, this transition is especially pronounced in maritime glaciers as the mass loss is less homogenous compared with more continental locations. There is a rapid decline in the mass balance in all Norwegian glaciers combined with weakening NAO phases, decreased P_{acc} , and rising summer temperatures. As summer temperatures increase beyond a point where summer ablation overcompensates winter accumulation, it leads to mass loss. These factors collectively account for the glaciers' mass deficits post-2000.

The key findings identified are:

- 1) The NAO, precipitation, and temperature have a strong influence on glacier mass balance, but their relative influence has evolved over time.
- 2) A maritime-continental gradient exists, with maritime glaciers displaying a higher mass turnover and stronger coupling with the atmospheric drivers than the continental glaciers.
- 3) A post-2000 transition for some glaciers towards a stronger summer temperature and surface solar radiation sensitivity, combined with a weakened relationship with the NAO—indicating a shift towards summer mass balance dominated glacier regime.
- 4) A shift from pre-2000 winter mass balance controlled B_a to a post-2000 summer mass balance dominated control for 10 out of 11 glaciers confirming the regime shift.

5.2. Part B

The secondary objective of this project was to develop and evaluate empirical-statistical models for annual (B_a), winter (B_w), and summer (B_s) glacier mass balance using six regressors and three selectors. B_w emerged as the most predictable component, followed by B_a , with B_s showing the poorest performance. This hierarchy may be due to the increasing complexity of the underlying processes: B_a and B_w are more strongly linked to large-scale, seasonal climate drivers such as temperature, precipitation, and the NAO, which are easier to represent in empirical models. In contrast, B_s is more influenced by localized ablation processes, whose non-linear (physical) relationships are harder to capture statistically.

The key findings identified are:

- 1) Linear models (ARD, Ridge CV, Bayesian Ridge) outperformed the non-linear ones (Bagging, Random Forest, XGBoost), across all mass balance components. This is likely due to the simpler and relatively more linear relationships between mass balance and large-scale climate drivers like NAO, precipitation, and temperature.
- 2) Glaciers with longer and more complete pre-2000 records (>15 years) demonstrated better predictive skill, underscoring the importance of a robust training dataset. Longer records allow for a more reliable pre-/post-2000 training–testing data split, improving model performance.
- 3) Maritime glaciers showed better performance than continental ones, likely due to their stronger coupling with large-scale climate indices and higher mass turnover.

These results support the observed post-2000 shift toward a more temperature-driven regime and offer a basis for applying this machine-learning framework to compare the performance of different models while making future predictions using RCM/GCM data (e.g. CMIP6).

Bibliography

- Åkesson, H., Nisancioglu, K. H., Giesen, R. H., & Morlighem, M. (2016). *Simulating asymmetric growth and retreat of Hardangerjøkulen ice cap in southern Norway since the mid-Holocene*. Climate Interactions. <https://doi.org/10.5194/tc-2016-62>
- Andreassen, L. M., & Elvehøy, H. (2021). *Norwegian Glacier Reference Dataset for Climate Change Studies*. www.nve.no
- Andreassen, L. M., Elvehøy, H., Kjollmoen, B., & Belart, J. M. C. (2020). Glacier change in Norway since the 1960s—An overview of mass balance, area, length and surface elevation changes. *Journal of Glaciology*, 66(256), 313–328. <https://doi.org/10.1017/jog.2020.10>
- Andreassen, L. M., Elvehøy, H., Kjøllmoen, B., Engeset, R. V., & Haakensen, N. (2005a). *Glacier mass-balance and length variation in Norway*. <http://www.ipcc.ch>
- Andreassen, L. M., Elvehøy, H., Kjøllmoen, B., Engeset, R. V., & Haakensen, N. (2005b). Glacier mass-balance and length variation in Norway. *Annals of Glaciology*, 42, 317–325. <https://doi.org/10.3189/172756405781812826>
- Andreassen, L. M., KJøllmoen, B., Rasmussen, A., Melvold, K., & Nordli, Ø. (2012, June). Langfjordjøkelen, a rapidly shrinking glacier in northern Norway. In *Journal of Glaciology* (Vol. 58, Issue 209, pp. 581–593). <https://doi.org/10.3189/2012JoG11J014>
- Andreassen, L. M., Nordli, Ø., Rasmussen, A., Melvold, K., & Nordli, Ø. (2012). Langfjordjøkelen, a rapidly shrinking glacier in northern Norway. *Journal of Glaciology*, 58(209), 581–593. <https://doi.org/10.3189/2012JoG11J014>
- Andreassen, L. M., & Oerlemans, J. (2009). Modelling long-term summer and winter balances and the climate sensitivity of storbreen, norway. *Geografiska Annaler: Series A*,

- Physical Geography*, 91(4), 233–251. <https://doi.org/10.1111/j.1468-0459.2009.00366.x>
- Andreassen, L. M., & Winsvold, S. H. (2012). *Inventory of Norwegian Glaciers*.
- Anilkumar, R., Bharti, R., Chutia, D., & Aggarwal, S. P. (2023). Modelling point mass balance for the glaciers of the Central European Alps using machine learning techniques. *The Cryosphere*, 17(7), 2811–2828. <https://doi.org/10.5194/tc-17-2811-2023>
- Bach, E., Radic, V., & Schoof, C. (2018). How sensitive are mountain glaciers to climate change? Insights from a block model. *Journal of Glaciology*, 64(244), 247–258. <https://doi.org/10.1017/jog.2018.15>
- Baldwin, M. P. (2008). *Spatial Weighting and Iterative Projection Methods for EOFs*. <https://journals.ametsoc.org/view/journals/clim/22/2/2008jcli2147.1.xml>
- Barnston, A. G., & Livezey, R. E. (1987). Classification, seasonality and persistence of low-frequency atmospheric circulation patterns. *Monthly Weather Review*, 115(6), 1083–1126.
- Beniston, M., Farinotti, D., Stoffel, M., Andreassen, L. M., Coppola, E., Eckert, N., Fantini, A., Giacoma, F., Hauck, C., Huss, M., Huwald, H., Lehning, M., López-Moreno, J.-I., Magnusson, J., Marty, C., Morán-Tejeda, E., Morin, S., Naaim, M., Provenzale, A., ... Vincent, C. (2018). The European mountain cryosphere: A review of its current state, trends, and future challenges. *The Cryosphere*, 12(2), 759–794. <https://doi.org/10.5194/tc-12-759-2018>
- Beylich, A. A. (Ed.). (2021). *Landscapes and Landforms of Norway*. Springer International Publishing. <https://doi.org/10.1007/978-3-030-52563-7>
- Bizzotto, E. C., Villa, S., Vaj, C., & Vighi, M. (2009). Comparison of glacial and non-glacial-fed streams to evaluate the loading of persistent organic pollutants through seasonal snow/ice melt. *Chemosphere*, 74(7), 924–930. <https://doi.org/10.1016/j.chemosphere.2008.10.013>

- Boateng, D., & Mutz, S. G. (2023). pyESDv1.0.1: An open-source Python framework for empirical-statistical downscaling of climate information. *Geoscientific Model Development*, 16(22), 6479–6514. <https://doi.org/10.5194/gmd-16-6479-2023>
- Bogdal, C., Schmid, P., Zennegg, M., Anselmetti, F. S., Scheringer, M., & Hungerbühler, K. (2009). Blast from the past: Melting glaciers as a relevant source for persistent organic pollutants. *Environmental Science and Technology*, 43(21), 8173–8177. <https://doi.org/10.1021/es901628x>
- Bonan, D. B., Christian, J. E., & Christianson, K. (2019). Influence of North Atlantic climate variability on glacier mass balance in Norway, Sweden and Svalbard. *Journal of Glaciology*, 65(252), 580–594. <https://doi.org/10.1017/jog.2019.35>
- Breiman, L. (2001). Random Forests. *Machine Learning*, 45(1), 5–32. <https://doi.org/10.1023/A:1010933404324>
- Buttstädt, M., Möller, M., Iturraspe, R., & Schneider, C. (2009). Mass balance evolution of Martial Este Glacier, Tierra del Fuego (Argentina) for the period 1960–2099. *Advances in Geosciences*, 22, 117–124.
- Calvin, K., Dasgupta, D., Krinner, G., Mukherji, A., Thorne, P. W., Trisos, C., Romero, J., Aldunce, P., Barrett, K., Blanco, G., Cheung, W. W. L., Connors, S., Denton, F., Diongue-Niang, A., Dodman, D., Garschagen, M., Geden, O., Hayward, B., Jones, C., ... Péan, C. (2023). *IPCC, 2023: Climate Change 2023: Synthesis Report. Contribution of Working Groups I, II and III to the Sixth Assessment Report of the Intergovernmental Panel on Climate Change [Core Writing Team, H. Lee and J. Romero (eds.)]*. IPCC, Geneva, Switzerland. (First). Intergovernmental Panel on Climate Change (IPCC). <https://doi.org/10.59327/IPCC/AR6-9789291691647>
- Chen, T., & Guestrin, C. (2016). XGBoost: A Scalable Tree Boosting System. *Proceedings of the 22nd ACM SIGKDD International Conference on Knowledge Discovery and Data Mining*, 785–794. <https://doi.org/10.1145/2939672.2939785>

- Comas-Bru, L., & Hernández, A. (2018). Reconciling North Atlantic climate modes: Revised monthly indices for the East Atlantic and the Scandinavian patterns beyond the 20th century. *Earth System Science Data*, 10(4), 2329–2344.
- Dahl, S. O., Nesje, A., Lie, Ø., Fjordheim, K., & Matthews, J. A. (2002). Timing, equilibrium-line altitudes and climatic implications of two early-Holocene glacier readvances during the Erdalen Event at Jostedalsbreen, western Norway. *The Holocene*, 12(1), 17–25. <https://doi.org/10.1191/0959683602hl516rp>
- Daly, G. L., & Wania, F. (2005, January). Organic contaminants in mountains. In *Environmental Science and Technology* (Vol. 39, Issue 2, pp. 385–398). <https://doi.org/10.1021/es048859u>
- Davis, R. E. (1976). Predictability of sea surface temperature and sea level pressure anomalies over the North Pacific Ocean. *Journal of Physical Oceanography*, 6(3), 249–266.
- Dyurgerov, M. (2003). Mountain and subpolar glaciers show an increase in sensitivity to climate warming and intensification of the water cycle. *Journal of Hydrology*, 282(1–4), 164–176. [https://doi.org/10.1016/S0022-1694\(03\)00254-3](https://doi.org/10.1016/S0022-1694(03)00254-3)
- Dyurgerov, M. B., & Meier, M. F. (2000). *Twentieth century climate change: Evidence from small glaciers*. www.pnas.org
- Engelhardt, M., Schuler, T. V., & Andreassen, L. M. (2013). Glacier mass balance of Norway 1961–2010 calculated by a temperature-index model. *Annals of Glaciology*, 54(63), 32–40.
- Folland, C. K., Knight, J., Linderholm, H. W., Fereday, D., Ineson, S., & Hurrell, J. W. (2009). The summer North Atlantic Oscillation: Past, present, and future. *Journal of Climate*, 22(5), 1082–1103.
- Gabrielli, P., Cozzi, G., Torcini, S., Cescon, P., & Barbante, C. (2008). Trace elements in winter snow of the Dolomites (Italy): A statistical study of natural and anthropogenic

- contributions. *Chemosphere*, 72(10), 1504–1509.
<https://doi.org/10.1016/j.chemosphere.2008.04.076>
- Giesen, R. H., & Oerlemans, J. (2010). Response of the ice cap Hardangerjøkulen in southern Norway to the 20th and 21st century climates. *The Cryosphere*, 4(2), 191–213.
- Han, P., Long, D., Zhao, F., & Slater, L. J. (2023). Response of Two Glaciers in Different Climate Settings of the Tibetan Plateau to Climate Change Through Year 2100 Using a Hybrid Modeling Approach. *Water Resources Research*, 59(4), e2022WR033618.
<https://doi.org/10.1029/2022WR033618>
- Hanssen-Bauer, I., & Førland, E. (2000). *Temperature and precipitation variations in Norway 1900–1994 and their links to atmospheric circulation—Hanssen-Bauer—2000—International Journal of Climatology—Wiley Online Library*.
[https://rmets.onlinelibrary.wiley.com/doi/abs/10.1002/1097-0088\(20001130\)20:14%3C1693::AID-JOC567%3E3.0.CO;2-7?casa_token=GfYjiFfsdcYAAAAA%3AvST6zZaXoq8d4KFBIgM-QMmbhZj_4vYclgnsJd-9Em6yGUbVrULKie1jTg_RHyXCDFzD_o8GHjXjVKwkdQ](https://rmets.onlinelibrary.wiley.com/doi/abs/10.1002/1097-0088(20001130)20:14%3C1693::AID-JOC567%3E3.0.CO;2-7?casa_token=GfYjiFfsdcYAAAAA%3AvST6zZaXoq8d4KFBIgM-QMmbhZj_4vYclgnsJd-9Em6yGUbVrULKie1jTg_RHyXCDFzD_o8GHjXjVKwkdQ)
- Hersbach, H., Bell, B., Berrisford, P., Hirahara, S., Horányi, A., Muñoz-Sabater, J., Nicolas, J., Peubey, C., Radu, R., Schepers, D., Simmons, A., Soci, C., Abdalla, S., Abellan, X., Balsamo, G., Bechtold, P., Biavati, G., Bidlot, J., Bonavita, M., ... Thépaut, J.-N. (2020). The ERA5 global reanalysis. *Quarterly Journal of the Royal Meteorological Society*, 146(730), 1999–2049. <https://doi.org/10.1002/qj.3803>
- Hewitson, B. C., Daron, J., Crane, R. G., Zermoglio, M. F., & Jack, C. (2014). Interrogating empirical-statistical downscaling. *Climatic Change*, 122(4), 539–554.
<https://doi.org/10.1007/s10584-013-1021-z>

- Hock, R. (2005). Glacier melt: A review of processes and their modelling. In *Progress in Physical Geography* (Vol. 29, Issue 3, pp. 362–391). Arnold.
<https://doi.org/10.1191/0309133305pp453ra>
- Hock, R., Radić, V., & De Woul, M. (2007). Climate sensitivity of Storglaciären, Sweden: An intercomparison of mass-balance models using ERA-40 re-analysis and regional climate model data. *Annals of Glaciology*, 46, 342–348.
- Hodson, A. J. (2014). Understanding the dynamics of black carbon and associated contaminants in glacial systems. *Wiley Interdisciplinary Reviews: Water*, 1(2), 141–149. <https://doi.org/10.1002/wat2.1016>
- Hoerl, A. E., & Kennard, R. W. (1970). Ridge Regression: Biased Estimation for Nonorthogonal Problems. *Technometrics*, 12(1), 55–67.
<https://doi.org/10.1080/00401706.1970.10488634>
- Hughes, P. D., Gibbard, P. L., & Ehlers, J. (2013). Timing of glaciation during the last glacial cycle: Evaluating the concept of a global ‘Last Glacial Maximum’ (LGM). *Earth-Science Reviews*, 125, 171–198. <https://doi.org/10.1016/j.earscirev.2013.07.003>
- Hurrell, J. W. (1995). Decadal Trends in the North Atlantic Oscillation: Regional Temperatures and Precipitation. *Science*, 269(5224), 676–679.
<https://doi.org/10.1126/science.269.5224.676>
- Hurrell, James &, Phillips, Adam & National Center for Atmospheric Research Staff (Eds). Last modified 2023-07-10 "The Climate Data Guide: Hurrell North Atlantic Oscillation (NAO) Index (station-based)." Retrieved from <https://climatedataguide.ucar.edu/climate-data/hurrell-north-atlantic-oscillation-nao-index-station-based> on 2025-07-14.
- Iversen, E., & Burningham, H. (2015). Relationship between NAO and wind climate over Norway. *Climate Research*, 63(2), 115–134. <https://doi.org/10.3354/cr01277>

- Jolliffe, I. (2002). Principal Component Analysis. In *International Encyclopedia of Statistical Science* (pp. 1094–1096). Springer, Berlin, Heidelberg. https://doi.org/10.1007/978-3-642-04898-2_455
- Jolliffe, I. (2011). Principal Component Analysis. In *International Encyclopedia of Statistical Science* (pp. 1094–1096). Springer, Berlin, Heidelberg. https://doi.org/10.1007/978-3-642-04898-2_455
- Ketzler, G. et al. (2021). “The Climate of Norway”. In: pp. 7–29.
- Kjøllmoen, B. (2011). *Glaciological investigations in Norway in 2010*.
- Kraaijenbrink, P. D. A., Bierkens, M. F. P., Lutz, A. F., & Immerzeel, W. W. (2017). Impact of a global temperature rise of 1.5 degrees Celsius on Asia’s glaciers. *Nature*, 549(7671), 257–260. <https://doi.org/10.1038/nature23878>
- Laumann, T., & Nesje, A. (2009). A simple method of simulating the future frontal position of Briksdalsbreen, western Norway. *The Holocene*, 19(2), 221–228. <https://doi.org/10.1177/0959683608100566>
- Laumann, T., & Nesje, A. (2014). Spørteggbreen, western Norway, in the past, present and future: Simulations with a two-dimensional dynamical glacier model. *The Holocene*, 24(7), 842–852. <https://doi.org/10.1177/0959683614530446>
- Lemke, P, Ren, J, Alley, R B, Allison, I, Carrasco, J, Flato, G, Fujii, Y, Kaser, G, Mote, P, Thomas, R H, & Zhang, T. Observations. Changes in Snow, Ice and Frozen Ground. Chapter 4. United Kingdom.
- Liestøl, O. (1967). *Storbreen glacier in Jotunheimen, Norway*. <https://brage.npolar.no/xmlui/bitstream/handle/11250/173862/Skrifter141.pdf?sequence=2>
- Lingis, P., & Michaelides, S. C. (2009). Teleconnection patterns of the Siberian Anticyclone and precipitation over Cyprus. *Atmospheric Research*, 94(4), 663–674. <https://doi.org/10.1016/j.atmosres.2009.05.013>

- Lorenz, E. N. (1956). Empirical orthogonal functions and statistical weather prediction. (*No Title*). <https://cir.nii.ac.jp/crid/1370004237455296143>
- Mangerud, J., Gyllencreutz, R., Lohne, Ø., & Svendsen, J. I. (2011). Glacial History of Norway. In *Developments in Quaternary Sciences* (Vol. 15, pp. 279–298). Elsevier. <https://doi.org/10.1016/B978-0-444-53447-7.00022-2>
- Marzeion, B., Hofer, M., Jarosch, A. H., Kaser, G., & Mölg, T. (2012). A minimal model for reconstructing interannual mass balance variability of glaciers in the European Alps. *The Cryosphere*, 6(1), 71–84.
- Masiokas, M. H., Christie, D. A., Le Quesne, C., Pitte, P., Ruiz, L., Villalba, R., Luckman, B. H., Berthier, E., Nussbaumer, S. U., & González-Reyes, Á. (2016). Reconstructing the annual mass balance of the Echaurren Norte glacier (Central Andes, 33.5 S) using local and regional hydroclimatic data. *The Cryosphere*, 10(2), 927–940.
- Matthews, J. A., & Karlén, W. (1992). Asynchronous neoglaciation and Holocene climatic change reconstructed from Norwegian glaciolacustrine sedimentary sequences. *Geology*, 20(11), 991. [https://doi.org/10.1130/0091-7613\(1992\)020<0991:ANAHCC>2.3.CO;2](https://doi.org/10.1130/0091-7613(1992)020<0991:ANAHCC>2.3.CO;2)
- Medwedeff, W. G., & Roe, G. H. (2017). Trends and variability in the global dataset of glacier mass balance. *Climate Dynamics*, 48(9), 3085–3097. <https://doi.org/10.1007/s00382-016-3253-x>
- Mellado-Cano, J., Barriopedro, D., García-Herrera, R., Trigo, R. M., & Hernández, A. (2019). Examining the north atlantic oscillation, east atlantic pattern, and jet variability since 1685. *Journal of Climate*, 32(19), 6285–6298. <https://doi.org/10.1175/JCLI-D-19-0135.1>
- Mutz, S., & Aschauer, J. (2022). *Empirical glacier mass-balance models for South America | Journal of Glaciology | Cambridge Core*. <https://www.cambridge.org/core/journals/journal-of-glaciology/article/empirical->

glacier-massbalance-models-for-south-
america/5858720EDDF9D02938D728114E408764

Mutz, S. G., Scherrer, S., Muceniece, I., & Ehlers, T. A. (2021). Twenty-first century regional temperature response in Chile based on empirical-statistical downscaling. *Climate Dynamics*, 56(9), 2881–2894. <https://doi.org/10.1007/s00382-020-05620-9>

Mutz, S., Paeth, H., & Winkler, S. (2016). Modelling of future mass balance changes of Norwegian glaciers by application of a dynamical–statistical model. *Climate Dynamics*, 46(5–6), 1581–1597. <https://doi.org/10.1007/s00382-015-2663-5>

National Center for Atmospheric Research Staff (Eds). Last modified 22 Jul 2013. "The Climate Data Guide: Empirical Orthogonal Function (EOF) Analysis and Rotated EOF Analysis." Retrieved from <https://climatedataguide.ucar.edu/climate-data-tools-and-analysis/empirical-orthogonal-function-eof-analysis-and-rotated-eof-analysis>.

Nesje, A. (2023). Future state of Norwegian glaciers: Estimating glacier mass balance and equilibrium line responses to projected 21st century climate change. *The Holocene*, 33(10), 1257–1271. <https://doi.org/10.1177/09596836231183069>

Nesje, A., & Bakke, J. (2007). *Norwegian mountain glaciers in the past, present and future*.

Nesje, A., & Dahl, S. O. (2000). *Key Issues in Environmental Change*.

Nesje, A., Lie, Ø., & Dahl, S. O. (2000). Is the North Atlantic Oscillation reflected in Scandinavian glacier mass balance records? *Journal of Quaternary Science*, 15(6), 587–601. [https://doi.org/10.1002/1099-1417\(200009\)15:6<587::AID-JQS533>3.0.CO;2-2](https://doi.org/10.1002/1099-1417(200009)15:6<587::AID-JQS533>3.0.CO;2-2)

Nesje, A., Matthews, J. A., Dahl, S. O., Berrisford, M. S., & Andersson, C. (2001). Holocene glacier fluctuations of Flatebreen and winter-precipitation changes in the Jostedalsbreen region, western Norway, based on glaciolacustrine sediment records. *The Holocene*, 11(3), 267–280. <https://doi.org/10.1191/095968301669980885>

- Nesje, A., Matthews, J. A., Dahl, S. O., Berrisford2, M. S., & Andersson', C. (2001). Holocene glacier fluctuations of Flatebreen and winter-precipitation changes in the Jostedalsbreen region, western Norway, based on glaciolacustrine sediment records. In *The Holocene* (Vol. 11, pp. 267–280).
- Obukhov, A. M. (1947). Statistically homogeneous fields on a sphere. *Usp. Mat. Nauk*, 2(2), 196–198.
- O’Neel, S., Hood, E., Arendt, A., & Sass, L. (2014). Assessing streamflow sensitivity to variations in glacier mass balance. *Climatic Change*, 123(2), 329–341. <https://doi.org/10.1007/s10584-013-1042-7>
- Østrem, G., & Brugman, M. (1991). *Østrem_Brugman_GlacierMassBalanceMeasurements_1991*.
- Østrem, G., & Haakensen, N. (1973). *GLACIERS OF NORWAY Meddelelse nr 82 fra Hydrologisk avdelingg 1993 CONTENTS*.
- Østrem, G., & Haakensen, N. (1993). *Glaciers of Europe-GLACIERS OF NORWAY SATELLITE IMAGE ATLAS OF GLACIERS OF THE WORLD*.
- Østrem, G., & Haakensen, N. (1993). *Ostrem_glaciers_of_norway*.
- Østrem, G., & Stanley, A. (1966). *GLACIER MASS BALANCE MEASUREMENTS A MANUAL FOR FIELD WORK*.
- Peings, Y., Cattiaux, J., Vavrus, S. J., & Magnusdottir, G. (2018). Projected squeezing of the wintertime North-Atlantic jet. *Environmental Research Letters*, 13(7), 074016.
- Pinto, J. G., & Raible, C. C. (2012). Past and recent changes in the North Atlantic oscillation. *WIREs Climate Change*, 3(1), 79–90. <https://doi.org/10.1002/wcc.150>
- Rasmussen, L. A., Andreassen, L. M., & Conway, H. (2007). Reconstruction of mass balance of glaciers in southern Norway back to 1948. *Annals of Glaciology*, 46, 255–260.
- Rasmussen, L. A., & Conway, H. (2005). Influence of upper-air conditions on glaciers in Scandinavia. *Annals of Glaciology*, 42, 402–408.

- Robertson, A. W., Qian, J.-H., Tippett, M. K., Moron, V., & Lucero, A. (2012). *Downscaling of Seasonal Rainfall over the Philippines: Dynamical versus Statistical Approaches*. <https://doi.org/10.1175/MWR-D-11-00177.1>
- Schneider, D. P., C. Deser, J. Fasullo, and K. E. Trenberth, 2013: Climate Data Guide Spurs Discovery and Understanding. *Eos Trans. AGU*, 94, 121–122, <https://doi.org/10.1002/2013eo130001>
- Schöner, W., & Böhm, R. (2007). A statistical mass-balance model for reconstruction of LIA ice mass for glaciers in the European Alps. *Annals of Glaciology*, 46, 161–169.
- Schuler, T. V., Hock, R., Jackson, M., Elvehøy, H., Braun, M., Brown, I., & Hagen, J.-O. (2005). Distributed mass-balance and climate sensitivity modelling of Engabreen, Norway. *Annals of Glaciology*, 42, 395–401.
- Seppälä, M. (Ed.). (2005). *The physical geography of Fennoscandia*. Oxford University Press.
- Slemmons, K. E. H., Saros, J. E., & Simon, K. (2013, October). The influence of glacial meltwater on alpine aquatic ecosystems: A review. In *Environmental Sciences: Processes and Impacts* (Vol. 15, Issue 10, pp. 1794–1806). <https://doi.org/10.1039/c3em00243h>
- SSB (2012) Electricity, annual figures, 2025. <https://www.ssb.no/en/energi-og-industri/energi/statistikk/elektrisitet>
- Trachsel, M., & Nesje, A. (2015). Modelling annual mass balances of eight Scandinavian glaciers using statistical models. *The Cryosphere*, 9(4), 1401–1414.
- Trigo, R. M., Osborn, T. J., & Corte-Real, J. M. (2002). The North Atlantic Oscillation influence on Europe: Climate impacts and associated physical mechanisms. *Climate Research*, 20(1), 9–17.
- Vaughan, D. G., Comiso, J. C., Allison, I., Carrasco, J., Kaser, G., Kwok, R., Mote, P., Murray, T., Paul, F., Ren, J., Rignot, E., Solomina, O., Steffen, K., Zhang, T., Stocker, Qin, D., Plattner, G.-K., Tignor, M., Allen, S. K., ... Kwok, R. (2013). *Observations*:

- Cryosphere. In: Climate Change 2013: The Physical Science Basis. Contribution of Working Group I to the Fifth Assessment Report of the Intergovernmental Panel on Climate Change Coordinating Lead Authors: Lead Authors.*
- Vicente-Serrano, S. M., & López-Moreno, J. I. (2008). Nonstationary influence of the North Atlantic Oscillation on European precipitation. *Journal of Geophysical Research: Atmospheres*, 113(D20), 2008JD010382. <https://doi.org/10.1029/2008JD010382>
- Villa, S., Negrelli, C., Finizio, A., Flora, O., & Vighi, M. (2006). Organochlorine compounds in ice melt water from Italian Alpine rivers. *Ecotoxicology and Environmental Safety*, 63(1), 84–90. <https://doi.org/10.1016/j.ecoenv.2005.05.010>
- Wilks, D. S. (2011). Chapter 12—Principal Component (EOF) Analysis. In D. S. Wilks (Ed.), *International Geophysics* (Vol. 100, pp. 519–562). Academic Press. <https://doi.org/10.1016/B978-0-12-385022-5.00012-9>
- Winkler, S., Chinn, T., Gärtnner-Roer, I., Nussbaumer, S. U., Zemp, M., & Zumbühl, H. J. (2010). An introduction to mountain glaciers as climate indicators with spatial and temporal diversity. *Erdkunde*, 97–118.
- Winsvold, S. H., Andreassen, L. M., & Kienholz, C. (2014). Glacier area and length changes in Norway from repeat inventories. *Cryosphere*, 8(5), 1885–1903. <https://doi.org/10.5194/tc-8-1885-2014>
- Xu, M., Yan, M., Kang, J., & Ren, J. (2012). Comparative studies of glacier mass balance and their climatic implications in Svalbard, Northern Scandinavia, and Southern Norway. *Environmental Earth Sciences*, 67(5), 1407–1414. <https://doi.org/10.1007/s12665-012-1585-3>
- Yao, T., Thompson, L., Yang, W., Yu, W., Gao, Y., Guo, X., Yang, X., Duan, K., Zhao, H., Xu, B., Pu, J., Lu, A., Xiang, Y., Kattel, D. B., & Joswiak, D. (2012). Different glacier status with atmospheric circulations in Tibetan Plateau and surroundings. *Nature Climate Change*, 2(9), 663–667. <https://doi.org/10.1038/nclimate1580>

Zemp, M., Huss, M., Thibert, E., Eckert, N., McNabb, R., Huber, J., Barandun, M., Machguth, H., Nussbaumer, S. U., Gärtner-Roer, I., Thomson, L., Paul, F., Maussion, F., Kutuzov, S., & Cogley, J. G. (2019). Global glacier mass changes and their contributions to sea-level rise from 1961 to 2016. *Nature*, 568(7752), 382–386.
<https://doi.org/10.1038/s41586-019-1071-0>

Appendix

I. EOF Analysis

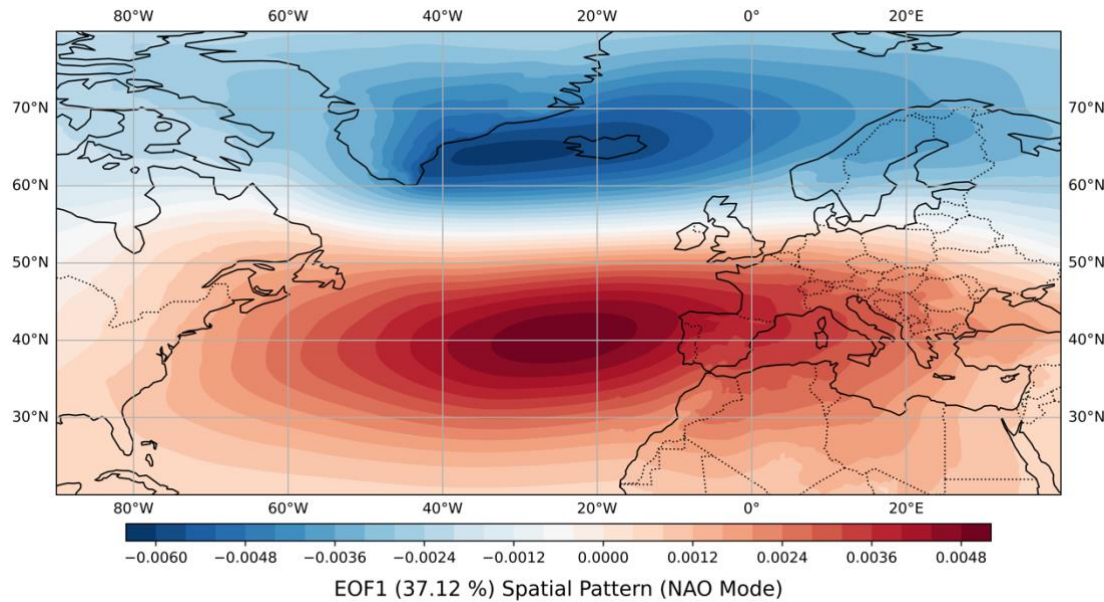


Fig. A1: First mode (North Atlantic Oscillation) from the EOF analysis of the mean sea level pressure data for the Northern Hemisphere domain (20°N - 80°N ; -90°W – 40°E), for the accumulation season (Dec-Feb). The classic NAO dipole over Azores (high) – Iceland (low) can be seen.

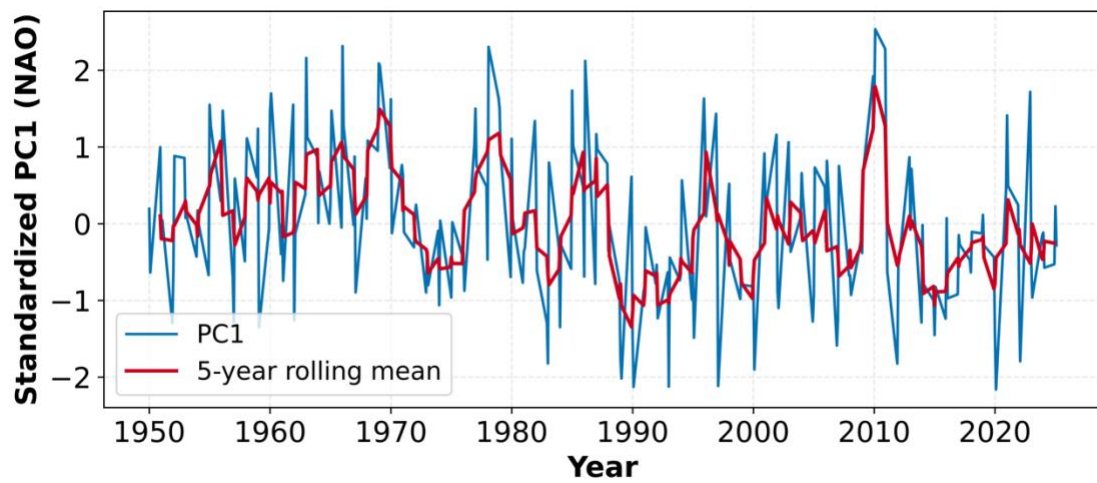


Fig. A2: Standardized PC1 corresponding to the first mode (EOF1). The blue line shows annual PC1 values. This is the raw PC1 (mean = 0, SD = 1) obtained directly from the PCA, with no seasonal aggregation. The red line is a 5-year centered rolling mean, highlighting lower frequency variability.

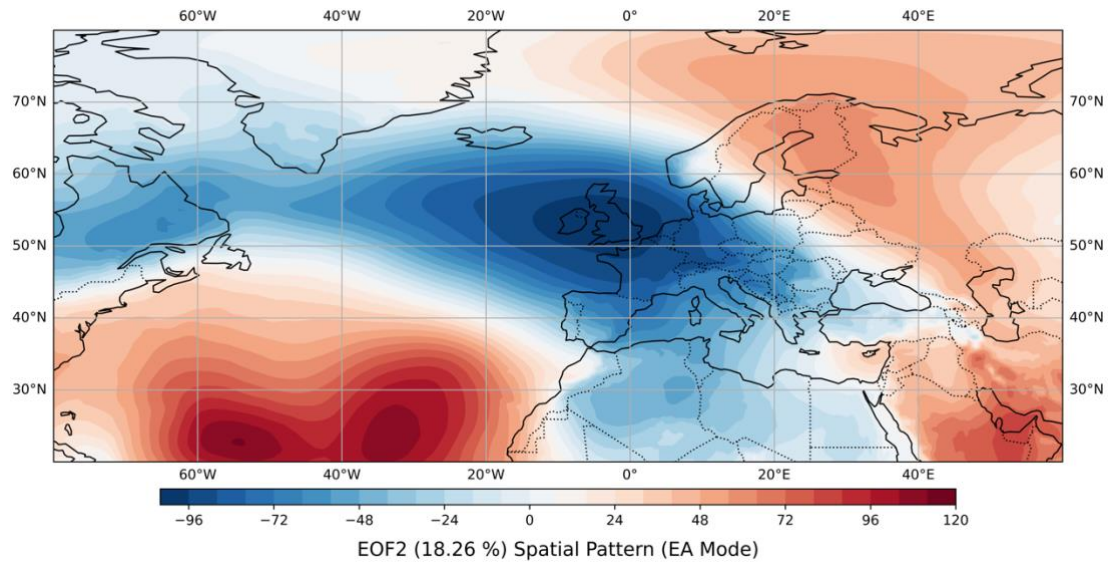


Fig. A3: Second mode (East Atlantic Oscillation) from the EOF analysis of the mean sea level pressure data for the Northern Hemisphere domain (20°N - 80°N ; -90°W – 40°E), for the accumulation season (Dec-Feb). A more zonally oriented dipole (compared to NAO) can be seen.

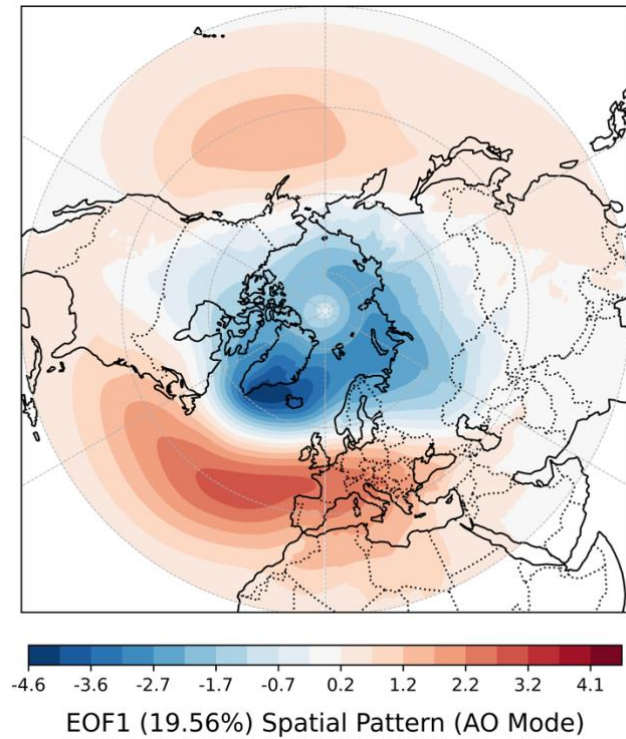


Fig. A4: First mode (Arctic Oscillation) from the EOF analysis of the mean sea level pressure data for the Northern Hemisphere domain (20°N - 90°N ; -180°W – 180°E). A nearly annular dipole pattern, with opposing SLP anomalies between the Arctic and mid-latitudes (characteristic of AO) can be seen.

II. Comparison between Hurrell's NAO and EOF derived NAO

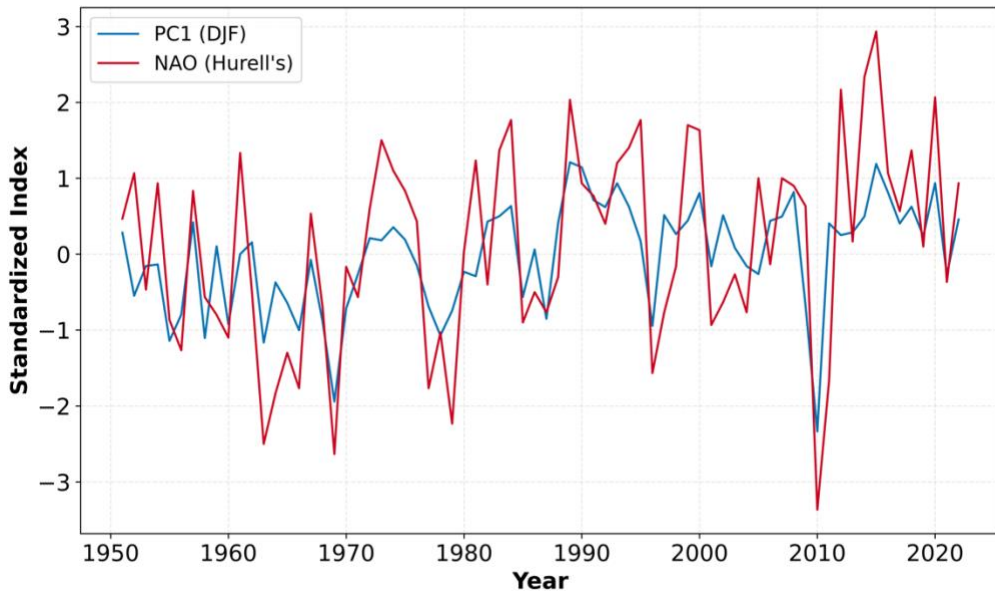


Fig. A5: Comparison of standardized Hurrell's NAO and the EOF derived NAO (PC1), 1950-2023. Both computed as DJF (Dec-Feb) seasonal means. We can observe a high degree of similarity in the patterns and phases of the EOF-derived NAO and Hurrell's NAO.

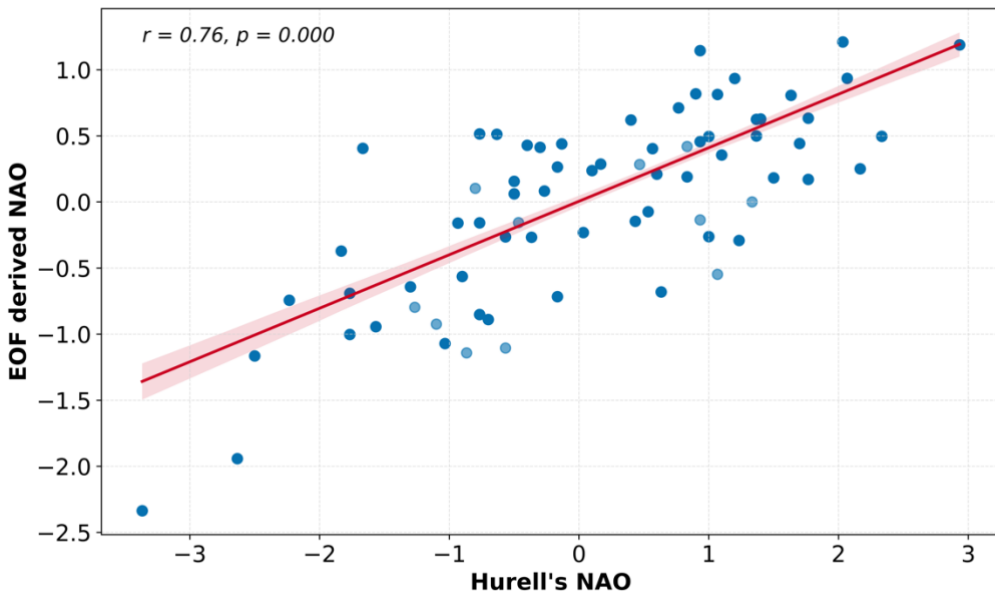


Fig. A6: Scatterplot of Hurrell's NAO and EOF derived NAO (PC1). The red line represents the linear regression fit, and the shaded area indicates the 95% CI. A strong positive correlation ($r=0.76$) proves a high degree of similarity, and that the EOF-derived NAO index captures the same large-scale atmospheric variability as a station-based index (Hurrell's).

III. Regime Shift in $B_w \sim$ NAO Coupling

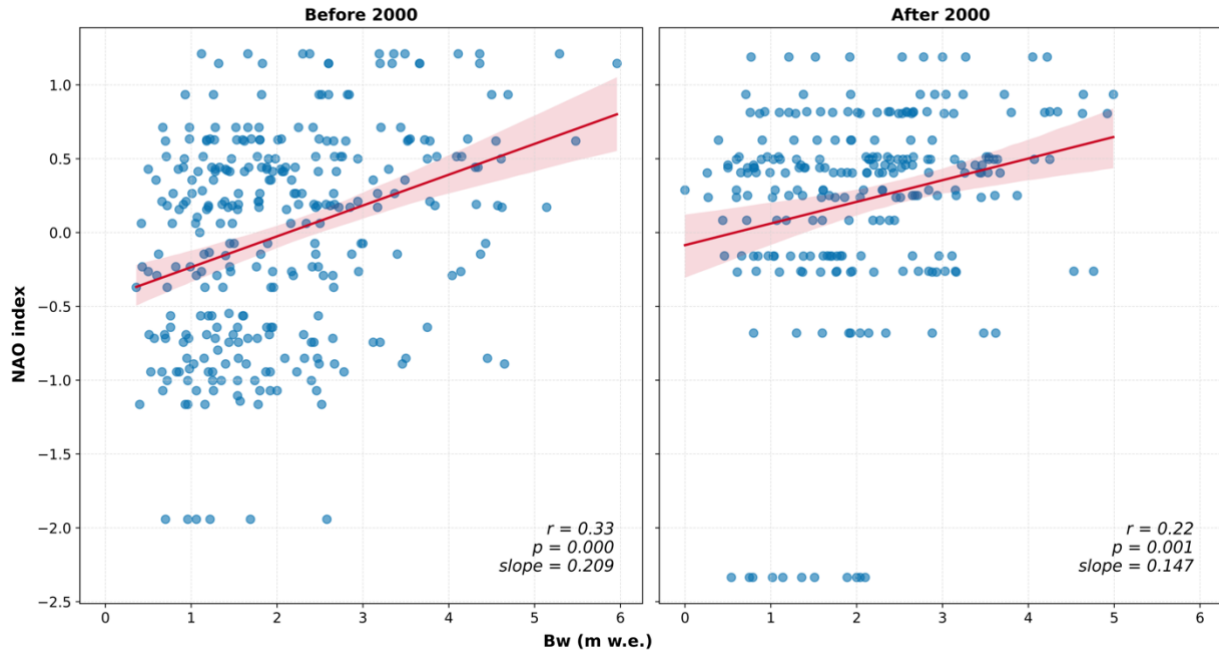


Fig. A7: Scatterplots showing the relationship between winter balance (B_w) and the North Atlantic Oscillation (NAO) index for all glaciers combined, separated into the periods before 2000 (left) and after 2000 (right). The red line represents the linear regression fit, with the shaded area indicating the 95% CI. A statistically significant weakening in the $B_w \sim$ NAO relationship is evident after 2000, with both the correlation coefficient and slope decreasing compared to the earlier period.

IV. Complete Glacier-wise Modelling Results

Location of glaciers included in this study: Alf- Ålfotbreen, Aus- Austdalsbreen, Eng-Engabreen, Grås- Gråsubreen, Grå- Gråfjellsbrea, Han- Hansebreen, Hell- Hellstugubreen, Lan- Langfjordjøkelen, Nig- Nigardsbreen, Rem-Rembesdalskåka, Sto- Storbreen.

Table A1: Annual Mass Balance (B_a)

| Glacier | Model Combination | Model Type | R ² Score | RMSE |
|---------|-------------------|------------|----------------------|-------|
| Alf | Ridge + Rec | Non-linear | 0.654 | 0.496 |
| Alf | Ridge + Seq | Non-linear | 0.601 | 0.532 |
| Alf | Ridge + Tree | Non-linear | 0.57 | 0.552 |
| Alf | Bag + Rec | Non-linear | 0.47 | 0.613 |
| Alf | Bag + Seq | Non-linear | 0.413 | 0.645 |
| Alf | Bag + Tree | Non-linear | 0.564 | 0.556 |
| Alf | ARD + Rec | Linear | 0.662 | 0.489 |
| Alf | ARD + Seq | Linear | 0.598 | 0.534 |
| Alf | ARD + Tree | Linear | 0.584 | 0.543 |
| Alf | RF + Rec | Non-linear | 0.455 | 0.622 |
| Alf | RF + Seq | Non-linear | 0.428 | 0.636 |
| Alf | RF + Tree | Non-linear | 0.525 | 0.58 |
| Alf | XGB + Rec | Non-linear | 0.256 | 0.726 |
| Alf | XGB + Seq | Non-linear | -0.012 | 0.847 |
| Alf | XGB + Tree | Non-linear | 0.349 | 0.679 |
| Alf | BYR + Rec | Non-linear | 0.651 | 0.498 |
| Alf | BYR + Seq | Non-linear | 0.601 | 0.532 |
| Alf | BYR + Tree | Non-linear | 0.573 | 0.55 |
| Aus | Ridge + Rec | Non-linear | 0.522 | 0.645 |
| Aus | Ridge + Seq | Non-linear | 0.324 | 0.768 |
| Aus | Ridge + Tree | Non-linear | 0.685 | 0.524 |
| Aus | Bag + Rec | Non-linear | 0.705 | 0.507 |
| Aus | Bag + Seq | Non-linear | 0.381 | 0.735 |
| Aus | Bag + Tree | Non-linear | 0.647 | 0.555 |
| Aus | ARD + Rec | Linear | 0.441 | 0.698 |
| Aus | ARD + Seq | Linear | 0.15 | 0.861 |
| Aus | ARD + Tree | Linear | 0.652 | 0.551 |
| Aus | RF + Rec | Non-linear | 0.708 | 0.504 |
| Aus | RF + Seq | Non-linear | 0.369 | 0.742 |
| Aus | RF + Tree | Non-linear | 0.642 | 0.559 |
| Aus | XGB + Rec | Non-linear | 0.754 | 0.464 |
| Aus | XGB + Seq | Non-linear | -0.228 | 1.035 |
| Aus | XGB + Tree | Non-linear | 0.496 | 0.663 |
| Aus | BYR + Rec | Non-linear | 0.303 | 0.78 |
| Aus | BYR + Seq | Non-linear | 0.317 | 0.772 |

| | | | | |
|------|--------------|------------|--------|-------|
| Aus | BYR + Tree | Non-linear | 0.149 | 0.862 |
| Eng | Ridge + Rec | Non-linear | 0.473 | 0.767 |
| Eng | Ridge + Seq | Non-linear | 0.444 | 0.789 |
| Eng | Ridge + Tree | Non-linear | 0.444 | 0.789 |
| Eng | Bag + Rec | Non-linear | 0.319 | 0.873 |
| Eng | Bag + Seq | Non-linear | 0.223 | 0.932 |
| Eng | Bag + Tree | Non-linear | 0.223 | 0.932 |
| Eng | ARD + Rec | Linear | 0.595 | 0.673 |
| Eng | ARD + Seq | Linear | 0.595 | 0.673 |
| Eng | ARD + Tree | Linear | 0.595 | 0.673 |
| Eng | RF + Rec | Non-linear | 0.345 | 0.856 |
| Eng | RF + Seq | Non-linear | 0.213 | 0.938 |
| Eng | RF + Tree | Non-linear | 0.213 | 0.938 |
| Eng | XGB + Rec | Non-linear | 0.069 | 1.02 |
| Eng | XGB + Seq | Non-linear | -0.113 | 1.116 |
| Eng | XGB + Tree | Non-linear | -0.311 | 1.211 |
| Eng | BYR + Rec | Non-linear | 0.448 | 0.785 |
| Eng | BYR + Seq | Non-linear | 0.489 | 0.756 |
| Eng | BYR + Tree | Non-linear | 0.489 | 0.756 |
| Graf | Ridge + Rec | Non-linear | 0.424 | 0.877 |
| Graf | Ridge + Seq | Non-linear | 0.531 | 0.792 |
| Graf | Ridge + Tree | Non-linear | 0.4 | 0.896 |
| Graf | Bag + Rec | Non-linear | 0.23 | 1.014 |
| Graf | Bag + Seq | Non-linear | 0.275 | 0.984 |
| Graf | Bag + Tree | Non-linear | 0.211 | 1.027 |
| Graf | ARD + Rec | Linear | 0.497 | 0.82 |
| Graf | ARD + Seq | Linear | 0.375 | 0.914 |
| Graf | ARD + Tree | Linear | 0.496 | 0.82 |
| Graf | RF + Rec | Non-linear | 0.243 | 1.006 |
| Graf | RF + Seq | Non-linear | 0.303 | 0.965 |
| Graf | RF + Tree | Non-linear | 0.191 | 1.04 |
| Graf | XGB + Rec | Non-linear | 0.224 | 1.018 |
| Graf | XGB + Seq | Non-linear | 0.187 | 1.042 |
| Graf | XGB + Tree | Non-linear | -0.032 | 1.174 |
| Graf | BYR + Rec | Non-linear | 0.241 | 1.007 |
| Graf | BYR + Seq | Non-linear | 0.241 | 1.007 |
| Graf | BYR + Tree | Non-linear | 0.413 | 0.886 |
| Gras | Ridge + Rec | Non-linear | 0.101 | 0.878 |
| Gras | Ridge + Seq | Non-linear | 0.102 | 0.878 |
| Gras | Ridge + Tree | Non-linear | 0.011 | 0.921 |
| Gras | Bag + Rec | Non-linear | 0.021 | 0.916 |
| Gras | Bag + Seq | Non-linear | 0.276 | 0.788 |
| Gras | Bag + Tree | Non-linear | 0.367 | 0.737 |
| Gras | ARD + Rec | Linear | -0.139 | 0.988 |

| | | | | |
|------|--------------|------------|--------|-------|
| Gras | ARD + Seq | Linear | 0.074 | 0.891 |
| Gras | ARD + Tree | Linear | 0.073 | 0.892 |
| Gras | RF + Rec | Non-linear | 0.025 | 0.915 |
| Gras | RF + Seq | Non-linear | 0.289 | 0.781 |
| Gras | RF + Tree | Non-linear | 0.381 | 0.729 |
| Gras | XGB + Rec | Non-linear | -0.315 | 1.062 |
| Gras | XGB + Seq | Non-linear | 0.227 | 0.814 |
| Gras | XGB + Tree | Non-linear | 0.026 | 0.914 |
| Gras | BYR + Rec | Non-linear | -0.017 | 0.934 |
| Gras | BYR + Seq | Non-linear | 0.093 | 0.882 |
| Gras | BYR + Tree | Non-linear | -0.025 | 0.938 |
| Han | Ridge + Rec | Non-linear | 0.573 | 0.553 |
| Han | Ridge + Seq | Non-linear | 0.507 | 0.594 |
| Han | Ridge + Tree | Non-linear | 0.5 | 0.598 |
| Han | Bag + Rec | Non-linear | 0.646 | 0.503 |
| Han | Bag + Seq | Non-linear | 0.456 | 0.624 |
| Han | Bag + Tree | Non-linear | 0.637 | 0.51 |
| Han | ARD + Rec | Linear | 0.7 | 0.464 |
| Han | ARD + Seq | Linear | 0.525 | 0.583 |
| Han | ARD + Tree | Linear | 0.594 | 0.539 |
| Han | RF + Rec | Non-linear | 0.643 | 0.505 |
| Han | RF + Seq | Non-linear | 0.452 | 0.626 |
| Han | RF + Tree | Non-linear | 0.603 | 0.533 |
| Han | XGB + Rec | Non-linear | 0.327 | 0.694 |
| Han | XGB + Seq | Non-linear | 0.188 | 0.762 |
| Han | XGB + Tree | Non-linear | 0.258 | 0.728 |
| Han | BYR + Rec | Non-linear | 0.228 | 0.743 |
| Han | BYR + Seq | Non-linear | 0.489 | 0.604 |
| Han | BYR + Tree | Non-linear | 0.552 | 0.566 |
| Hell | Ridge + Rec | Non-linear | 0.295 | 0.884 |
| Hell | Ridge + Seq | Non-linear | 0.264 | 0.903 |
| Hell | Ridge + Tree | Non-linear | 0.291 | 0.887 |
| Hell | Bag + Rec | Non-linear | 0.438 | 0.79 |
| Hell | Bag + Seq | Non-linear | -0.086 | 1.097 |
| Hell | Bag + Tree | Non-linear | 0.398 | 0.817 |
| Hell | ARD + Rec | Linear | 0.236 | 0.921 |
| Hell | ARD + Seq | Linear | 0.299 | 0.882 |
| Hell | ARD + Tree | Linear | 0.23 | 0.924 |
| Hell | RF + Rec | Non-linear | 0.422 | 0.801 |
| Hell | RF + Seq | Non-linear | -0.022 | 1.065 |
| Hell | RF + Tree | Non-linear | 0.164 | 0.963 |
| Hell | XGB + Rec | Non-linear | 0.399 | 0.816 |
| Hell | XGB + Seq | Non-linear | -0.2 | 1.154 |
| Hell | XGB + Tree | Non-linear | 0.073 | 1.014 |

| | | | | |
|------|--------------|------------|--------|-------|
| Hell | BYR + Rec | Non-linear | 0.018 | 1.044 |
| Hell | BYR + Seq | Non-linear | 0.244 | 0.916 |
| Hell | BYR + Tree | Non-linear | 0.32 | 0.868 |
| Lan | Ridge + Rec | Non-linear | 0.05 | 1.089 |
| Lan | Ridge + Seq | Non-linear | 0.124 | 1.046 |
| Lan | Ridge + Tree | Non-linear | -0.193 | 1.221 |
| Lan | Bag + Rec | Non-linear | -0.082 | 1.163 |
| Lan | Bag + Seq | Non-linear | -0.128 | 1.187 |
| Lan | Bag + Tree | Non-linear | -0.162 | 1.205 |
| Lan | ARD + Rec | Linear | -0.099 | 1.172 |
| Lan | ARD + Seq | Linear | 0.094 | 1.064 |
| Lan | ARD + Tree | Linear | -0.102 | 1.174 |
| Lan | RF + Rec | Non-linear | -0.076 | 1.16 |
| Lan | RF + Seq | Non-linear | -0.121 | 1.184 |
| Lan | RF + Tree | Non-linear | -0.236 | 1.243 |
| Lan | XGB + Rec | Non-linear | -0.501 | 1.37 |
| Lan | XGB + Seq | Non-linear | -0.845 | 1.518 |
| Lan | XGB + Tree | Non-linear | -0.566 | 1.399 |
| Lan | BYR + Rec | Non-linear | 0.018 | 1.108 |
| Lan | BYR + Seq | Non-linear | 0.116 | 1.051 |
| Lan | BYR + Tree | Non-linear | 0.011 | 1.112 |
| Nig | Ridge + Rec | Non-linear | 0.549 | 0.627 |
| Nig | Ridge + Seq | Non-linear | 0.59 | 0.598 |
| Nig | Ridge + Tree | Non-linear | 0.491 | 0.666 |
| Nig | Bag + Rec | Non-linear | 0.501 | 0.659 |
| Nig | Bag + Seq | Non-linear | 0.331 | 0.764 |
| Nig | Bag + Tree | Non-linear | 0.42 | 0.711 |
| Nig | ARD + Rec | Linear | 0.659 | 0.545 |
| Nig | ARD + Seq | Linear | 0.596 | 0.593 |
| Nig | ARD + Tree | Linear | 0.659 | 0.545 |
| Nig | RF + Rec | Non-linear | 0.508 | 0.655 |
| Nig | RF + Seq | Non-linear | 0.314 | 0.773 |
| Nig | RF + Tree | Non-linear | 0.416 | 0.713 |
| Nig | XGB + Rec | Non-linear | 0.369 | 0.742 |
| Nig | XGB + Seq | Non-linear | 0.045 | 0.912 |
| Nig | XGB + Tree | Non-linear | 0.634 | 0.564 |
| Nig | BYR + Rec | Non-linear | 0.345 | 0.756 |
| Nig | BYR + Seq | Non-linear | 0.622 | 0.574 |
| Nig | BYR + Tree | Non-linear | 0.558 | 0.621 |
| Rem | Ridge + Rec | Non-linear | 0.614 | 0.559 |
| Rem | Ridge + Seq | Non-linear | 0.676 | 0.512 |
| Rem | Ridge + Tree | Non-linear | 0.704 | 0.489 |
| Rem | Bag + Rec | Non-linear | 0.389 | 0.703 |
| Rem | Bag + Seq | Non-linear | 0.482 | 0.647 |

| | | | | |
|-----|--------------|------------|--------|-------|
| Rem | Bag + Tree | Non-linear | 0.409 | 0.692 |
| Rem | ARD + Rec | Linear | 0.565 | 0.593 |
| Rem | ARD + Seq | Linear | 0.814 | 0.388 |
| Rem | ARD + Tree | Linear | 0.587 | 0.578 |
| Rem | RF + Rec | Non-linear | 0.376 | 0.71 |
| Rem | RF + Seq | Non-linear | 0.474 | 0.652 |
| Rem | RF + Tree | Non-linear | 0.396 | 0.699 |
| Rem | XGB + Rec | Non-linear | 0.14 | 0.834 |
| Rem | XGB + Seq | Non-linear | 0.004 | 0.898 |
| Rem | XGB + Tree | Non-linear | -0.179 | 0.977 |
| Rem | BYR + Rec | Non-linear | 0.622 | 0.553 |
| Rem | BYR + Seq | Non-linear | 0.811 | 0.391 |
| Rem | BYR + Tree | Non-linear | 0.742 | 0.457 |
| Sto | Ridge + Rec | Non-linear | 0.407 | 0.771 |
| Sto | Ridge + Seq | Non-linear | 0.222 | 0.883 |
| Sto | Ridge + Tree | Non-linear | 0.049 | 0.977 |
| Sto | Bag + Rec | Non-linear | 0.448 | 0.744 |
| Sto | Bag + Seq | Non-linear | 0.364 | 0.799 |
| Sto | Bag + Tree | Non-linear | 0.408 | 0.771 |
| Sto | ARD + Rec | Linear | 0.413 | 0.768 |
| Sto | ARD + Seq | Linear | 0.399 | 0.777 |
| Sto | ARD + Tree | Linear | 0.413 | 0.768 |
| Sto | RF + Rec | Non-linear | 0.442 | 0.749 |
| Sto | RF + Seq | Non-linear | 0.369 | 0.796 |
| Sto | RF + Tree | Non-linear | 0.405 | 0.773 |
| Sto | XGB + Rec | Non-linear | 0.254 | 0.865 |
| Sto | XGB + Seq | Non-linear | 0.066 | 0.968 |
| Sto | XGB + Tree | Non-linear | 0.065 | 0.969 |
| Sto | BYR + Rec | Non-linear | 0.478 | 0.724 |
| Sto | BYR + Seq | Non-linear | 0.291 | 0.844 |
| Sto | BYR + Tree | Non-linear | 0.18 | 0.907 |

Table A2: Winter Mass Balance (B_w):

| Glacier | Model Combination | Model Type | R ² Score | RMSE |
|---------|-------------------|------------|----------------------|-------|
| Alf | Ridge + Rec | Non-linear | 0.113 | 0.627 |
| Alf | Ridge + Seq | Non-linear | -0.387 | 0.784 |
| Alf | Ridge + Tree | Non-linear | -0.317 | 0.764 |
| Alf | Bag + Rec | Non-linear | -0.209 | 0.732 |
| Alf | Bag + Seq | Non-linear | -0.435 | 0.798 |
| Alf | Bag + Tree | Non-linear | -0.395 | 0.787 |
| Alf | ARD + Rec | Linear | 0.257 | 0.574 |
| Alf | ARD + Seq | Linear | -0.34 | 0.771 |
| Alf | ARD + Tree | Linear | 0.257 | 0.574 |

| | | | | |
|-----|--------------|------------|--------|-------|
| Alf | RF + Rec | Non-linear | -0.23 | 0.739 |
| Alf | RF + Seq | Non-linear | -0.423 | 0.795 |
| Alf | RF + Tree | Non-linear | -0.403 | 0.789 |
| Alf | XGB + Rec | Non-linear | -0.284 | 0.755 |
| Alf | XGB + Seq | Non-linear | -1.166 | 0.98 |
| Alf | XGB + Tree | Non-linear | -0.464 | 0.806 |
| Alf | BYR + Rec | Non-linear | 0.06 | 0.646 |
| Alf | BYR + Seq | Non-linear | -0.357 | 0.776 |
| Alf | BYR + Tree | Non-linear | -0.34 | 0.771 |
| Aus | Ridge + Rec | Non-linear | 0.361 | 0.563 |
| Aus | Ridge + Seq | Non-linear | -0.055 | 0.723 |
| Aus | Ridge + Tree | Non-linear | 0.648 | 0.418 |
| Aus | Bag + Rec | Non-linear | 0.539 | 0.478 |
| Aus | Bag + Seq | Non-linear | -0.149 | 0.755 |
| Aus | Bag + Tree | Non-linear | 0.324 | 0.579 |
| Aus | ARD + Rec | Linear | 0.603 | 0.444 |
| Aus | ARD + Seq | Linear | -0.012 | 0.708 |
| Aus | ARD + Tree | Linear | 0.602 | 0.444 |
| Aus | RF + Rec | Non-linear | 0.509 | 0.493 |
| Aus | RF + Seq | Non-linear | -0.185 | 0.766 |
| Aus | RF + Tree | Non-linear | 0.48 | 0.508 |
| Aus | XGB + Rec | Non-linear | 0.57 | 0.461 |
| Aus | XGB + Seq | Non-linear | -0.305 | 0.804 |
| Aus | XGB + Tree | Non-linear | 0.25 | 0.61 |
| Aus | BYR + Rec | Non-linear | 0.326 | 0.578 |
| Aus | BYR + Seq | Non-linear | -0.05 | 0.721 |
| Aus | BYR + Tree | Non-linear | 0.609 | 0.44 |
| Eng | Ridge + Rec | Non-linear | 0.523 | 0.558 |
| Eng | Ridge + Seq | Non-linear | 0.429 | 0.611 |
| Eng | Ridge + Tree | Non-linear | 0.466 | 0.591 |
| Eng | Bag + Rec | Non-linear | 0.316 | 0.669 |
| Eng | Bag + Seq | Non-linear | -0.103 | 0.849 |
| Eng | Bag + Tree | Non-linear | -0.103 | 0.849 |
| Eng | ARD + Rec | Linear | 0.572 | 0.529 |
| Eng | ARD + Seq | Linear | 0.572 | 0.529 |
| Eng | ARD + Tree | Linear | 0.572 | 0.529 |
| Eng | RF + Rec | Non-linear | 0.292 | 0.68 |
| Eng | RF + Seq | Non-linear | -0.101 | 0.848 |
| Eng | RF + Tree | Non-linear | 0.131 | 0.754 |
| Eng | XGB + Rec | Non-linear | -0.046 | 0.827 |
| Eng | XGB + Seq | Non-linear | -0.462 | 0.977 |
| Eng | XGB + Tree | Non-linear | -0.462 | 0.977 |
| Eng | BYR + Rec | Non-linear | 0.453 | 0.598 |
| Eng | BYR + Seq | Non-linear | 0.43 | 0.61 |

| | | | | |
|------|--------------|------------|--------|-------|
| Eng | BYR + Tree | Non-linear | 0.466 | 0.591 |
| Graf | Ridge + Rec | Non-linear | -0.134 | 1.536 |
| Graf | Ridge + Seq | Non-linear | 0.078 | 1.385 |
| Graf | Ridge + Tree | Non-linear | 0.316 | 1.193 |
| Graf | Bag + Rec | Non-linear | 0.179 | 1.307 |
| Graf | Bag + Seq | Non-linear | 0.324 | 1.186 |
| Graf | Bag + Tree | Non-linear | 0.453 | 1.067 |
| Graf | ARD + Rec | Linear | 0.341 | 1.171 |
| Graf | ARD + Seq | Linear | 0.339 | 1.173 |
| Graf | ARD + Tree | Linear | 0.339 | 1.173 |
| Graf | RF + Rec | Non-linear | 0.199 | 1.291 |
| Graf | RF + Seq | Non-linear | 0.309 | 1.2 |
| Graf | RF + Tree | Non-linear | 0.46 | 1.06 |
| Graf | XGB + Rec | Non-linear | 0.305 | 1.203 |
| Graf | XGB + Seq | Non-linear | 0.105 | 1.365 |
| Graf | XGB + Tree | Non-linear | 0.403 | 1.115 |
| Graf | BYR + Rec | Non-linear | 0.078 | 1.385 |
| Graf | BYR + Seq | Non-linear | 0.028 | 1.422 |
| Graf | BYR + Tree | Non-linear | 0.154 | 1.327 |
| Gras | Ridge + Rec | Non-linear | -0.223 | 0.854 |
| Gras | Ridge + Seq | Non-linear | -0.458 | 0.933 |
| Gras | Ridge + Tree | Non-linear | -0.04 | 0.788 |
| Gras | Bag + Rec | Non-linear | -0.024 | 0.782 |
| Gras | Bag + Seq | Non-linear | -0.37 | 0.904 |
| Gras | Bag + Tree | Non-linear | 0.061 | 0.749 |
| Gras | ARD + Rec | Linear | -0.212 | 0.851 |
| Gras | ARD + Seq | Linear | -0.357 | 0.9 |
| Gras | ARD + Tree | Linear | 0.138 | 0.718 |
| Gras | RF + Rec | Non-linear | 0.049 | 0.753 |
| Gras | RF + Seq | Non-linear | -0.352 | 0.898 |
| Gras | RF + Tree | Non-linear | 0.131 | 0.72 |
| Gras | XGB + Rec | Non-linear | -0.123 | 0.819 |
| Gras | XGB + Seq | Non-linear | -1.279 | 1.166 |
| Gras | XGB + Tree | Non-linear | -0.143 | 0.826 |
| Gras | BYR + Rec | Non-linear | -0.225 | 0.855 |
| Gras | BYR + Seq | Non-linear | -0.411 | 0.918 |
| Gras | BYR + Tree | Non-linear | -0.131 | 0.822 |
| Han | Ridge + Rec | Non-linear | 0.059 | 0.734 |
| Han | Ridge + Seq | Non-linear | -0.218 | 0.835 |
| Han | Ridge + Tree | Non-linear | -0.218 | 0.835 |
| Han | Bag + Rec | Non-linear | -0.197 | 0.828 |
| Han | Bag + Seq | Non-linear | -0.393 | 0.893 |
| Han | Bag + Tree | Non-linear | -0.393 | 0.893 |
| Han | ARD + Rec | Linear | 0.476 | 0.548 |

| | | | | |
|------|--------------|------------|--------|-------|
| Han | ARD + Seq | Linear | 0.474 | 0.549 |
| Han | ARD + Tree | Linear | 0.474 | 0.549 |
| Han | RF + Rec | Non-linear | -0.17 | 0.818 |
| Han | RF + Seq | Non-linear | -0.368 | 0.885 |
| Han | RF + Tree | Non-linear | -0.368 | 0.885 |
| Han | XGB + Rec | Non-linear | -0.544 | 0.94 |
| Han | XGB + Seq | Non-linear | -0.537 | 0.938 |
| Han | XGB + Tree | Non-linear | -0.537 | 0.938 |
| Han | BYR + Rec | Non-linear | 0.041 | 0.741 |
| Han | BYR + Seq | Non-linear | -0.208 | 0.831 |
| Han | BYR + Tree | Non-linear | -0.208 | 0.831 |
| Hell | Ridge + Rec | Non-linear | 0.054 | 0.817 |
| Hell | Ridge + Seq | Non-linear | 0.307 | 0.699 |
| Hell | Ridge + Tree | Non-linear | 0.384 | 0.659 |
| Hell | Bag + Rec | Non-linear | 0.264 | 0.72 |
| Hell | Bag + Seq | Non-linear | 0.056 | 0.816 |
| Hell | Bag + Tree | Non-linear | 0.173 | 0.764 |
| Hell | ARD + Rec | Linear | 0.209 | 0.747 |
| Hell | ARD + Seq | Linear | 0.365 | 0.669 |
| Hell | ARD + Tree | Linear | 0.187 | 0.757 |
| Hell | RF + Rec | Non-linear | 0.24 | 0.732 |
| Hell | RF + Seq | Non-linear | 0.053 | 0.817 |
| Hell | RF + Tree | Non-linear | 0.209 | 0.747 |
| Hell | XGB + Rec | Non-linear | -0.049 | 0.86 |
| Hell | XGB + Seq | Non-linear | -0.078 | 0.872 |
| Hell | XGB + Tree | Non-linear | 0.132 | 0.782 |
| Hell | BYR + Rec | Non-linear | -0.061 | 0.865 |
| Hell | BYR + Seq | Non-linear | 0.297 | 0.704 |
| Hell | BYR + Tree | Non-linear | 0.297 | 0.704 |
| Lan | Ridge + Rec | Non-linear | 0.298 | 0.84 |
| Lan | Ridge + Seq | Non-linear | 0.317 | 0.829 |
| Lan | Ridge + Tree | Non-linear | 0.142 | 0.929 |
| Lan | Bag + Rec | Non-linear | 0.182 | 0.907 |
| Lan | Bag + Seq | Non-linear | 0.352 | 0.807 |
| Lan | Bag + Tree | Non-linear | 0.207 | 0.893 |
| Lan | ARD + Rec | Linear | 0.085 | 0.959 |
| Lan | ARD + Seq | Linear | -0.079 | 1.042 |
| Lan | ARD + Tree | Linear | 0.174 | 0.911 |
| Lan | RF + Rec | Non-linear | 0.141 | 0.93 |
| Lan | RF + Seq | Non-linear | 0.331 | 0.82 |
| Lan | RF + Tree | Non-linear | 0.186 | 0.905 |
| Lan | XGB + Rec | Non-linear | -0.419 | 1.195 |
| Lan | XGB + Seq | Non-linear | 0.002 | 1.002 |
| Lan | XGB + Tree | Non-linear | -0.046 | 1.026 |

| | | | | |
|-----|--------------|------------|--------|-------|
| Lan | BYR + Rec | Non-linear | 0.301 | 0.839 |
| Lan | BYR + Seq | Non-linear | 0.318 | 0.828 |
| Lan | BYR + Tree | Non-linear | 0.407 | 0.772 |
| Nig | Ridge + Rec | Non-linear | 0.351 | 0.67 |
| Nig | Ridge + Seq | Non-linear | 0.084 | 0.796 |
| Nig | Ridge + Tree | Non-linear | 0.055 | 0.808 |
| Nig | Bag + Rec | Non-linear | 0.462 | 0.61 |
| Nig | Bag + Seq | Non-linear | -0.25 | 0.929 |
| Nig | Bag + Tree | Non-linear | 0.466 | 0.607 |
| Nig | ARD + Rec | Linear | 0.589 | 0.533 |
| Nig | ARD + Seq | Linear | -0.104 | 0.873 |
| Nig | ARD + Tree | Linear | 0.526 | 0.573 |
| Nig | RF + Rec | Non-linear | 0.433 | 0.626 |
| Nig | RF + Seq | Non-linear | -0.269 | 0.937 |
| Nig | RF + Tree | Non-linear | 0.444 | 0.62 |
| Nig | XGB + Rec | Non-linear | 0.18 | 0.753 |
| Nig | XGB + Seq | Non-linear | -0.633 | 1.063 |
| Nig | XGB + Tree | Non-linear | -0.093 | 0.869 |
| Nig | BYR + Rec | Non-linear | 0.336 | 0.677 |
| Nig | BYR + Seq | Non-linear | 0.01 | 0.827 |
| Nig | BYR + Tree | Non-linear | -0.104 | 0.873 |
| Rem | Ridge + Rec | Non-linear | 0.598 | 0.41 |
| Rem | Ridge + Seq | Non-linear | 0.399 | 0.501 |
| Rem | Ridge + Tree | Non-linear | 0.19 | 0.581 |
| Rem | Bag + Rec | Non-linear | 0.448 | 0.48 |
| Rem | Bag + Seq | Non-linear | 0.471 | 0.47 |
| Rem | Bag + Tree | Non-linear | 0.322 | 0.532 |
| Rem | ARD + Rec | Linear | 0.686 | 0.362 |
| Rem | ARD + Seq | Linear | 0.149 | 0.596 |
| Rem | ARD + Tree | Linear | 0.79 | 0.296 |
| Rem | RF + Rec | Non-linear | 0.413 | 0.495 |
| Rem | RF + Seq | Non-linear | 0.489 | 0.462 |
| Rem | RF + Tree | Non-linear | 0.34 | 0.525 |
| Rem | XGB + Rec | Non-linear | 0.298 | 0.541 |
| Rem | XGB + Seq | Non-linear | -0.393 | 0.762 |
| Rem | XGB + Tree | Non-linear | -0.037 | 0.658 |
| Rem | BYR + Rec | Non-linear | 0.664 | 0.374 |
| Rem | BYR + Seq | Non-linear | 0.389 | 0.505 |
| Rem | BYR + Tree | Non-linear | 0.149 | 0.596 |
| Sto | Ridge + Rec | Non-linear | 0.239 | 0.653 |
| Sto | Ridge + Seq | Non-linear | 0.203 | 0.668 |
| Sto | Ridge + Tree | Non-linear | 0.261 | 0.643 |
| Sto | Bag + Rec | Non-linear | 0.312 | 0.62 |
| Sto | Bag + Seq | Non-linear | 0.194 | 0.672 |

| | | | | |
|-----|------------|------------|--------|-------|
| Sto | Bag + Tree | Non-linear | 0.127 | 0.699 |
| Sto | ARD + Rec | Linear | 0.289 | 0.631 |
| Sto | ARD + Seq | Linear | 0.244 | 0.651 |
| Sto | ARD + Tree | Linear | 0.271 | 0.639 |
| Sto | RF + Rec | Non-linear | 0.313 | 0.62 |
| Sto | RF + Seq | Non-linear | 0.18 | 0.677 |
| Sto | RF + Tree | Non-linear | 0.115 | 0.704 |
| Sto | XGB + Rec | Non-linear | 0.436 | 0.562 |
| Sto | XGB + Seq | Non-linear | -0.346 | 0.868 |
| Sto | XGB + Tree | Non-linear | -0.365 | 0.874 |
| Sto | BYR + Rec | Non-linear | 0.256 | 0.645 |
| Sto | BYR + Seq | Non-linear | 0.217 | 0.662 |
| Sto | BYR + Tree | Non-linear | 0.404 | 0.578 |

Table A3: Summer Mass Balance (B_s)

| Glacier | Model Combination | Model Type | R ² Score | RMSE |
|---------|-------------------|------------|----------------------|-------|
| Alf | Ridge + Rec | Non-linear | 0.367 | 0.74 |
| Alf | Ridge + Seq | Non-linear | -0.032 | 0.945 |
| Alf | Ridge + Tree | Non-linear | 0.236 | 0.813 |
| Alf | Bag + Rec | Non-linear | 0.093 | 0.886 |
| Alf | Bag + Seq | Non-linear | 0.063 | 0.9 |
| Alf | Bag + Tree | Non-linear | -0.141 | 0.993 |
| Alf | ARD + Rec | Linear | 0.151 | 0.857 |
| Alf | ARD + Seq | Linear | 0.05 | 0.906 |
| Alf | ARD + Tree | Linear | 0.147 | 0.859 |
| Alf | RF + Rec | Non-linear | 0.04 | 0.911 |
| Alf | RF + Seq | Non-linear | 0.044 | 0.909 |
| Alf | RF + Tree | Non-linear | -0.231 | 1.032 |
| Alf | XGB + Rec | Non-linear | -0.254 | 1.041 |
| Alf | XGB + Seq | Non-linear | -0.376 | 1.091 |
| Alf | XGB + Tree | Non-linear | -0.556 | 1.16 |
| Alf | BYR + Rec | Non-linear | 0.202 | 0.831 |
| Alf | BYR + Seq | Non-linear | -0.043 | 0.95 |
| Alf | BYR + Tree | Non-linear | -0.016 | 0.937 |
| Aus | Ridge + Rec | Non-linear | 0.208 | 0.84 |
| Aus | Ridge + Seq | Non-linear | 0.069 | 0.91 |
| Aus | Ridge + Tree | Non-linear | -0.069 | 0.976 |
| Aus | Bag + Rec | Non-linear | 0.131 | 0.88 |
| Aus | Bag + Seq | Non-linear | 0.477 | 0.682 |
| Aus | Bag + Tree | Non-linear | 0.113 | 0.888 |
| Aus | ARD + Rec | Linear | 0.07 | 0.91 |
| Aus | ARD + Seq | Linear | 0.272 | 0.805 |
| Aus | ARD + Tree | Linear | 0.271 | 0.806 |

| | | | | |
|------|--------------|------------|--------|-------|
| Aus | RF + Rec | Non-linear | 0.14 | 0.875 |
| Aus | RF + Seq | Non-linear | 0.448 | 0.701 |
| Aus | RF + Tree | Non-linear | 0.091 | 0.9 |
| Aus | XGB + Rec | Non-linear | 0.019 | 0.934 |
| Aus | XGB + Seq | Non-linear | -0.086 | 0.983 |
| Aus | XGB + Tree | Non-linear | 0.297 | 0.791 |
| Aus | BYR + Rec | Non-linear | 0.118 | 0.886 |
| Aus | BYR + Seq | Non-linear | 0.069 | 0.91 |
| Aus | BYR + Tree | Non-linear | -0.038 | 0.961 |
| Eng | Ridge + Rec | Non-linear | 0.162 | 0.826 |
| Eng | Ridge + Seq | Non-linear | 0.178 | 0.819 |
| Eng | Ridge + Tree | Non-linear | 0.137 | 0.839 |
| Eng | Bag + Rec | Non-linear | 0.347 | 0.73 |
| Eng | Bag + Seq | Non-linear | 0.017 | 0.895 |
| Eng | Bag + Tree | Non-linear | 0.082 | 0.865 |
| Eng | ARD + Rec | Linear | 0.19 | 0.813 |
| Eng | ARD + Seq | Linear | 0.165 | 0.825 |
| Eng | ARD + Tree | Linear | 0.165 | 0.825 |
| Eng | RF + Rec | Non-linear | 0.383 | 0.709 |
| Eng | RF + Seq | Non-linear | -0.026 | 0.914 |
| Eng | RF + Tree | Non-linear | 0.172 | 0.821 |
| Eng | XGB + Rec | Non-linear | -0.164 | 0.974 |
| Eng | XGB + Seq | Non-linear | -0.677 | 1.169 |
| Eng | XGB + Tree | Non-linear | -0.688 | 1.173 |
| Eng | BYR + Rec | Non-linear | -0.05 | 0.925 |
| Eng | BYR + Seq | Non-linear | 0.165 | 0.825 |
| Eng | BYR + Tree | Non-linear | -0.05 | 0.925 |
| Graf | Ridge + Rec | Non-linear | -1.048 | 2.293 |
| Graf | Ridge + Seq | Non-linear | -0.418 | 1.908 |
| Graf | Ridge + Tree | Non-linear | -0.925 | 2.223 |
| Graf | Bag + Rec | Non-linear | -1.321 | 2.44 |
| Graf | Bag + Seq | Non-linear | -1.356 | 2.459 |
| Graf | Bag + Tree | Non-linear | -1.389 | 2.476 |
| Graf | ARD + Rec | Linear | -0.541 | 1.989 |
| Graf | ARD + Seq | Linear | -0.539 | 1.988 |
| Graf | ARD + Tree | Linear | -0.528 | 1.98 |
| Graf | RF + Rec | Non-linear | -1.343 | 2.452 |
| Graf | RF + Seq | Non-linear | -1.31 | 2.435 |
| Graf | RF + Tree | Non-linear | -1.512 | 2.539 |
| Graf | XGB + Rec | Non-linear | -0.838 | 2.172 |
| Graf | XGB + Seq | Non-linear | -0.835 | 2.17 |
| Graf | XGB + Tree | Non-linear | -0.88 | 2.197 |
| Graf | BYR + Rec | Non-linear | -0.496 | 1.959 |
| Graf | BYR + Seq | Non-linear | -0.47 | 1.942 |

| | | | | |
|------|--------------|------------|--------|-------|
| Graf | BYR + Tree | Non-linear | -0.86 | 2.185 |
| Gras | Ridge + Rec | Non-linear | 0.113 | 0.936 |
| Gras | Ridge + Seq | Non-linear | 0.021 | 0.983 |
| Gras | Ridge + Tree | Non-linear | 0.075 | 0.956 |
| Gras | Bag + Rec | Non-linear | 0.068 | 0.959 |
| Gras | Bag + Seq | Non-linear | 0.249 | 0.861 |
| Gras | Bag + Tree | Non-linear | 0.301 | 0.83 |
| Gras | ARD + Rec | Linear | 0.057 | 0.965 |
| Gras | ARD + Seq | Linear | 0.057 | 0.965 |
| Gras | ARD + Tree | Linear | 0.057 | 0.965 |
| Gras | RF + Rec | Non-linear | 0.09 | 0.948 |
| Gras | RF + Seq | Non-linear | 0.247 | 0.862 |
| Gras | RF + Tree | Non-linear | 0.111 | 0.937 |
| Gras | XGB + Rec | Non-linear | 0.032 | 0.977 |
| Gras | XGB + Seq | Non-linear | -0.122 | 1.053 |
| Gras | XGB + Tree | Non-linear | 0.433 | 0.748 |
| Gras | BYR + Rec | Non-linear | 0.017 | 0.985 |
| Gras | BYR + Seq | Non-linear | 0.017 | 0.985 |
| Gras | BYR + Tree | Non-linear | -0.005 | 0.996 |
| Han | Ridge + Rec | Non-linear | 0.215 | 0.754 |
| Han | Ridge + Seq | Non-linear | 0.161 | 0.779 |
| Han | Ridge + Tree | Non-linear | -0.169 | 0.919 |
| Han | Bag + Rec | Non-linear | 0.063 | 0.823 |
| Han | Bag + Seq | Non-linear | -0.02 | 0.859 |
| Han | Bag + Tree | Non-linear | 0.075 | 0.818 |
| Han | ARD + Rec | Linear | 0.114 | 0.8 |
| Han | ARD + Seq | Linear | 0.246 | 0.739 |
| Han | ARD + Tree | Linear | -0.07 | 0.879 |
| Han | RF + Rec | Non-linear | 0.131 | 0.793 |
| Han | RF + Seq | Non-linear | -0.028 | 0.862 |
| Han | RF + Tree | Non-linear | -0.197 | 0.93 |
| Han | XGB + Rec | Non-linear | 0.071 | 0.82 |
| Han | XGB + Seq | Non-linear | -0.233 | 0.944 |
| Han | XGB + Tree | Non-linear | -0.137 | 0.907 |
| Han | BYR + Rec | Non-linear | -0.043 | 0.869 |
| Han | BYR + Seq | Non-linear | 0.232 | 0.745 |
| Han | BYR + Tree | Non-linear | -0.07 | 0.88 |
| Hell | Ridge + Rec | Non-linear | 0.208 | 0.974 |
| Hell | Ridge + Seq | Non-linear | 0.187 | 0.986 |
| Hell | Ridge + Tree | Non-linear | 0.19 | 0.985 |
| Hell | Bag + Rec | Non-linear | 0.331 | 0.895 |
| Hell | Bag + Seq | Non-linear | 0.346 | 0.885 |
| Hell | Bag + Tree | Non-linear | 0.337 | 0.891 |
| Hell | ARD + Rec | Linear | 0.14 | 1.015 |

| | | | | |
|------|--------------|------------|--------|-------|
| Hell | ARD + Seq | Linear | 0.14 | 1.015 |
| Hell | ARD + Tree | Linear | 0.138 | 1.016 |
| Hell | RF + Rec | Non-linear | 0.345 | 0.886 |
| Hell | RF + Seq | Non-linear | 0.358 | 0.877 |
| Hell | RF + Tree | Non-linear | 0.143 | 1.013 |
| Hell | XGB + Rec | Non-linear | 0.275 | 0.932 |
| Hell | XGB + Seq | Non-linear | 0.264 | 0.939 |
| Hell | XGB + Tree | Non-linear | -0.417 | 1.302 |
| Hell | BYR + Rec | Non-linear | 0.03 | 1.078 |
| Hell | BYR + Seq | Non-linear | 0.174 | 0.994 |
| Hell | BYR + Tree | Non-linear | 0.141 | 1.014 |
| Lan | Ridge + Rec | Non-linear | 0.134 | 1.184 |
| Lan | Ridge + Seq | Non-linear | 0.167 | 1.161 |
| Lan | Ridge + Tree | Non-linear | 0.186 | 1.147 |
| Lan | Bag + Rec | Non-linear | 0.146 | 1.176 |
| Lan | Bag + Seq | Non-linear | -0.009 | 1.278 |
| Lan | Bag + Tree | Non-linear | 0.114 | 1.197 |
| Lan | ARD + Rec | Linear | 0.147 | 1.175 |
| Lan | ARD + Seq | Linear | 0.147 | 1.175 |
| Lan | ARD + Tree | Linear | 0.147 | 1.175 |
| Lan | RF + Rec | Non-linear | 0.141 | 1.179 |
| Lan | RF + Seq | Non-linear | -0.01 | 1.279 |
| Lan | RF + Tree | Non-linear | 0.125 | 1.19 |
| Lan | XGB + Rec | Non-linear | 0.074 | 1.224 |
| Lan | XGB + Seq | Non-linear | -0.165 | 1.373 |
| Lan | XGB + Tree | Non-linear | -0.059 | 1.309 |
| Lan | BYR + Rec | Non-linear | -0.031 | 1.292 |
| Lan | BYR + Seq | Non-linear | 0.147 | 1.175 |
| Lan | BYR + Tree | Non-linear | 0.116 | 1.196 |
| Nig | Ridge + Rec | Non-linear | 0.413 | 0.725 |
| Nig | Ridge + Seq | Non-linear | 0.172 | 0.861 |
| Nig | Ridge + Tree | Non-linear | 0.407 | 0.729 |
| Nig | Bag + Rec | Non-linear | 0.177 | 0.858 |
| Nig | Bag + Seq | Non-linear | -0.174 | 1.025 |
| Nig | Bag + Tree | Non-linear | -0.289 | 1.075 |
| Nig | ARD + Rec | Linear | 0.401 | 0.733 |
| Nig | ARD + Seq | Linear | 0.312 | 0.785 |
| Nig | ARD + Tree | Linear | 0.401 | 0.733 |
| Nig | RF + Rec | Non-linear | 0.139 | 0.878 |
| Nig | RF + Seq | Non-linear | -0.193 | 1.034 |
| Nig | RF + Tree | Non-linear | -0.244 | 1.056 |
| Nig | XGB + Rec | Non-linear | -0.176 | 1.027 |
| Nig | XGB + Seq | Non-linear | -0.197 | 1.035 |
| Nig | XGB + Tree | Non-linear | -0.377 | 1.111 |

| | | | | |
|-----|--------------|------------|--------|-------|
| Nig | BYR + Rec | Non-linear | 0.327 | 0.776 |
| Nig | BYR + Seq | Non-linear | 0.106 | 0.895 |
| Nig | BYR + Tree | Non-linear | 0.121 | 0.887 |
| Rem | Ridge + Rec | Non-linear | 0.369 | 0.774 |
| Rem | Ridge + Seq | Non-linear | 0.251 | 0.843 |
| Rem | Ridge + Tree | Non-linear | 0.302 | 0.813 |
| Rem | Bag + Rec | Non-linear | 0.041 | 0.954 |
| Rem | Bag + Seq | Non-linear | -0.362 | 1.136 |
| Rem | Bag + Tree | Non-linear | 0.069 | 0.94 |
| Rem | ARD + Rec | Linear | 0.229 | 0.855 |
| Rem | ARD + Seq | Linear | 0.259 | 0.838 |
| Rem | ARD + Tree | Linear | 0.261 | 0.837 |
| Rem | RF + Rec | Non-linear | 0.044 | 0.952 |
| Rem | RF + Seq | Non-linear | -0.348 | 1.131 |
| Rem | RF + Tree | Non-linear | 0.042 | 0.953 |
| Rem | XGB + Rec | Non-linear | -0.267 | 1.096 |
| Rem | XGB + Seq | Non-linear | -1.386 | 1.504 |
| Rem | XGB + Tree | Non-linear | 0.019 | 0.965 |
| Rem | BYR + Rec | Non-linear | 0.324 | 0.801 |
| Rem | BYR + Seq | Non-linear | 0.217 | 0.862 |
| Rem | BYR + Tree | Non-linear | 0.293 | 0.819 |
| Sto | Ridge + Rec | Non-linear | 0.168 | 1.022 |
| Sto | Ridge + Seq | Non-linear | -0.014 | 1.128 |
| Sto | Ridge + Tree | Non-linear | 0.169 | 1.021 |
| Sto | Bag + Rec | Non-linear | 0.128 | 1.046 |
| Sto | Bag + Seq | Non-linear | 0.422 | 0.852 |
| Sto | Bag + Tree | Non-linear | 0.265 | 0.961 |
| Sto | ARD + Rec | Linear | 0.16 | 1.026 |
| Sto | ARD + Seq | Linear | 0.16 | 1.026 |
| Sto | ARD + Tree | Linear | 0.16 | 1.027 |
| Sto | RF + Rec | Non-linear | 0.129 | 1.045 |
| Sto | RF + Seq | Non-linear | 0.413 | 0.858 |
| Sto | RF + Tree | Non-linear | 0.184 | 1.012 |
| Sto | XGB + Rec | Non-linear | -0.373 | 1.313 |
| Sto | XGB + Seq | Non-linear | 0.287 | 0.946 |
| Sto | XGB + Tree | Non-linear | -0.062 | 1.155 |
| Sto | BYR + Rec | Non-linear | 0.008 | 1.115 |
| Sto | BYR + Seq | Non-linear | -0.07 | 1.159 |
| Sto | BYR + Tree | Non-linear | -0.061 | 1.154 |